Molecular Pharmacology Fast Forward. Published on July 10, 2019 as DOI: 10.1124/mol.119.116764
This article has not been copyedited and formatted. The final version may differ from this version.

Investigating the influence of tracer kinetics on competition-kinetic association binding assays; identifying the optimal conditions for assessing the kinetics of low affinity compounds.

David A Sykes[1,2], Palash Jain[1,2] & Steven J Charlton[1,2,3]

[1]School of Life Sciences, Queen's Medical Centre, University of Nottingham, Nottingham NG7 2UH, UK

[2]Centre of Membrane and Protein and Receptors (COMPARE), University of Birmingham and University of Nottingham, Midlands, UK.

[3]Excellerate Bioscience Ltd, Discovery Building, BioCity, Pennyfoot Street, Nottingham, NG1 1GF, UK

Downloaded from molpharm.aspetjournals.org at ASPET Journals on April 19, 2024

Molecular Pharmacology Fast Forward. Published on July 10, 2019 as DOI: 10.1124/mol.119.116764
This article has not been copyedited and formatted. The final version may differ from this version.

Running title: Optimizing the design of competition association assays.

Addresses for correspondence:

Prof Steven Charlton

School of Life Sciences

Queen's Medical Centre

University of Nottingham

Nottingham NG7 2UH

E-mail: steven.charlton@nottingham.ac.uk

David Sykes

School of Life Sciences

Queen's Medical Centre

University of Nottingham

Nottingham NG7 2UH

E-mail: David.Sykes@nottingham.ac.uk

Downloaded from molpharm.aspetjournals.org at ASPET Journals on April 19, 2024

Molecular Pharmacology Fast Forward. Published on July 10, 2019 as DOI: 10.1124/mol.119.116764
This article has not been copyedited and formatted. The final version may differ from this version.

Abbreviations:

CPM, counts per minute; SPA, scintillation proximity assays; TR-FRET time-resolved FRET; HTRF, homogeneous time resolved fluorescence; SKR structure-kinetic relationships; PPHT-red, ((±)-2-(n-phenethyl-n-propyl)amino-5-hydroxytetralin hydrochloride;1-Naphthalenol, 5,6,7,8-tetrahydro-6-[(2-phenylethyl)propylamino]) derivative labeled with a red fluorescent probe

Downloaded from molpharm.aspetjournals.org at ASPET Journals on April 19, 2024

Molecular Pharmacology Fast Forward. Published on July 10, 2019 as DOI: 10.1124/mol.119.116764
This article has not been copyedited and formatted. The final version may differ from this version.

Abstract

There is an increased appreciation of the importance of optimizing drug-binding kinetics leading to the development of various different techniques for measuring the kinetics of unlabelled compounds. One approach is the competition-association kinetic binding method, first described in the 1980s. The kinetic characteristics of the tracer employed greatly affects the reliability of estimated kinetic parameters, a barrier to successfully introducing these kinetic assays earlier in the drug discovery process.

Using a modeling and Monte Carlo simulation approach we identify the optimal tracer characteristics for determining the kinetics of the range of unlabeled ligands typically encountered during the different stages of a drug discovery program (i.e. rapidly-dissociating eg. k_{off} = 10min^{-1} low-affinity "hits" through to slowly-dissociating eg. k_{off} = 0.01min^{-1} high-affinity "candidates"). For more rapidly dissociating ligands (eg. k_{off} = 10min^{-1}) the key to obtaining accurate kinetic parameters was to employ a tracer with a relatively fast off-rate (eg. k_{off} = 1min^{-1}), or alternatively to increase the tracer concentration. Reductions in assay start-time ≤1sec, and read frequency ≤5sec significantly improved the reliability of curve fitting. Timing constraints are largely dictated by the method of detection, its inherent sensitivity (eg TR-FRET verses radiometric detection), and the ability to inject samples online. Furthermore we include data from TR-FRET experiments which validates this simulation approach confirming its practical utility.

These insights into the optimal experimental parameters for development of competition-association assays provide a framework for identifying and testing novel tracers necessary for profiling unlabelled competitors, particularly rapidly-dissociating low affinity competitors.

Downloaded from molpharm.aspetjournals.org at ASPET Journals on April 19, 2024

Molecular Pharmacology Fast Forward. Published on July 10, 2019 as DOI: 10.1124/mol.119.116764
This article has not been copyedited and formatted. The final version may differ from this version.

Introduction

Historically most drug discovery programs have relied upon equilibrium dissociation constant measurements when assessing the potential of future lead-drug candidates, rather than the kinetic parameters that comprise it (K_d = k_{off} / k_{on}). However, it is becoming more widely appreciated that optimising the kinetics of drug binding (k_{off} and k_{on}) can enhance both compound efficacy and duration of action (Sykes et al., 2009; Guo et al., 2012; Vauquelin, 2016; Copeland, 2016). This has resulted in the introduction of novel methods to assess ligand binding kinetics at earlier stages in the drug discovery process, allowing the development of structure-kinetic relationships (SKR) (Schmidtke et al., 2011; Georgi et al., 2018). A commonly applied method to assess the kinetics of unlabeled compounds is surface plasmon resonance (SPR) spectroscopy, but this is still not widely utilized for membrane proteins due to issues with protein purification and stability. To overcome this competition-association kinetic binding assays using radioactive probes have been employed successfully to determine the kinetic values for both antagonists (Gillard and Chatelain 2006; Slack et al., 2011; Fleck et al., 2012; Sykes et al., 2014; Sykes et al, 2016) and agonists (Sykes et al., 2009; Sykes and Charlton 2012) acting at a variety of G protein-coupled receptors (GPCRs) at physiological temperature, and even more recently at non-GPCR targets (Yu *et al*., 2015).

Despite their undoubtable high sensitivity the use of radioactive probes as tracers in kinetic competition binding assays presents a number of challenges. Classic radioactive binding requires the need for multiple washing steps to separate bound and free radioligand, adding complexity to the procedure and reducing throughput. Importantly the wash step requirement also prevents any possibility of multiple single sample reads. More recently scintillation proximity assays (SPA) have been

Downloaded from molpharm.aspetjournals.org at ASPET Journals on April 19, 2024

Molecular Pharmacology Fast Forward. Published on July 10, 2019 as DOI: 10.1124/mol.119.116764
This article has not been copyedited and formatted. The final version may differ from this version.

formulated which can be performed in homogeneous conditions, but signal-drift due to bead settling can complicate interpretation at early time points (Xia et al., 2016).

The emergence of time-resolved RET-based methods, (Schiele et al., 2014; Klein-Herenbrink et al., 2016) and bioluminescence based methods (Stoddart et al., 2018; Bouzo-Lorenzo et al., 2019) offers an alternative to radioactive binding assays and represent higher throughput methods to assess unlabelled ligand kinetics. With separation of bound and unbound-label no longer necessary multiple reads can be made from the same well (Emami-Nemini et al., 2013; Stoddart et al., 2015). Using the simple technique of time-resolved fluorescent resonance energy transfer (TR-FRET) we successfully characterised the binding of a series of dopamine D_2 specific agonists and clinically used antipsychotics employing a SNAP-tagged receptor labelled with terbium and a fluorescent tracer (Klein-Herenbrink et al., 2016; Sykes et al, 2017).

A key observation made during these studies was that the kinetic characteristics of the tracer had a profound effect on the reliability of the estimated kinetic parameters of unlabelled competitors (Klein-Herenbrink et al., 2016). This was most evident when using a slowly dissociating tracer to assess rapidly dissociating, low affinity ligands. This represents a potential barrier to successfully introducing kinetic assays earlier in the drug discovery process (e.g. hit identification/validation) as tracers need to be capable of determining the kinetics of low affinity “hits” (in the μM range). Thus the aim of the current study was to use a modeling and simulation approach to identify the optimal tracer characteristics for determining the kinetics of a variety of unlabeled ligands typically encountered during different stages of a drug discovery program (i.e. low affinity “hits” through to high affinity “candidates”).

Downloaded from molpharm.aspetjournals.org at ASPET Journals on April 19, 2024

Molecular Pharmacology Fast Forward. Published on July 10, 2019 as DOI: 10.1124/mol.119.116764
This article has not been copyedited and formatted. The final version may differ from this version.

Using Monte Carlo simulations we have assessed the ability of the global association method to accurately determine the kinetics of different model tracers. The global association method is a way of simultaneously fitting multiple tracer association curves (eg different tracer concentrations) to find best-fit k_{off} and k_{on} parameters across the whole dataset. Additionally using Monte Carlo simulations we have explored the utility of these model tracers to predict the kinetic parameters of unlabeled ligands in competition-association binding mode. Furthermore, we have explored the influence of experimental design on the accuracy of kinetic parameter estimation, testing the impact of increasing tracer concentrations, and investigating different plate reader configurations, particularly the influence of read frequency time and on-line (direct reagent injection into sample wells) versus off-line (reagent addition into plate prior to insertion into reader) reagent addition.

Finally we test the validity of this modelling approach through the detailed characterisation of two dopamine D_2R specific fluorescent tracers; spiperone-d2 and PPHT-red. Assessing their ability to determine the kinetics of D_2R specific ligands with very varied kinetic characteristics, from the rapidly dissociating chlorpromazine to the very slowly dissociating butaclamol.

The analysis presented has important implications for the design of competition-kinetic approaches to assess unlabelled compound kinetics, providing a framework for the identification and testing of suitable tracers. In particular we have identified the optimal tracer characteristics and experimental design for assessing low affinity competitors, enabling the utilisation of kinetics assays much earlier in the drug discovery process.

.

Downloaded from molpharm.aspetjournals.org at ASPET Journals on April 19, 2024

Molecular Pharmacology Fast Forward. Published on July 10, 2019 as DOI: 10.1124/mol.119.116764
This article has not been copyedited and formatted. The final version may differ from this version.

Materials and Methods

Determining the kinetics of the tracer for use in competition kinetic binding studies

Monte Carlo simulations are useful to investigate the behaviour of a system under controlled situations and may be thought of as statistical experiments. They provide an estimation of variance for complex models, which ultimately helps researchers with experimental design and provides confidence in a particular experimental approach prior to testing. The underlying principle is to take a simulated dataset that is based on a set of 'ideal' model parameters, add random error to the 'dataset' and then recreate the resulting dataset many times to obtain the parameters of interest. In this case the 'dataset' comprises an XY table where X is time and Y is % specific binding of the tracer. This process allows a frequency distribution to be built from the resulting parameter estimates allowing an understanding of the associated error of each parameter estimate under the conditions employed (Christopoulos 2001).

The competition association assay model (Motulsky and Mahan, 1984) relies on an accurate assessment of the kinetic properties of the labelled tracer, both the association rate constant (k_{on} *or* $k1$) and the dissociation rate constant (k_{off} *or* $k2$). Since the introduction of fitting software, such as GraphPad Prism, a popular experimental procedure to estimate the kinetics of the tracer is to monitor the binding of two or more different concentrations of tracer over time until equilibrium is reached, in doing so it is possible to calculate the k_{on} and k_{off} values of the tracer by simultaneously fitting all curves to generate global estimates for these rate parameters.

Downloaded from molpharm.aspetjournals.org at ASPET Journals on April 19, 2024

Molecular Pharmacology Fast Forward. Published on July 10, 2019 as DOI: 10.1124/mol.119.116764
This article has not been copyedited and formatted. The final version may differ from this version.

For the purposes of this study tracer association was simulated using GraphPad Prism 6.0 employing the following equation where k_{ob} equals the observed rate of association and k_{on} and k_{off} are the association and dissociation-rate constants respectively of the tracer:

$$k_{ob} = [L]*k_{on} + k_{off} \quad \text{(Eq. 1)}$$

$$Y = Y_{max}*(1-\exp(-1*k_{ob}*X))$$

In this globally fitted model of tracer binding, tracer concentrations [L] are fixed, k_{on} and k_{off} are shared parameters and independent of tracer concentration. Here, Y is the level of receptor-bound tracer, Y_{max} is the level of tracer binding at equilibrium, X is in units of time (eg. min) and k_{obs} (min^{-1}) is the rate in which equilibrium is approached.

Tracer binding simulations were performed to assess the effect of on-line and off-line reagent addition on our ability to accurately estimate the kinetics of a variety of model tracers with varied kinetics parameters, consistent with the properties of compounds discovered in the various phases of the drug discovery cascade, the details of which are provided in Table 1. Tracer Monte Carlo simulations were performed using the following parameters; the k_{on} and k_{off} of each model tracer studied was allowed to vary, whilst the concentrations of tracer (L) employed were fixed at various multiples of the tracer's affinity, specifically 30, 10, 3, 1, 0.3, 0.1 xK_d. Unless otherwise stated the assay start time was fixed at either 1 sec to mimic on-line addition of reagents via plate reader injectors, or 30 sec to mimic the delay in the time to read following off-line addition of membranes prior to insertion the assay plate into the plate reader. Read frequency (i.e. the time between each well read) was varied at 1, 5, 10, 20 & 60 seconds. Random error was added to the generated y values by taking each

Downloaded from molpharm.aspetjournals.org at ASPET Journals on April 19, 2024

Molecular Pharmacology Fast Forward. Published on July 10, 2019 as DOI: 10.1124/mol.119.116764
This article has not been copyedited and formatted. The final version may differ from this version.

theoretical (i.e. 'correct') value and adding to it a random number taken from a uniformly distributed population with a standard deviation equal to one. The random error chosen for simulation was Guassian absolute to directly reflect the pattern of error observed in our experimental data. The resulting simulated data sets were then individually fit to the association kinetic model (two or more concentration of hot, GraphPad Prism 6.0) and 'Global (shared) parameters' including tracer k_{off} and k_{on} values were tabulated. In total 200 simulations were performed per test condition.

Determining the suitability of the tracer for competition kinetic binding studies

The interactions of the tracer and unlabelled competitor with receptor is described by two differential equations which when solved yield a single equation describing the binding of the tracer as a function of time (Motulsky and Mahan, 1984). This model was used to simulate competition association curves to a variety of unlabelled compounds with different association-rate constants (k_{on} *or* $k3$) and dissociation-rate constants (k_{off} *or* $k4$), according to the following equations:

$$K_A = k_1[L] + k_2$$

$$K_B = k_3[I] + k_4$$

$$S = \sqrt{((K_A - K_A)^2 + 4 \cdot k_1 \cdot k_3 \cdot L \cdot I \cdot 10^{-18})}$$

$$K_F = 0.5 \cdot (K_A + K_B + S)$$

$$K_S = 0.5 \cdot (K_A + K_B - S)$$

$$DIFF = K_F - K_S$$

Downloaded from molpharm.aspetjournals.org at ASPET Journals on April 19, 2024

Molecular Pharmacology Fast Forward. Published on July 10, 2019 as DOI: 10.1124/mol.119.116764
This article has not been copyedited and formatted. The final version may differ from this version.

$$Q = \frac{B_{max} \cdot K_1 \cdot L \cdot 10^{-9}}{DIFF}$$

$$Y = Q \cdot \left(\frac{k_4 \cdot DIFF}{K_F \cdot K_S} + \frac{k_4 - K_F}{K_F} \cdot \exp(-K_F \cdot X) - \frac{k_4 - K_s}{K_s} \cdot \exp(-K_S \cdot X) \right) \qquad \text{(Eq. 2)}$$

Where: X = Time (min), Y = Specific binding (eg. CPM or HTRF units), k_1 = k_{on} tracer (M^{-1} min^{-1}), k_2 = k_{off} tracer (min^{-1}), L = Concentration of tracer used (nM), I = Concentration unlabeled ligand (nM). Fixing the above parameters allows the following to be calculated: k_3 = Association-rate constant of unlabeled ligand (M^{-1} min^{-1}), k_4 = Dissociation-rate constant of unlabeled ligand (min^{-1}), B_{max} = Maximal specific binding of the system at equilibrium binding (eg CPM or HTRF units),

All competition kinetic association simulations were performed using the model tracers described in Table 1. These Monte Carlo simulation studies were designed to assess the effect of tracer kinetics on the ability of the Motulsky-Mahan model to distinguish compounds typically encountered in a drug discovery program with a wide range of kinetic off-rates ranging from the more rapidly dissociating (eg. k_{off} = $100min^{-1}$ representative of low affinity fragments) to the more slowly dissociating (eg. k_{off} = $0.01min^{-1}$ representative of a lead candidate compound).

Unless otherwise stated the concentration of tracer (L) employed was fixed at 3x K_d. The concentration of unlabelled competitor (I) was routinely fixed at various multiples of its own affinity, specifically 100, 30, 10, 3, 1x K_d. Also taken into consideration was on-line verses off-line addition protocols and their effect on our ability to accurately estimate the kinetics of unlabeled compounds with varied kinetics parameters. Start time was fixed at either 1 second (to mimic on-line addition) or 30 seconds (to mimic

Downloaded from molpharm.aspetjournals.org at ASPET Journals on April 19, 2024

Molecular Pharmacology Fast Forward. Published on July 10, 2019 as DOI: 10.1124/mol.119.116764
This article has not been copyedited and formatted. The final version may differ from this version.

off-line addition) and the read frequency was varied using either 1, 5, 10, 20 & 60 seconds unless otherwise stated.

Random error was added to the generated y values by taking each theoretical (i.e. 'correct') value and adding to it a random number taken from a uniformly distributed population with a standard deviation equal to one. The random error chosen for simulation was Guassian absolute to directly reflect the pattern of error observed in our experimental data. The resulting simulated data sets were then individually fit to the competition association model (Kinetics of competitive binding, GraphPad Prism 6.0) model and 'Global (shared) parameters' including tracer k_{off} and k_{on} values were tabulated. In total 200 simulations were performed per test condition.

In order to test the effect of tracer concentration on our ability to estimate the kinetic parameters of unlabelled compounds we performed a further series of simulations but this time we employed tracer concentrations (L) at 1x, 10x and 30x K_d. The concentrations of unlabelled competitor (I) was varied accordingly. This allowed us to test the effect of decreasing and increasing tracer competition on the accuracy of unlabelled compound kinetic determinations.

In another series of competition kinetic association simulations, the ability of a rapidly dissociating tracer to assess the kinetics of low affinity (1-1000 μM) unlabelled fragments was explored in both double and single concentration screening modes. All Monte Carlo simulations were performed using the following parameters; the k_{on} and k_{off} of the model tracer studied was fixed at $3x10^7$ M^{-1} min^{-1} and 10 min^{-1} respectively, with the concentration of tracer (L) employed fixed at 3x K_d whilst the concentrations of the fragments were fixed specifically at 10 and 100 μM (typical of a fragment screen where affinity of the fragments is unknown). Start time was fixed at 1 second (to mimic on-

Downloaded from molpharm.aspetjournals.org at ASPET Journals on April 19, 2024

Molecular Pharmacology Fast Forward. Published on July 10, 2019 as DOI: 10.1124/mol.119.116764
This article has not been copyedited and formatted. The final version may differ from this version.

line addition) and a standard read frequency of 5 seconds was employed. The resulting simulated data sets were then individually fit to the competition association model and 'Global (shared) parameters' including tracer k_{off} and k_{on} values were tabulated. In total 200 simulations were performed per test condition. All the experiments described above assume that the Laws of Mass Action are obeyed and that ligand depletion does not occur under any of the conditions of tracer and competitor binding explored (Carter et al., 2007).

Monte Carlo simulation data analysis

All Monte Carlo simulations were performed in Prism 6.0. In total 200 simulations were performed per test condition using an associated error equivalent to a standard deviation of one. 'Global (shared) parameters' associated with Equations 1 and 2 were recorded and an outlier test (using an iterative Grubb's test, α=0.0001) was performed on reported k_{on} and k_{off} values for tracers and unlabelled competitors. Outliers and ambiguous fits (those for which confidence intervals were extremely wide) were removed from the analysis before calculation of mean and % coefficient of variance (CV) values (i.e. (standard deviation/mean)*100), which are indications of accuracy and variation around the expected input value. Mean fitting values were considered a reliably "good fit" if >90% of fits (i.e. >180//200 fits were returned without being judged as either outliers and/or ambiguous fits). Ambiguous fits are those for which confidence intervals are extremely wide and therefore not reported (Motulsky n.d.). Graphical representation of Monte Carlo data was also performed in using R and competition association data was fitted in Prism 6.0.

Fluorescent ligand binding assays.

Downloaded from molpharm.aspetjournals.org at ASPET Journals on April 19, 2024

Molecular Pharmacology Fast Forward. Published on July 10, 2019 as DOI: 10.1124/mol.119.116764
This article has not been copyedited and formatted. The final version may differ from this version.

Materials

PPHT ((±)-2-(n-phenethyl-n-propyl)amino-5-hydroxytetralin hydrochloride;1-Naphthalenol, 5,6,7,8-tetrahydro-6-[(2-phenylethyl)propylamino]) derivative labeled with a red fluorescent probe (PPHT-red) was obtained from Cisbio Bioassays (Bagnolssur-Cèze, France). Ninety-six-well polypropylene plates (Corning) were purchased from Fisher Scientific UK (Loughborough, UK) and 384-well optiplate plates were purchased from PerkinElmer (Beaconsfield, UK). GppNHp, risperidone, chlorpromazine hydrochloride and (+)-butaclamol used in competition assays were obtained from Sigma-Aldrich (Poole, UK). Domperidone, and haloperidol hydrochloride used for competition assays were obtained from Tocris Bioscience (Avonmouth, Bristol). Pergolide and ropinirole were kind gifts from Dr Robert Lane (Monash University), whilst bromocriptine was a kind gift of Dr Nicholas Holliday (Nottingham University).

Determination of D_2R fluorescent ligand binding kinetics. All fluorescent binding experiments using PPHT-red and spiperone-d2, were conducted in white 384-well Optiplate plates, in assay binding buffer, HBSS containing 5mM HEPES, 1% DMSO and 0.02% pluronic acid pH 7.4, 0.1mM GppNHp. GppNHp was included to remove the G protein–coupled population of receptors that can result in two distinct populations of binding sites in membrane preparations, since the Motulsky–Mahan model is only appropriate for ligands competing at a single site. In all cases, nonspecific binding was determined in the presence of 10 μM haloperidol.

To accurately determine association-rate (k_{on}) and dissociation-rate (k_{off}) values, the observed rate of association (k_{ob}) was calculated using at least four different concentrations of either PPHT-red or spiperone-d2. SNAP-tagged terbium labelled

Downloaded from molpharm.aspetjournals.org at ASPET Journals on April 19, 2024

Molecular Pharmacology Fast Forward. Published on July 10, 2019 as DOI: 10.1124/mol.119.116764
This article has not been copyedited and formatted. The final version may differ from this version.

human dopamine D_{2L} receptors expressed in CHO cell membranes (2 µg per well) were injected into wells containing six different concentrations of the fluorescent tracers PPHT-red (50-1.56 nM) or spiperone-d2 (10-0.3 nM) in a final assay volume of 40 µL. A detailed description of the terbium labelling procedure can be found in Sykes et al., 2017.

The degree of PPHT-red or spiperone-d2 bound to the receptor was assessed at multiple time points by HTRF detection to allow construction of association kinetic curves. The resulting data were globally fitted to the association kinetic model (Equation 1) to derive a single best-fit estimate for k_{on} and k_{off} as described under Data analysis and data detection.

Competition binding kinetics. To determine the association and dissociation-rates of D_2R ligands, we used a competition kinetic binding assay we recently described to profile the kinetics of a series of D_2R agonists (Klein-Herenbrink *et al*., 2016). This approach involves the addition of a receptor preparation to wells containing fluorescent ligand and competitor, so that at t = 0 all receptors are unoccupied.

12.5 nM PPHT-red (~1x K_d, a concentration which avoids ligand depletion in this assay volume, (see Carter *et al*., 2007) was added simultaneously with the unlabeled compound (at t = 0) to CHO cell membranes containing the human dopamine D_{2L} receptor (2 µg per well) in 40 µL of assay buffer.

Specifically Human dopamine D_{2L} CHO cell membranes (2 µg per well) were injected into wells containing six different concentrations of the fluorescent tracers PPHT-red (50-1.56 nM) or spiperone-d2 (10-0.3 nM) and varying concentrations of unlabeled compound in a final assay volume of 40 µL. Online addition is best achieved by

Downloaded from molpharm.aspetjournals.org at ASPET Journals on April 19, 2024

Molecular Pharmacology Fast Forward. Published on July 10, 2019 as DOI: 10.1124/mol.119.116764
This article has not been copyedited and formatted. The final version may differ from this version.

injecting an equal volume of receptor (20 µL membranes) to the assay plate containing the ligands of interest (eg. tracer and/or competitor 20 µL) to ensure complete and adequate mixing of all reagents. The degree of PPHT-red bound to the receptor was assessed at multiple time points by HTRF detection. The kinetic parameters of PPHT-red and spiperone-d2 plus those of unlabeled compounds were determined using a start time of ~1sec and a read frequency of 5sec.

Nonspecific binding was determined as the amount of HTRF signal detected in the presence of haloperidol (10 µM) and was subtracted from each time point, meaning that t = 0 was always equal to zero. Each time point was conducted on the same 384-well plate incubated at room temperature with orbital mixing (1sec of 100 RPM/cycle).

Data were globally fitted using Equation 2 to simultaneously calculate k_{on} and k_{off} of the unlabeled compounds. Different competitor concentration ranges were chosen, as compounds with a long residence time equilibrate more slowly, so a higher relative concentration is required to ensure the experiments reach equilibrium within a reasonable time frame (20 minutes), while still maintaining a good signal-to-noise.

Data analysis and signal detection

For the binding experiments described signal detection was performed on a Pherastar FS (BMG Labtech, Offenburg, Germany) using standard HTRF settings. The terbium donor was always excited with up to 6 laser flashes at a wavelength of 337 nm. A kinetic TR-FRET signal was collected at 5 seconds intervals both at 665 nm and 620 nm, when using red acceptor. HTRF ratios were obtained by dividing the acceptor signal (665 nm) by the donor signal (620 nm) and multiplying this value by 10,000.

Downloaded from molpharm.aspetjournals.org at ASPET Journals on April 19, 2024

Molecular Pharmacology Fast Forward. Published on July 10, 2019 as DOI: 10.1124/mol.119.116764
This article has not been copyedited and formatted. The final version may differ from this version.

Results

Monte Carlo simulations

Accurate determination of model tracer kinetic parameters

In order to accurately calculate the kinetic on (k_{on}) and off-rates (k_{off}) of unlabelled competitor compounds the kinetic parameters of the tracer used must first be determined by fitting tracer association data to a global kinetic model (see Equation 1). Simulations were performed for four model tracers whose rates of dissociation differed up to 1000-fold (see Table 1).

For each tracer tested a family of association kinetic curves were constructed using 6 concentrations of each tracer, ranging from ~30 to 0.1x K_d with each association curve being monitored to the point of equilibrium; such that Y_{max} is reached allowing for the most accurate estimation of tracer kinetic parameters, k_{on} and k_{off} (see Figure 1A & C).

To construct Figure 1A & C using Monte Carlo simulations the k_{on} input value for the very rapidly dissociating tracer was fixed at 3 x10^7 M^{-1} min^{-1} and k_{off} input value at 10 min^{-1}. Figure 1A and C differ only in their initial start time 1 sec (representative of on-line injection) and 30 sec (representative of off-line addition) respectively with read frequency fixed every 10 sec thereafter. What is immediately apparent under these simulation conditions is that the equilibrium between a very rapidly dissociating tracer (k_{off} 10min^{-1}) and receptor is reached rapidly within the first 30 sec and as a consequence an accurate determination of tracer association is improbable with a 30 sec start time. This is reflected in the graphical plots, Figure 1B and D showing the relationship between input tracer k_{off} and output k_{off} with read frequency. With a start time of 1 sec tracer kinetic determinations (data fits) are on the whole extremely

Downloaded from molpharm.aspetjournals.org at ASPET Journals on April 19, 2024

Molecular Pharmacology Fast Forward. Published on July 10, 2019 as DOI: 10.1124/mol.119.116764
This article has not been copyedited and formatted. The final version may differ from this version.

reliable, with a 'good fit' achieved on > 90% of the 200 fits. See Figure 1B & C and Supplemental Table 1. In contrast reliable determinations of tracer kinetics, as judged through off-rate monitoring, following a 30 sec start time representative of off-line addition, is only possible when the off-rate of the tracer is less that $1min^{-1}$.

Also apparent is the effect of read frequency on the variation in reported k_{off} values with shorter read frequencies resulting in an improved quality of fit as highlighted by a reduction in the variability of the estimated output of tracer off-rate values. The results of Monte Carlo simulations using the kinetic association model equations are summarized in Supplemental Table 1. It must be emphasized that although our analysis focuses on the kinetic parameter k_{off}, the variability of k_{on} is also documented in these Supplemental Tables.

Competition kinetic binding between tracer and unlabelled competitor mimicking an off-line addition protocol

In order to accurately determine the kinetics of unlabelled competitor compounds it is conventional to construct a family of association kinetic curves using a fixed tracer concentration (~3x K_d) and varying concentrations of the unlabelled compound with each association curve being monitored until equilibrium (see Figure 2A & B). In the case of the most slowly dissociating tracer, association curves were monitored for 180 min to reflect practical limitations. The resulting data were then fitted to the Motulsky–Mahan model which describes the interaction between an unlabelled compound and a labelled tracer and allows us to calculate the k_{on} and k_{off} of the unlabelled compound (Equation 2).

Downloaded from molpharm.aspetjournals.org at ASPET Journals on April 19, 2024

Molecular Pharmacology Fast Forward. Published on July 10, 2019 as DOI: 10.1124/mol.119.116764
This article has not been copyedited and formatted. The final version may differ from this version.

Example results of Monte Carlo simulations using the Motulsky-Mahan model equation are shown in Figure 2A & B. In each case the very rapidly dissociating tracer was employed; with input values of k_{on} for the tracer fixed at 3 x10^7 M^{-1} min^{-1} and k_{off} fixed at 10 min^{-1}. Figure 2A & B differ only in respect of the kinetic properties of the unlabelled compound in competition with the tracer, with initial start times fixed at 1 sec and with read frequency fixed every 10 sec thereafter. Under these simulation conditions and in the presence of a rapidly dissociating unlabelled compound (with kinetic parameters; k_{off} of 10 min^{-1}, k_{on} of 1x10^6 M^{-1} min^{-1}), equilibrium between the rapidly dissociating tracer, competitor compound and receptor is reached rapidly within the first 30 sec (see Figure 2A).

In direct contrast in the presence of a more slowly dissociating competitor (with kinetic parameters; k_{off} of 1min^{-1}, k_{on} of 1x10^7 M^{-1} min^{-1}) then the time to equilibrium is markedly increased with a characteristic 'overshoot' in the initial binding of the tracer (see Figure 2B). The data contained in Figure 2 represents a single simulation and is illustrative of the whole data set which is summarized in Figure 3.

State of the art radioligand-based competition association binding assays are routinely formulated using only 12 time points (Sykes et al., 2010) employing either a single concentration of competitor (Sykes et al., 2014; Martella et al., 2017) or up to three concentrations of competitor (Sykes et al., 2009; Sykes et al., 2010) and a tracer concentration in the range of 1-10x its own K_d. Current knowledge of FRET-based competition association binding assays is based on a small number of studies which in general have employed an offline addition protocol to improve experimental throughput but also to allow greater temperature control during the initial mixing step (Klein-Herenbrink et al., 2016; Sykes et al., 2017; Sykes and Charlton 2018).

Downloaded from molpharm.aspetjournals.org at ASPET Journals on April 19, 2024

Molecular Pharmacology Fast Forward. Published on July 10, 2019 as DOI: 10.1124/mol.119.116764
This article has not been copyedited and formatted. The final version may differ from this version.

Figure 3A-D shows summary off-rate data from the Motulsky-Mahan fits to the Monte-Carlo kinetic simulations exploring the effect of sample time and tracer kinetics on our ability to accurately determine competitor kinetic parameters (k_{off} range from 100 to 0.01 min^{-1}), and is representative of an off-line addition protocol with a 30 sec start time. In all cases tracers were employed at a concentration 3x their own K_d value. These results demonstrate that even the very rapidly dissociating tracer examined (k_{off} = 10 min^{-1}) is not able to accurately determine the kinetics of unlabeled compounds with off-rates ranging from 100 – 10 min^{-1} (see Figure 3A). This represents a limitation in the kinetic quantification of unlabelled compounds using the competition association method where reagents are added offline from the plate reader.

Also apparent was the influence of read frequency on our ability to accurately predict the kinetics of unlabeled competitor compounds with slower dissociation rates, i.e. those in the range of 0.01 min^{-1}, reflecting the imprecise fitting of the tracer 'overshoot'. Interestingly, a tracer with a k_{off} of 1 min^{-1} under the conditions explored could not accurately fit the kinetics of unlabeled compounds with a k_{off} of 100 min^{-1} and is only suitable to unambiguously and accurately quantify the kinetics of unlabeled compounds with a k_{off} in the range of 10 min^{-1} if the read frequency remains at 1 sec (see Figure 3B). Almost identical patterns were observed for tracers with k_{off} values of 0.1 and 0.01min^{-1} (see Figure 3C and D). The results of Monte Carlo simulations using the Motulsky-Mahan model equation are summarized in Supplemental Tables 2-5.

Competition kinetic binding between tracer and unlabelled competitor mimicking an on-line injection protocol

Downloaded from molpharm.aspetjournals.org at ASPET Journals on April 19, 2024

Molecular Pharmacology Fast Forward. Published on July 10, 2019 as DOI: 10.1124/mol.119.116764
This article has not been copyedited and formatted. The final version may differ from this version.

Having established the limitation of the off-line injection protocol we decided to explore the potential of utilising on-board plate reader injectors and the increased resolution at very early time points to improve the goodness of fit (fit quality). Figure 4A-D shows summary dissociation rate estimates obtained by fitting Monte-Carlo simulations that explore the effect of read frequency and tracer kinetics on our ability to accurately determine competitor kinetic parameters (k_{off} range from 100 to 0.01 min^{-1}), and is representative of an injection protocol with a 1 sec start time. In all cases tracers were employed at a concentration 3x their own K_d value. These simulations demonstrate that the very rapidly dissociating tracer examined (k_{off} = 10 min^{-1}) is able to accurately determine the kinetics of unlabeled compounds with off-rates ranging from 100 – 0.01 min^{-1} (see Figure 4A). Interestingly under these tracer conditions employed the range of dissociation rate estimates markedly increases for the most rapidly dissociating unlabeled compounds examined (10-100 min^{-1}) representing the limit of kinetic detection for this type of competition kinetic binding approach (See Supplemental Table 2). Also apparent was the influence of increasing read frequency on our ability to accurately predict the kinetics of unlabeled compounds with slower dissociation rates in the range of 0.01 min^{-1}. Increased variation likely reflects the imprecise fitting of the tracer 'overshoot' which is reliant on early time points for accuracy. In contrast a tracer with a k_{off} of 1 min^{-1} is seemingly suitable for the determination of off-rates in the range of ~10 min^{-1}, but increasing variation in the mean is observed as the read frequency is increased from 1 to 60 seconds (see Figure 4B). Practically this wider degree of variation in the mean will become especially apparent if the number of observations for a particular compound is kept low (i.e. n ≤ 4). A different pattern is observed for a tracer with a k_{off} value equal to 0.1 min^{-1}, as shown in Figure 4C for compounds with rapid off-rates between 10-100 min^{-1} the number of ambiguous fits is

Downloaded from molpharm.aspetjournals.org at ASPET Journals on April 19, 2024

Molecular Pharmacology Fast Forward. Published on July 10, 2019 as DOI: 10.1124/mol.119.116764
This article has not been copyedited and formatted. The final version may differ from this version.

very high (see Supplemental Table 4), and it is only compounds with k_{off} value of ≤ 1 min^{-1} that can be measured without ambiguity at this concentration of tracer employed (i.e. 3x K_d). Interestingly the appearance of ambiguity in fitting estimates precedes any inaccuracies in the fitting estimates themselves. Finally a kinetic tracer with a k_{off} of 0.01min^{-1} employed at a concentration of 3x K_d, is only able to unambiguously (and accurately) determine the kinetics of compounds with k_{off} ≤ 1min^{-1} when the read frequency is shortened to 1 sec (see Figure 4D) and as a consequence is of limited value as a tracer for kinetic determinations of more rapidly dissociating compounds.

The figures which are derived from these Monte-Carlo simulations are useful guides to enable investigators interested in compound kinetics and associated SAR to set up kinetic screens and choose appropriate tracers to profile the properties of unlabeled compounds. To illustrate some key points, Monte-Carlo simulation results reproducing the experimentally observed effect of competitor off-rate on the competition profile observed with a rapidly dissociating tracer and a slowly dissociating tracer with varying start time are depicted in Figure 5A-D. Figure 5A shows competition between a fixed concentration (3x K_d) of a very slowly dissociating tracer (k_{off} of 0.01 min^{-1}, k_{on} of 1x10^9 M^{-1} min^{-1}) and unlabeled competitors with varying dissociation-rates. What becomes apparent is that despite the variation in the unlabeled compound off-rate (0.01- 100 min^{-1}) the tracer association curves in the presence of the compounds with a k_{off} > 0.01 become bunched to the point they become practically indistinguishable. Figure 5C was obtained under identical conditions apart from a 30 sec delay in start time, representative of off-line addition. The increased start time has little effect on the ability to discriminate between the kinetic off-rates of these compounds primarily as the tracer itself is slow to reach equilibrium with the receptor.

Downloaded from molpharm.aspetjournals.org at ASPET Journals on April 19, 2024

Molecular Pharmacology Fast Forward. Published on July 10, 2019 as DOI: 10.1124/mol.119.116764
This article has not been copyedited and formatted. The final version may differ from this version.

Figure 5B shows competition between a fixed concentration (3x K_d) of a rapidly dissociating tracer (k_{off} of 10 min^{-1}, k_{on} of $3x10^7$ M^{-1} min^{-1}) and unlabeled competitors with varying dissociation-rates (0.01- 100 min^{-1}), and demonstrates how it is possible to accurately determine the dissociation-rates of the more rapidly dissociating competitors using the injection protocol (k_{off} range 0.01–10 min^{-1}, assay start time 1 sec). Figure 5D was obtained under identical conditions apart from a 30 sec delay in start time representative of off-line addition. This time the increased start time has a major effect on the ability of this tracer to discriminate between the kinetic off-rates of these compounds primarily as the tracer itself very rapidly reaches equilibrium with the receptor. Interestingly this loss of early time points in the case of an unlabeled competitor with a k_{off} of 10 min^{-1} results in an apparent underestimation of the k_{off} of the unlabeled competitor as demonstrated by the apparent tracer 'overshoot'. This highlights the key importance of the early time points for accurate competitor characterization.

In line with previous kinetic studies (Klein-Herenbrink et al., 2016) the k_{off} of unlabeled compounds was poorly estimated when the tracer k_{off} is substantially slower than that of the unlabeled ligand. Increasing the k_{off} of the tracer from 0.1 to 10 vastly improved the precision with which the values of k_{on} and k_{off} were estimated for the more rapidly dissociating compounds (as illustrated in Supplemental Tables 2-5). In contrast k_{on} had no impact on the accuracy of the parameter estimate reflective of the fact that changes in k_{on} are completely compensated for by changes in the ligand concentration (data not shown) i.e. no change in k_{obs}.

Effect of tracer concentration on kinetic determination

The effect of tracer concentration on the accuracy of kinetic determinations was explored in further series of Monte Carlo simulations. Tracer concentration was both lowered to 1x K_d and increased to 10 and 30x K_d. We chose to highlight a tracer with

Downloaded from molpharm.aspetjournals.org at ASPET Journals on April 19, 2024

Molecular Pharmacology Fast Forward. Published on July 10, 2019 as DOI: 10.1124/mol.119.116764
This article has not been copyedited and formatted. The final version may differ from this version.

kinetic properties commonly encountered in drug-receptor screening campaigns; high affinity (1nM), fast on $1x10^8$ M^{-1} min^{-1} and slow off $0.1min^{-1}$. The results obtained with this tracer in competition with compounds with kinetic off-rates ranging from 100 to 0.01 min^{-1} following an on-line addition protocol are shown in Figure 6.

Simulations varying concentration following an on-line addition protocol were also performed for tracers with off-rates of 10, 1 and 0.01 as shown in Supplemental Figures 1, 2 and 3. k_{obs} $t_{1/2}$ values ($0.693/k_{obs}$) for the tracers with dissociation rates of 10, 1, 0.1, and 0.01 min^{-1} were 1.1 sec, 10.4 sec, 1.7 min and 17.3 min respectively at tracer concentrations 3x their respective K_d.

As a generality an increase in ligand concentration was associated with an improvement in both the accuracy of kinetic determinations but also the number of fits deemed unambiguous and in some cases effectively rescued the ability of a tracer to determine the kinetics of a more rapidly dissociating competitor. For example a competitor with an off-rate of 10 min^{-1} competing with a tracer with an off rate of $0.1min^{-1}$ could be readily resolved when the tracer concentration was increased from 3x K_d (Figure 6B) to 30x K_d (Figure 6D). k_{obs} $t_{1/2}$ values for a tracer with a dissociation rate of 0.1 min^{-1} ranged from 3.5 to 0.2 min, at concentrations of tracer, 1 to 30x K_d respectively. Data for a competitor with an off-rate of 10 min^{-1} competing with different concentrations of tracers with off-rates ranging from 0.01-10 min^{-1} are summarized in Figure 7.

Similarly the effect of tracer concentration was explored following an off-line addition protocol with the data summarized in Supplemental Figures 4 to 7. In the case of a tracer with an off-rate of 0.1 min^{-1}, increasing tracer concentration with the offline method did not improve the goodness of fit when quantifying competitors with off-rates in the region of 10 min^{-1} but tuning this particular experimental variable may still offer

Downloaded from molpharm.aspetjournals.org at ASPET Journals on April 19, 2024

Molecular Pharmacology Fast Forward. Published on July 10, 2019 as DOI: 10.1124/mol.119.116764
This article has not been copyedited and formatted. The final version may differ from this version.

some benefit to researchers without access to detection instruments with injectors, reducing the overall error associated with kinetic determinations.

Fragment screening using competition-kinetic association binding assays

Monte-Carlo simulations were performed to recreate the competition profile expected with low affinity fragments (31 in total with K_d values ranging from 1 μM to 1000 μM). These competitor fragments with varied kinetic parameters (k_{off} ranging from 3 to 200 min^{-1} and k_{on} from 3 $x10^6$ to 2 $x10^5$ M^{-1} min^{-1}) were simulated in competition with a fixed concentration (3x K_d) of a rapidly dissociating tracer (k_{off} of 10min^{-1}, k_{on} of 3$x10^7$ M^{-1} min^{-1}) . Supplemental Figure 8A shows the expected inhibition of tracer binding caused by a low affinity competitor, fragment 25 (affinity of 0.25 mM, k_{off} of 87.1 min^{-1}, k_{on} of 5 $x10^5$ M^{-1} min-1) tested at two concentrations, 10 and 100 μM. Using a start time of 1 sec and a read frequency of 5 sec it was possible to estimate the affinity of such fragments with a high degree of accuracy as shown by the correlation of input K_d with output K_d (see Supplemental Figure 8B). In contrast as the k_{off} of the fragment increases then the degree of error associated with the estimation of k_{off} and k_{on} is increased, (as judged by the increase in the overall standard deviation associated with the mean) however the overall correlation of input and output kinetic parameters remains extremely good, see Supplemental Figure 8C and D. In all cases using this 2-point method the number of ambiguous fits was below 5%. Interestingly this analysis demonstrates that the affinity of the fragments is estimated with a much higher degree of accuracy than the individual kinetic measurements, demonstrating the overriding influence of the final equilibrium position on kinetic parameter estimation. A similar analysis was performed using single concentrations of compound (10 or 100 μM) and clearly demonstrates the benefit of the 2-point approach with the errors associated with each estimate being larger and the number of ambiguous fits increasing proportionally (See Supplemental Figure 9A-F). Details on how to perform a Monte Carlo analysis and an example Monte Carlo Prism file

Downloaded from molpharm.aspetjournals.org at ASPET Journals on April 19, 2024

Molecular Pharmacology Fast Forward. Published on July 10, 2019 as DOI: 10.1124/mol.119.116764
This article has not been copyedited and formatted. The final version may differ from this version.

can be found in the Supplemental Methods, see 'How to conduct a Monte Carlo Analysis in GraphPad Prism'.

Downloaded from molpharm.aspetjournals.org at ASPET Journals on April 19, 2024

Molecular Pharmacology Fast Forward. Published on July 10, 2019 as DOI: 10.1124/mol.119.116764
This article has not been copyedited and formatted. The final version may differ from this version.

Experimental validation of the Monte Carlo simulation approach

In order to validate the findings of these Monte Carlo simulations exploring the effect of tracer characteristics on kinetic determinations using the Motulsky-Mahan approach we undertook an experimental study designed to explore the limits of a previously well characterized system, the dopamine D2L receptor using a TR-FRET-based system. In this study we chose to focus on a small number of compounds with diverse kinetics and employ the BMG pherastar FS (plate reader) injectors in order to make an assessment of tracer binding at the very earliest time points.

Determining the kinetic of D_2R fluorescent tracers

Representative kinetic association curves for PPHT-red and spiperone-d2 using a start time of ~1 sec and a read frequency of 5 sec are shown in Figure 8A and C respectively. The kinetic parameters determined from these plots are presented in Table 2. PPHT-red dissociated rapidly from the dopamine D_2R with a $t_{1/2}$ of 2.2 min ($0.693/k_{off}$) whereas spiperone-d2 dissociated more slowly ($t_{1/2}$ of 8.7 min). The removal of data points to reflect off-line addition (i.e. the first ~30 sec) or increasing read frequencies (10 to 60 sec) had little influence on the determination of the kinetic parameters of these two fluorescent tracers reflective of the fact that they are not so rapidly dissociating that the early time points are critical for an accurate estimation of their kinetic parameters. Figure 8B and D show the expected linear relationship between PPHT-red and spiperone-d2 concentration and the observed rate of association (or k_{obs}) and suggest that the Laws of Mass Action are observed.

Effect of tracer kinetics on dopamine D_2R ligand kinetic determinations

To experimentally test the effect of tracer kinetics on k_{off} estimates of unlabeled ligands, competition association experiments were performed for 5 dopamine D2 ligands; chlorpromazine, ropinerole, pergolide, domperidone and butaclamol (Figure

Downloaded from molpharm.aspetjournals.org at ASPET Journals on April 19, 2024

Molecular Pharmacology Fast Forward. Published on July 10, 2019 as DOI: 10.1124/mol.119.116764
This article has not been copyedited and formatted. The final version may differ from this version.

9). The associated errors and therefore the accuracy of kinetic determinations for rapidly dissociating compounds is highly dependent on the kinetic properties of the tracer employed to measure them. In contrast the error associated with more slowly dissociating compounds is largely comparable and seemingly independent of the tracers kinetic properties. This is illustrated in Figure 9A and Figure 9B and shows that the error associated with kinetic determinations made with the more slowly dissociating tracer spiperone-d2 is in general much larger than for the more rapidly dissociating tracer PPHT-red. This is evident from the spread of k_{off} values on the x axis (spiperone-d2) being wider than the spread of the k_{off} values on the y axis (PPHT-red). The errors associated with kinetic determinations of rapidly dissociating compounds following off-line addition of PPHT-red (Figure 9A) is little changed compared to on-line addition (Figure 9B), however there was a tendency for the error to increase for the more slowly dissociating compounds, this situation is replicated for spiperone-d2, (see Figure 9A and Figure 9B) and potentially represents the imprecise fitting of the tracer 'overshoot'.

Downloaded from molpharm.aspetjournals.org at ASPET Journals on April 19, 2024

Molecular Pharmacology Fast Forward. Published on July 10, 2019 as DOI: 10.1124/mol.119.116764
This article has not been copyedited and formatted. The final version may differ from this version.

Discussion

The growing awareness of the importance of optimising drug-binding kinetics has led to a rapid increase in the development and utilisation of assay systems capable of measuring the kinetics of unlabelled compounds. A popular format for investigating membrane-bound targets is the competition association binding assay, first described by Aranyi (1980), then popularized by Motulsky and Mahan (1984) and used extensively to characterise many different receptor systems (Gillard et al., 2002; Dowling & Charlton, 2006; Sullivan et al., 2006; Fleck et al., 2012; Sykes et al., 2014; Riddy et al., 2015; Nederpelt et al., 2016; Guo et al., 2017; Bouzo-Lorenzo et al., 2019). A key observation during this time has been that the accuracy of estimating kinetic parameters of rapidly dissociating molecules is poorer when using a slowly dissociating ligand as the tracer (Sykes et al., 2012; Klein-Herenbrink et al., 2016; Bosma et al., 2019).

The purpose of the current study was to explore the effect of tracer kinetics on our ability to accurately estimate the kinetics of unlabelled compounds using the competition-association binding method. In particular we were interested to test the limits of this model system in terms of its ability to assess the binding of very rapidly dissociating compounds likely to be representative of compounds identified in a screening campaign. In practical terms we were also keen to investigate the importance of read-frequency to assist with experimental design. To our knowledge, the current study is the first to fully explore these elements and provide clear guidance for the use of this assay format at all stages of the drug discovery process.

As shown in Figure 1 and Supplemental Tables 1, it was generally possible to derive accurate estimates (< 2-fold difference) of the tracer kinetic parameters using the

Downloaded from molpharm.aspetjournals.org at ASPET Journals on April 19, 2024

Molecular Pharmacology Fast Forward. Published on July 10, 2019 as DOI: 10.1124/mol.119.116764
This article has not been copyedited and formatted. The final version may differ from this version.

global association Equation 1 for simulated data sets. For the more rapidly dissociating tracers the key to obtaining more accurate kinetic parameters was to reduce the assay start-time and the read frequency. Our ability to control these parameters is largely instrument (reader)-dependent. For example, assay start-time is dependent upon the ability to inject sample whilst simultaneously reading from the same well. In addition, assay sensitivity determines the required sample acquisition time, which restricts minimal read frequency. Consequently the option to vary these parameters can be considered as critical factors in the process of determining unlabeled compound kinetics. This is readily illustrated in a comparison of Figure 1B and 1D. Provided an initial start time of 1 sec was used (representative of on-line injection) it was possible to accurately determine the kinetics of all model tracers with less than 10% variation around the mean. In contrast, employing a start time of 30 sec prevented accurate kinetic determinations for the most rapidly dissociating tracer even when the read frequency was restricted to 1 sec (Figure 2C and 2D), demonstrating the importance of on-line injection.

The situation with the Motulsky-Mahan Equation 2 for the estimation of unlabeled compound kinetics was a little more complicated. Although it was possible to derive accurate rate constant estimates for the majority of conditions, there were some combinations that failed to return reproducible estimates (Supplemental Tables 2–5). In general employing a tracer concentration at 3x its K_d it was not possible to reliably estimate k_{on} and k_{off} where the dissociation of the tracer was (≥ 10-fold) slower than the unlabeled competitor. For example, the accurate estimation of the rate constants of a rapidly dissociating ligand with k_{off} of 100 min^{-1} requires a tracer that is also rapidly dissociating, i.e. in the range of 10 min^{-1}. The initial read time was also critically important to determine the kinetics of unlabeled compounds. Where the simulations

Downloaded from molpharm.aspetjournals.org at ASPET Journals on April 19, 2024

Molecular Pharmacology Fast Forward. Published on July 10, 2019 as DOI: 10.1124/mol.119.116764
This article has not been copyedited and formatted. The final version may differ from this version.

were started from 1 sec, mimicking an on-line injection protocol, the kinetic parameters of unlabeled compounds were generally accurately estimated. In contrast, when measurements were started (sampled) 30 sec after the beginning of the experiment, mimicking off-line addition, the estimates were poorer, particularly for rapidly dissociating ligands. This highlights the importance of early time points measured before equilibrium is established. This problem is exacerbated as read frequency is increased since definition on the tracer association curves are lost. In contrast a short read frequency is associated with an increase in the number of data points, which is useful from an accuracy perspective (as illustrated by reduced % CV values see Supplemental Tables 2). However short read frequency will have a negative impact on throughput, which is an important consideration especially when profiling 100-1000s of compounds during screening.

To date, SPR has been the main method for measuring kinetics of fragments at receptors however this technique is traditionally limited to artificially stabilized receptors (Shepherd et al., 2014). Thus the competitive binding model presented is an attractive alternative to SPR and should theoretically allow the investigator to reveal the kinetics of low affinity fragments with off-rates in the order of 10 min^{-1} should an appropriate tracer be identified (see Supplemental Figure 8 and 9).

In a previous paper exploring dopamine D_2R agonist kinetics we were able to demonstrate the importance of tracer properties on our ability to determine the kinetics of rapidly dissociating ligands (Klein-Herenbrink et al., 2016). In the current study we have further explored this observation employing an on-line injection protocol. In the previous study [^{3}H]-spiperone was unable to accurately determine the kinetics of the most rapidly dissociating D_2R agonists. This is likely the result of a number of factors

Downloaded from molpharm.aspetjournals.org at ASPET Journals on April 19, 2024

Molecular Pharmacology Fast Forward. Published on July 10, 2019 as DOI: 10.1124/mol.119.116764
This article has not been copyedited and formatted. The final version may differ from this version.

including; its slower measured off-rate from the dopamine D_2R, the relatively lower concentration of spiperone employed in the competition binding experiments i.e. 3x [^{3}H]-spiperone (versus 10x K_d spiperone-d2 in the current study) and the decision to employ an initial start time of 30 sec.

As predicted by the Monte Carlo simulations PPHT-red a tracer with a relatively fast off-rate was more reliable at determining the kinetic off-rates of the most rapidly dissociating antagonists and agonists tested in this study. In contrast spiperone-d2 (10x K_d) although adequate at determining the off-rates of the more slowly dissociating compounds was prone to more variation in its determination of the off-rates of the most rapidly dissociating compounds. Importantly what this study clearly demonstrates is that a failure to demonstrate an accurate fit of the kinetics of a rapidly dissociating compound (10min^{-1}) can be overcome through the use of higher concentrations of a slowly dissociating tracer and the decision to employ a shortening start and read frequency (see Figure 7). As one might predict the use of higher tracer concentrations could not compensate for an increase in the assay start time, representative of an off-line addition protocol (see Supplemental Figure 6).

What is apparent from this study is that for a competitive binding approach to be utilized throughout the different phases of the drug discovery process then the kinetics of the tracer need to be tailored to the appropriate properties of the unlabeled compounds. For low affinity compounds, such as initial hits or fragments, a rapidly equilibrating tracer is required to accurately determine rate constants. This is fortunate as it opens the possibility to fluorescently label an early hit to serve as a tracer to discover and characterize new fragments. In this format, it would be necessary to read relatively small numbers of wells in rapid succession (i.e. a shortened read frequency)

Downloaded from molpharm.aspetjournals.org at ASPET Journals on April 19, 2024

Molecular Pharmacology Fast Forward. Published on July 10, 2019 as DOI: 10.1124/mol.119.116764
This article has not been copyedited and formatted. The final version may differ from this version.

using a repeat on-line injection protocol in order to resolve the kinetics of the most rapidly dissociating fragments. Also apparent is that as we move further along the drug discovery pathway towards lead optimization, it may be beneficial to label a more slowly dissociating compound, allowing the off-line addition of tissue and increased sample throughput through extended read frequency. The decision to employ shorter read times is ultimately a compromise between throughput and the accurate resolution of kinetic parameters.

In summary we have improved the current understanding of the Motulsky-Mahan approach providing clear guidelines on the use of tracers to measure the kinetics of unlabeled competitors. Based on the detailed Monte Carlo approach presented we propose the following four factors as being important considerations when formulating competition association binding experiments:

1. Tracer kinetics; fast off tracer in the region of 0.1-1 min^{-1} appear to be critical for the determination of unlabeled compounds with rapid off kinetics in the region of 1-10 min^{-1}.
2. Tracer concentration, appears to play a crucial role in our ability to determine the kinetics of binding with greater accuracy and can even increase the range of compounds off rates which we can reliably measure.
3. Online Injection capability, proved critical to determine the off-rates of compounds and tracers which dissociate with off-rates in the region of 10 min^{-1}.
4. Rapid read frequency, dramatically improves the goodness of fit and reduces experimental variability and like online injection can rescue our ability to resolve the kinetics of the most rapidly dissociating compounds.

Downloaded from molpharm.aspetjournals.org at ASPET Journals on April 19, 2024

Molecular Pharmacology Fast Forward. Published on July 10, 2019 as DOI: 10.1124/mol.119.116764
This article has not been copyedited and formatted. The final version may differ from this version.

Experimental conditions can also be manipulated to enhance our ability to measure the kinetics of a particular tracer or competitor ligand. For example reducing assay temperature will slow the off-rates of both the tracer and the competitor compound, a ploy that has been successfully used in the past to enable the determination of off-rates of more rapidly dissociating compounds using the off-line addition protocol (Contreras et al., 1986, Guo et al., 2012). It should be noted, however, that kinetic parameters calculated at lower temperatures are unlikely to reflect those in a physiological system, significantly limiting their translational utility.

Overall, the findings in this paper highlight the importance of considering tracer kinetics and assay read start and read frequency when developing competition association assays. Notably, these simulations suggest that under the right conditions, the kinetic parameters of very low affinity (mM) competitors can be measured, providing the opportunity for kinetic fragment-based receptor screens and the development of SKRs at all phases of the drug discovery cascade.

Acknowledgements

We would like to thank Dr Nick Holliday for his helpful suggestions during the preparation of this manuscript. In addition we would like to thank BMG Labtech Ltd. for their expert technical assistance and for personal sponsorship of David Sykes.

Authorship Contributions

Participated in research design: Sykes and Charlton

Conducted experiments: Sykes

Contributed new reagents or analytic tools: Jain

Downloaded from molpharm.aspetjournals.org at ASPET Journals on April 19, 2024

Molecular Pharmacology Fast Forward. Published on July 10, 2019 as DOI: 10.1124/mol.119.116764
This article has not been copyedited and formatted. The final version may differ from this version.

Performed data analysis: Sykes and Jain

Wrote or contributed to the writing of the manuscript: Sykes and Charlton

Downloaded from molpharm.aspetjournals.org at ASPET Journals on April 19, 2024

Molecular Pharmacology Fast Forward. Published on July 10, 2019 as DOI: 10.1124/mol.119.116764
This article has not been copyedited and formatted. The final version may differ from this version.

References

Arányi P (1980). Kinetics of the hormone-receptor interaction. Competition experiments with slowly equilibrating ligands. Biochim Biophys Acta. 628(2):220-7.

Bouzo-Lorenzo M, Stoddart LA, Xia L, IJzerman AP, Heitman LH, Briddon SJ, Hill SJ (2019). A live cell NanoBRET binding assay allows the study of ligand-binding kinetics to the adenosine A3 receptor. Purinergic Signal. Mar 27. doi: 10.1007/s11302-019-09650-9. [Epub ahead of print]

Bosma R, Stoddart LA, Georgi V, Bouzo-Lorenzo M, Bushby N, Inkoom L, Waring MJ, Briddon SJ, Vischer HF, Sheppard RJ, Fernández-Montalván A, Hill SJ, Leurs R (2019). Probe dependency in the determination of ligand binding kinetics at a prototypical G protein-coupled receptor. Sci Rep. 9(1):7906.

Contreras ML, Wolfe BB and Molinoff P B (1986). Kinetic analysis of the interactions of agonists and antagonists with beta adrenergic receptors. Journal of Pharmacology and Experimental Therapeutics, 239 (1) 136-143.

Carter CM, Leighton-Davies JR, Charlton SJ (2007). Miniaturized receptor binding assays: complications arising from ligand depletion. *J Biomol Screen* 12: 255-266.

Copeland RA (2016). The drug-target residence time model: a 10-year retrospective. *Nat Rev Drug Discov.* 15(2):87-95.

Christopoulos A (2001). From 'captive' agonism to insurmountable antagonism: demonstrating the power of analytical pharmacology. *Clin Exp Pharmacol Physiol.* 28(3):223-9.

Downloaded from molpharm.aspetjournals.org at ASPET Journals on April 19, 2024

Molecular Pharmacology Fast Forward. Published on July 10, 2019 as DOI: 10.1124/mol.119.116764
This article has not been copyedited and formatted. The final version may differ from this version.

Dowling MR, Charlton SJ (2006). Quantifying the association and dissociation-rates of unlabelled antagonists at the muscarinic M3 receptor. *Br J Pharmacol.* 148(7):927-37.

Emami-Nemini A, Roux T, Leblay M, Bourrier E, Lamarque L, Trinquet E, Lohse MJ (2013). Time-resolved fluorescence ligand binding for G protein-coupled receptors. *Nat Protoc.* 8(7):1307-20.

Fleck BA, Hoare SR, Pick RR, Bradbury MJ, Grigoriadis DE (2012). Binding kinetics redefine the antagonist pharmacology of the corticotropin-releasing factor type 1 receptor. J Pharmacol Exp Ther. 341(2):518-31.

Georgi V, Schiele F, Berger BT, Steffen A, Marin Zapata PA, Briem H, Menz S, Preusse C, Vasta JD, Robers MB, Brands M, Knapp S Fernández-Montalván A (2018). Binding Kinetics Survey of the Drugged Kinome. J Am Chem Soc. 140(46):15774-15782.

Gillard M, Van Der Perren C, Moguilevsky N, Massingham R, Chatelain P (2002). Binding characteristics of cetirizine and levocetirizine to human H(1) histamine receptors: contribution of Lys(191) and Thr(194). Mol Pharmacol. 61(2):391-9.

Guo D, Mulder-Krieger T, IJzerman AP, Heitman LH (2012). Functional efficacy of adenosine A_2A receptor agonists is positively correlated to their receptor residence time. Br J Pharmacol. 166(6):1846-59.

Guo D, Heitman LH, IJzerman AP (2017). Kinetic Aspects of the Interaction between Ligand and G Protein-Coupled Receptor: The Case of the Adenosine Receptors. Chem Rev. 2017 117(1):38-66.

Downloaded from molpharm.aspetjournals.org at ASPET Journals on April 19, 2024

Molecular Pharmacology Fast Forward. Published on July 10, 2019 as DOI: 10.1124/mol.119.116764
This article has not been copyedited and formatted. The final version may differ from this version.

Klein Herenbrink C, Sykes DA, Donthamsetti P, Canals M, Coudrat T, Shonberg J, Scammells PJ, Capuano B, Sexton PM, Charlton SJ, Javitch JA, Christopoulos A, Lane JR. The role of kinetic context in apparent biased agonism at GPCRs. *Nat Commun.* 2016; 7: 10842.

Martella A, Sijben H, Rufer AC, Grether U, Fingerle J, Ullmer C, Hartung T, IJzerman AP, van der Stelt M, Heitman LH (2017). A Novel Selective Inverse Agonist of the CB2 Receptor as a Radiolabeled Tool Compound for Kinetic Binding Studies. Mol Pharmacol. 92(4):389-400.

Motulsky HJ, Mahan LC (1984). The kinetics of competitive radioligand binding predicted by the law of mass action. *Mol Pharmacol* **25**: 1-9.

Motulsky HJ (n.d.). GraphPad Curve Fitting Guide. Accessed June 15th 2019. http://www.graphpad.com/guides/prism/7/curve-fitting/index.htm.

Nederpelt I, Georgi V, Schiele F, Nowak-Reppel K, Fernández-Montalván AE, IJzerman AP, Heitman LH (2016). Characterization of 12 GnRH peptide agonists - a kinetic perspective. Br J Pharmacol. 173(1):128-41.

Riddy DM, Valant C, Rueda P, Charman WN, Sexton PM, Summers RJ, Christopoulos A, Langmead CJ (2015). Label-Free Kinetics: Exploiting Functional Hemi-Equilibrium to Derive Rate Constants for Muscarinic Receptor Antagonists. Mol Pharmacol. 88(4):779-90.

Schiele F, Ayaz P, Fernández-Montalván A (2014). A universal homogeneous assay for high-throughput determination of binding kinetics. *Anal Biochem.* 468C:42-49.

Downloaded from molpharm.aspetjournals.org at ASPET Journals on April 19, 2024

Molecular Pharmacology Fast Forward. Published on July 10, 2019 as DOI: 10.1124/mol.119.116764
This article has not been copyedited and formatted. The final version may differ from this version.

Schmidtke P, Luque FJ, Murray JB, Barril X (2011). Shielded hydrogen bonds as structural determinants of binding kinetics: application in drug design. *J Am Chem Soc.* 133(46):18903-10.

Shepherd CA, Hopkins AL, Navratilova I (2014). Fragment screening by SPR and advanced application to GPCRs. *Prog Biophys Mol Biol.* 116(2-3):113-23.

Slack RJ, Russell LJ, Hall DA, Luttmann MA, Ford AJ, Saunders KA, Hodgson ST, Connor HE, Browning C, Clark KL (2011). Pharmacological characterization of GSK1004723, a novel, long-acting antagonist at histamine H(1) and H(3) receptors. Br J Pharmacol. 164(6):1627-41.

Stoddart LA, Johnstone EKM, Wheal AJ, Goulding J, Robers MB, Machleidt T, Wood KV, Hill SJ, Pfleger KDG (2015). Application of BRET to monitor ligand binding to GPCRs. Nat Methods. 12(7):661-663.

Stoddart LA, Vernall AJ, Bouzo-Lorenzo M, Bosma R, Kooistra AJ, de Graaf C, Vischer HF, Leurs R, Briddon SJ, Kellam B, Hill SJ (2018). Development of novel fluorescent histamine H1-receptor antagonists to study ligand-binding kinetics in living cells. Sci Rep. 8(1):1572.

Sullivan SK, Hoare SR, Fleck BA, Zhu YF, Heise CE, Struthers RS, Crowe PD (2006). Kinetics of nonpeptide antagonist binding to the human gonadotropin-releasing hormone receptor: Implications for structure-activity relationships and insurmountable antagonism. Biochem Pharmacol. 72(7):838-49.

Downloaded from molpharm.aspetjournals.org at ASPET Journals on April 19, 2024

Molecular Pharmacology Fast Forward. Published on July 10, 2019 as DOI: 10.1124/mol.119.116764
This article has not been copyedited and formatted. The final version may differ from this version.

Sykes DA, Dowling MR, Charlton SJ (2009). Exploring the mechanism of agonist efficacy: a relationship between efficacy and agonist dissociation-rate at the muscarinic M3 receptor. *Mol Pharmacol.* 76(3):543-51.

Sykes DA, Dowling MR, Charlton SJ (2010). Measuring receptor target coverage: a radioligand competition binding protocol for assessing the association and dissociation rates of unlabeled compounds. Curr Protoc Pharmacol. Chapter 9:Unit 9.14.

Sykes DA, Charlton SJ (2012). Slow receptor dissociation is not a key factor in the duration of action of inhaled long-acting β2-adrenoceptor agonists. *Br J Pharmacol.* 165(8):2672-83.

Sykes DA, Parry C, Reilly J, Wright P, Fairhurst RA, Charlton SJ (2014). Observed drug-receptor association-rates are governed by membrane affinity: the importance of establishing "micro-pharmacokinetic/pharmacodynamic relationships" at the β2-adrenoceptor. *Mol Pharmacol* **85**: 608-617.

Sykes DA, Bradley ME, Riddy DM, Willard E, Reilly J, Miah A, Bauer C, Watson SJ, Sandham DA, Dubois G, Charlton SJ (2016). Fevipiprant (QAW039), a Slowly Dissociating CRTh2 Antagonist with the Potential for Improved Clinical Efficacy. *Mol Pharmacol.* 89(5):593-605.

Sykes DA, Moore H, Stott L, Holliday N, Javitch JA, Lane JR, Charlton SJ (2017). Extrapyramidal side effects of antipsychotics are linked to their association kinetics at dopamine D2 receptors.Nat Commun. 2017 Oct 2;8(1):763.

Downloaded from molpharm.aspetjournals.org at ASPET Journals on April 19, 2024

Molecular Pharmacology Fast Forward. Published on July 10, 2019 as DOI: 10.1124/mol.119.116764
This article has not been copyedited and formatted. The final version may differ from this version.

Sykes DA, Lane JR, Szabo M, Capuano B, Javitch JA, Charlton SJ (2018). Reply to 'Antipsychotics with similar association kinetics at dopamine D2 receptors differ in extrapyramidal side-effects'. Nat Commun. 2018 9(1):3568.

Turner RJ, Charlton SJ (2005). Assessing the minimum number of data points required for accurate IC50 determination. *Assay Drug Dev Technol.* 3(5):525-531.

Yu Z, IJzerman AP, Heitman LH (2015). Kv 11.1 (hERG)-induced cardiotoxicity: a molecular insight from a binding kinetics study of prototypical Kv 11.1 (hERG) inhibitors. *Br J Pharmacol.* 172(3):940-55.

Vauquelin G (2016). Impact of target binding kinetics on in vivo drug efficacy: koff , kon and rebinding. *Br J Pharmacol.* 173(15):2319-34.

Xia L, de Vries H, IJzerman AP, Heitman LH (2016). Scintillation proximity assay (SPA) as a new approach to determine a ligand's kinetic profile. A case in point for the adenosine A1 receptor. *Purinergic Signal.* 12(1):115-26.

Downloaded from molpharm.aspetjournals.org at ASPET Journals on April 19, 2024

Molecular Pharmacology Fast Forward. Published on July 10, 2019 as DOI: 10.1124/mol.119.116764
This article has not been copyedited and formatted. The final version may differ from this version.

Legends for Figures

Figure 1. Monte-Carlo simulation results exploring the effect of sample time on the determination of tracer kinetic parameters. **(A)** Association with time (1sec start; 10sec interval) of various concentrations of a very rapidly dissociating tracer with the following kinetic parameters; k_{off} of $10min^{-1}$, k_{on} of $3x10^7$ M^{-1} min^{-1} representative of 200 simulations. In this globally fitted model (see Equation 1) of tracer binding, tracer concentrations [L] are fixed, k_{on} and k_{off} are shared parameters to be determined. **(B)** Effect of read frequency on the output k_{off} of a series of experimental tracers (L) with varied kinetics, absolute values are the average of 200 simulations. In this instance tracer simulations were performed with an initial start time of 1sec representative of injection of receptor to a reaction containing only tracer. Blue open symbols represent conditions which returned >90% reliable fits. Red open symbols represent conditions which returned <90% reliable fits. **(C)** Association with time (30sec start; 10sec interval) of various concentrations of a very rapidly dissociating tracer with the following kinetic parameters; k_{off} of $10min^{-1}$, k_{on} of $3x10^7$ M^{-1} min^{-1}, representative of 200 simulations. **(D)** Effect of read frequency on the output k_{off} of a series of experimental tracers (L) with varied kinetics. In this instance tracer simulations were performed with an initial start time of 30 sec representative of off-line addition of receptor to a reaction containing only tracer, absolute values are the average of 200 simulations. Line-circles indicate the position of example simulations **(A)** and **(C)** and represent a small fraction of the total number of simulations shown in the plots **(B)** and **(D)**.

Downloaded from molpharm.aspetjournals.org at ASPET Journals on April 19, 2024

Molecular Pharmacology Fast Forward. Published on July 10, 2019 as DOI: 10.1124/mol.119.116764
This article has not been copyedited and formatted. The final version may differ from this version.

Figure 2. Monte-Carlo simulation results exploring the effect of competitor off-rate on the competition profile observed with a rapidly dissociating tracer. **(A)** Competition between a fixed concentration (3x K_d) of a very rapidly dissociating tracer; k_{off} of 10 min^{-1}, k_{on} of $3x10^7$ M^{-1} min^{-1} and a rapidly dissociating competitor with the following kinetic parameters; k_{off} of $10min^{-1}$, k_{on} of $1x10^6$ M^{-1} min^{-1}, data shown are representative of 200 simulations. **(B)** Competition between a fixed concentration (3x K_d) of a very rapidly dissociating tracer and a slowly dissociating competitor with the following kinetic parameters; k_{off} of $1min^{-1}$, k_{on} of $1x10^7$ M^{-1} min^{-1}, data shown are representative of 200 simulations. In all cases tracer and competitor binding simulations were performed with an initial start time of 1sec (representative of injection of receptor to a reaction containing tracer) and a read frequency of 10sec.

Downloaded from molpharm.aspetjournals.org at ASPET Journals on April 19, 2024

Molecular Pharmacology Fast Forward. Published on July 10, 2019 as DOI: 10.1124/mol.119.116764
This article has not been copyedited and formatted. The final version may differ from this version.

Figure 3. Monte-Carlo simulation results exploring the effect of sample time and tracer kinetics on the accurate determination of competitor k_{off} representative of an off-line addition protocol. Individual figures show the effect of assay read frequency time on the measured k_{off} of unlabelled competitor compounds with varied kinetics in competition with a fixed concentration (3x K_d) of; **(A)** a very rapidly dissociating tracer with the following kinetic parameters; k_{off} of $10min^{-1}$, k_{on} of $3x10^7$ M^{-1} min^{-1}, (**B)** a rapidly dissociating tracer with the following kinetic parameters; k_{off} of $1min^{-1}$, k_{on} of $1x10^7$ M^{-1} min^{-1}, (**C)** a slowly dissociating tracer with kinetic parameters; k_{off} of $0.1min^{-1}$, k_{on} of $1x10^8$ M^{-1} min^{-1}, and (**D)** a very slowly dissociating tracer with kinetic parameters; k_{off} of $0.01min^{-1}$, k_{on} of $1x10^9$ M^{-1} min^{-1}. Blue open symbols represent conditions which returned >90% reliable fits. Red open symbols represent conditions which returned <90% reliable fits. In all cases tracer simulations were performed with an initial start time of 30sec representative of off-line addition of receptor to a reaction containing free tracer (L) and unlabelled competitor (I), absolute values are the average of 200 simulations.

Downloaded from molpharm.aspetjournals.org at ASPET Journals on April 19, 2024

Molecular Pharmacology Fast Forward. Published on July 10, 2019 as DOI: 10.1124/mol.119.116764
This article has not been copyedited and formatted. The final version may differ from this version.

Figure 4. Monte-Carlo simulation results exploring the effect of tracer kinetics and sample time on the accurate determination of competitor k_{off} representative of an injection protocol. Individual figures show the effect of assay read frequency on the measured k_{off} of unlabelled competitor compounds with varied kinetics in competition with a fixed concentration (3x K_d) of; **(A)** a very rapidly dissociating tracer with the following kinetic parameters; k_{off} of 10min^{-1}, k_{on} of 3x10^{7} M^{-1} min^{-1}, **(B)** a rapidly dissociating tracer with kinetic parameters; k_{off} of 1min^{-1}, k_{on} of 1x10^{7} M^{-1} min^{-1}, **(C)** a slowly dissociating tracer with kinetic parameters; k_{off} of 0.1 min^{-1}, k_{on} of 1x10^{8} M^{-1} min^{-1}, and **(D)** a very slowly dissociating tracer with kinetic parameters; k_{off} of 0.01min^{-1}, k_{on} of 1x10^{9} M^{-1} min^{-1}. Blue open symbols represent conditions which returned >90% reliable fits. Red open symbols represent conditions which returned <90% reliable fits. In all cases tracer simulations were performed with an initial start time of 1sec representative of injection of receptor to a reaction containing free tracer (L) and unlabelled competitor (I), absolute values are the average of 200 simulations. k_{obs} $t_{1/2}$ values (0.693/k_{obs}) for the tracers with dissociation rates of 10, 1, 0.1, and 0.01 min^{-1} were 1.1 sec, 10.4 sec, 1.7 min and 17.3 min respectively.

Downloaded from molpharm.aspetjournals.org at ASPET Journals on April 19, 2024

Molecular Pharmacology Fast Forward. Published on July 10, 2019 as DOI: 10.1124/mol.119.116764
This article has not been copyedited and formatted. The final version may differ from this version.

Figure 5. Monte-Carlo simulation results reproducing the experimentally observed effect of competitor off-rate on the competition profile observed with a rapidly dissociating tracer and a slowly dissociating tracer at varying start times. **(A)** and **(C)** show competition between a fixed concentration (3x K_d) of a very slowly dissociating tracer with the following kinetic parameters; k_{off} of 0.01min^{-1}, k_{on} of 1x10^{9} M^{-1} min^{-1}, and competitors with varying dissociation-rates. **(B)** and **(D)** show competition between a fixed concentration (3x K_d) of a rapidly dissociating tracer with the following kinetic parameters; k_{off} of 10min^{-1}, k_{on} of 3x10^{7} M^{-1} min^{-1}, and competitors with varying dissociation-rates. In the case of **(A)** and **(B)** tracer and competitor binding simulations were performed with an initial start time of 1sec (representative of on-line injection of receptor to a reaction containing tracer and competitor) whereas **(C)** and **(D)** were performed with a start time of 30 sec (representative of off-line addition of receptor). All simulations have a read frequency of 10 sec. and the data shown are representative of 200 simulations.

Downloaded from molpharm.aspetjournals.org at ASPET Journals on April 19, 2024

Molecular Pharmacology Fast Forward. Published on July 10, 2019 as DOI: 10.1124/mol.119.116764
This article has not been copyedited and formatted. The final version may differ from this version.

Figure 6. Monte-Carlo simulation results exploring the effect of tracer concentration and sample time on the accurate determination of competitor k_{off} representative of an injection protocol. Effect of assay read frequency on measured k_{off} of unlabelled competitor compounds with varied kinetics in competition with different concentrations of a slowly dissociating tracer with kinetic parameters; k_{off} of 0.1min^{-1}, k_{on} of 1x10^{8} M^{-1} min^{-1}. Tracer concentrations were **(A)** 1x K_d, **(B)** 3x K_d, **(C)** 10x K_d and **(D)** 30x K_d. Blue open symbols represent conditions which returned >90% reliable fits. Red open symbols represent conditions which returned <90% reliable fits. In all cases tracer simulations were performed with an initial start time of 1sec representative of injection of receptor to a reaction containing free tracer (L) and unlabelled competitor (I), absolute values are the average of 200 simulations. k_{obs} $t_{1/2}$ values (0.693/k_{obs}) for a tracer with a dissociation rate of 0.1 min^{-1}, with increasing concentration of tracer 1, 3, 10 and 30x K_d were 3.5, 1.7, 0.6 and 0.2 min respectively.

Downloaded from molpharm.aspetjournals.org at ASPET Journals on April 19, 2024

Molecular Pharmacology Fast Forward. Published on July 10, 2019 as DOI: 10.1124/mol.119.116764
This article has not been copyedited and formatted. The final version may differ from this version.

Figure 7. Monte-Carlo simulation results exploring the effect of tracer kinetics, concentration and sample time on the accurate determination of k_{off} of a rapidly dissociating competitor representative of an on-line addition protocol. Effect of tracer concentration (1-30*K_d) and read frequency (1-60 sec) on the measured k_{off} of an unlabelled competitor compound with a k_{off} of 10 min^{-1} in competition with different concentrations of a tracers with varied kinetic k_{off} rates ranging from 0.01 min^{-1},- 10 min^{-1}. Tracer off-rates were **(A)** 0.01 min^{-1}, **(B)** 0.1 min^{-1}, **(C)** 1 $min^{-1}$and **(D)** 10 min^{-1}. Blue open symbols represent conditions which returned >90% reliable fits. Red open symbols represent conditions which returned <90% reliable fits. In all cases tracer simulations were performed with an initial start time of 1sec representative of addition of receptor to a reaction containing free tracer (L) and unlabelled competitor (I), absolute values are the average of 200 simulations.

Downloaded from molpharm.aspetjournals.org at ASPET Journals on April 19, 2024

Molecular Pharmacology Fast Forward. Published on July 10, 2019 as DOI: 10.1124/mol.119.116764
This article has not been copyedited and formatted. The final version may differ from this version.

Figure 8. Determination of PPHT-red and spiperone-d2 kinetic binding parameters. **(A)** Observed association of PPHT-red binding to the human dopamine D_2R. CHO–D_2R cell membranes (2 µg per well) were incubated for 20 min with gentle agitation with increasing concentrations of PPHT-red. Data are presented in singlet form from a representative of 4 experiments. **(B)** Plot of PPHT-red concentration versus k_{obs}. Binding followed a simple Law of Mass Action model, k_{obs} increasing in a linear manner with fluorescent ligand concentration. Data are representative of a total of 4 experiments. **(C)** Observed association of spiperone-d2 binding to the human dopamine D_2R. CHO-D_2R cell membranes (2 µg per well) were incubated for 20 min with gentle agitation with increasing concentrations of spiperone-d2. Data are presented in singlet form from a representative of 4 experiments. **(D)** Plot of spiperone-d2 concentration versus. k_{obs}. Binding followed a simple Law of Mass Action model, k_{obs} increasing in a linear manner with fluorescent ligand concentration. Data are representative of a total of 4 experiments. All binding reactions were performed in the presence of GppNHp (0.1 mM) with nonspecific-binding levels determined by inclusion of haloperidol (10 µM).

Downloaded from molpharm.aspetjournals.org at ASPET Journals on April 19, 2024

Molecular Pharmacology Fast Forward. Published on July 10, 2019 as DOI: 10.1124/mol.119.116764
This article has not been copyedited and formatted. The final version may differ from this version.

Figure 9. Effect of tracer properties and assay configuration on the determination of unlabeled compound kinetic parameters at the human dopamine D_2 receptor. Comparison of unlabelled compound k_{off} values with determined using spiperone-d2 and PPHT-red, **(A)** following an off-line injection protocol with a 5sec interval and **(B)** an on-line addition protocol with a 5sec interval. CHO-D_2R cell membranes (2 µg per well) were incubated for 20 min with gentle agitation with a fixed concentration of PPHT-red or spiperone-d2 and increasing concentrations of competitor. Data are presented as individual estimates from 4 experiments

Downloaded from molpharm.aspetjournals.org at ASPET Journals on April 19, 2024

Molecular Pharmacology Fast Forward. Published on July 10, 2019 as DOI: 10.1124/mol.119.116764
This article has not been copyedited and formatted. The final version may differ from this version.

Tables

Table 1. Equilibrium affinity and kinetic properties of the tracer compounds used to construct Figure 1 to 9 and Supplemental Figures 1 to 7 and typical of the kinetic parameters of compounds discovered at all phases of the drug discovery screening cascade.

Tracer K_D (nM)	Tracer k_{off} (min^{-1})	Tracer k_{on} (M^{-1} min^{-1})	Characteristic of tracer
0.01	0.01	$1x10^9$	Very high affinity candidate, very slow off
1	0.1	$1x10^8$	High affinity candidate, slow off
100	1	$1x10^7$	Lead-like, fast off
300	10	$3x10^7$	Hit-like, very fast off

Downloaded from molpharm.aspetjournals.org at ASPET Journals on April 19, 2024

Molecular Pharmacology Fast Forward. Published on July 10, 2019 as DOI: 10.1124/mol.119.116764
This article has not been copyedited and formatted. The final version may differ from this version.

Table 2. Kinetic binding parameters of the tracers PPHT-red and spiperoine-d2 determined from association binding studies using human dopamine D_{2L} CHO cell membranes. Data are mean s.e.m. from n separate experiments.

Tracer	**Tracer K_D (nM)**	**Tracer k_{off} (min^{-1})**	**Tracer k_{on} (M^{-1} min^{-1})**	**Nº of observations (n)**
PPHT-red	16.9 ± 1.1	0.32 ± 0.02	1.93 ± 0.21 $x10^7$	4
Spiperone-d2	0.62 ± 0.08	0.08 ± 0.01	1.30 ± 0.17 $x10^8$	4

.

Downloaded from molpharm.aspetjournals.org at ASPET Journals on April 19, 2024

Molecular Pharmacology Fast Forward. Published on July 10, 2019 as DOI: 10.1124/mol.119.116764
This article has not been copyedited and formatted. The final version may differ from this version.

Figures

Figure 1

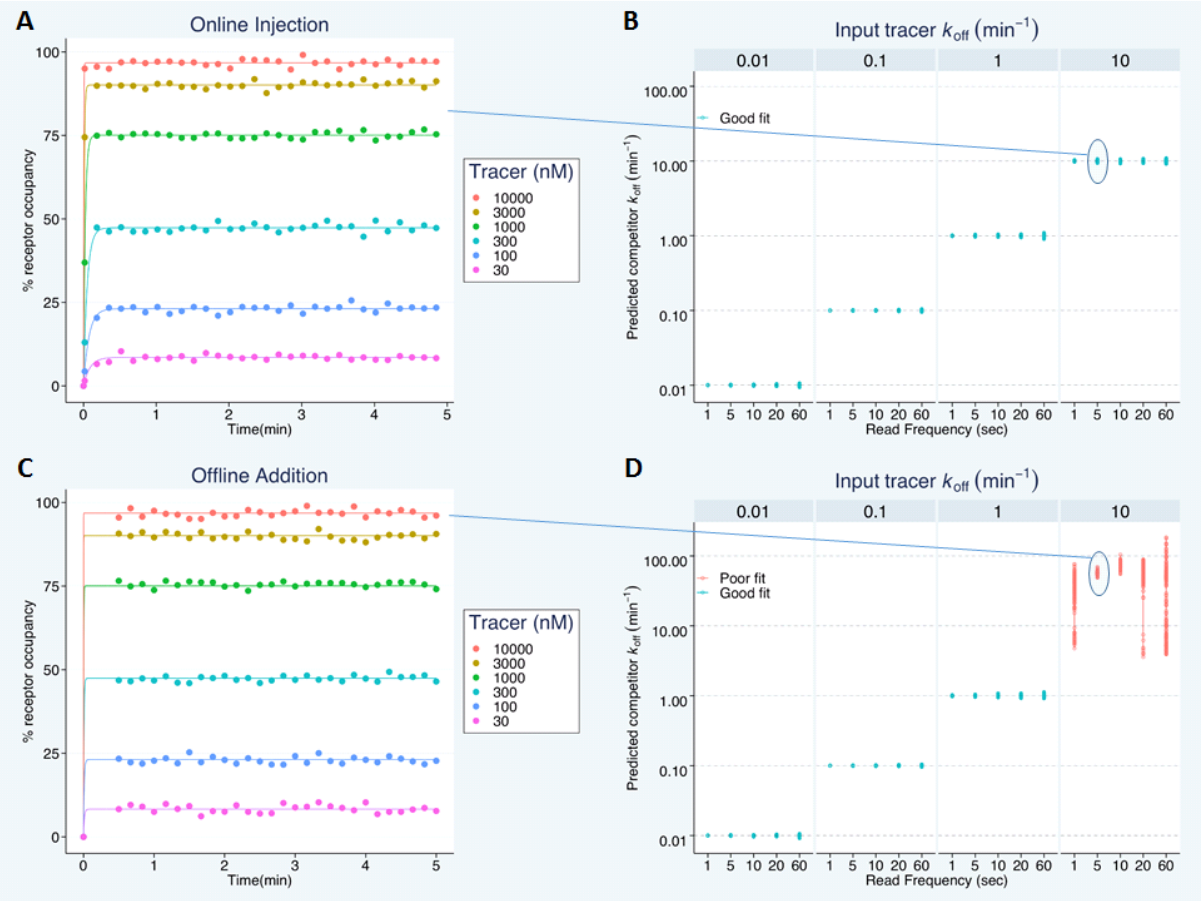

Downloaded from molpharm.aspetjournals.org at ASPET Journals on April 19, 2024

Molecular Pharmacology Fast Forward. Published on July 10, 2019 as DOI: 10.1124/mol.119.116764
This article has not been copyedited and formatted. The final version may differ from this version.

Figure 2

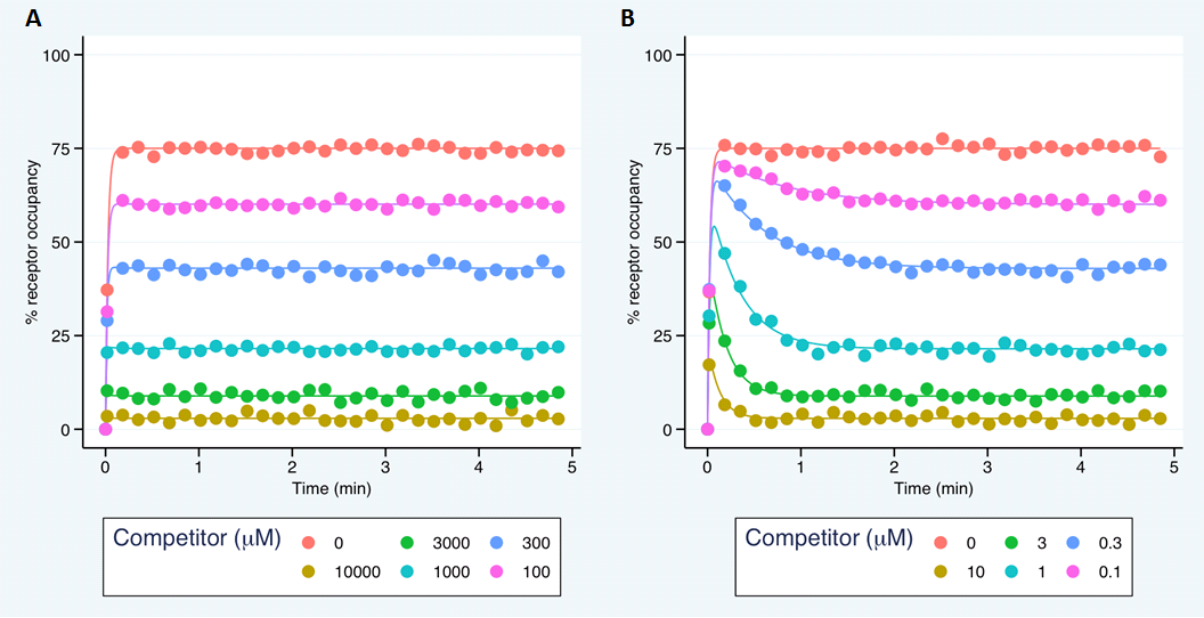

Downloaded from molpharm.aspetjournals.org at ASPET Journals on April 19, 2024

Molecular Pharmacology Fast Forward. Published on July 10, 2019 as DOI: 10.1124/mol.119.116764
This article has not been copyedited and formatted. The final version may differ from this version.

Figure 3

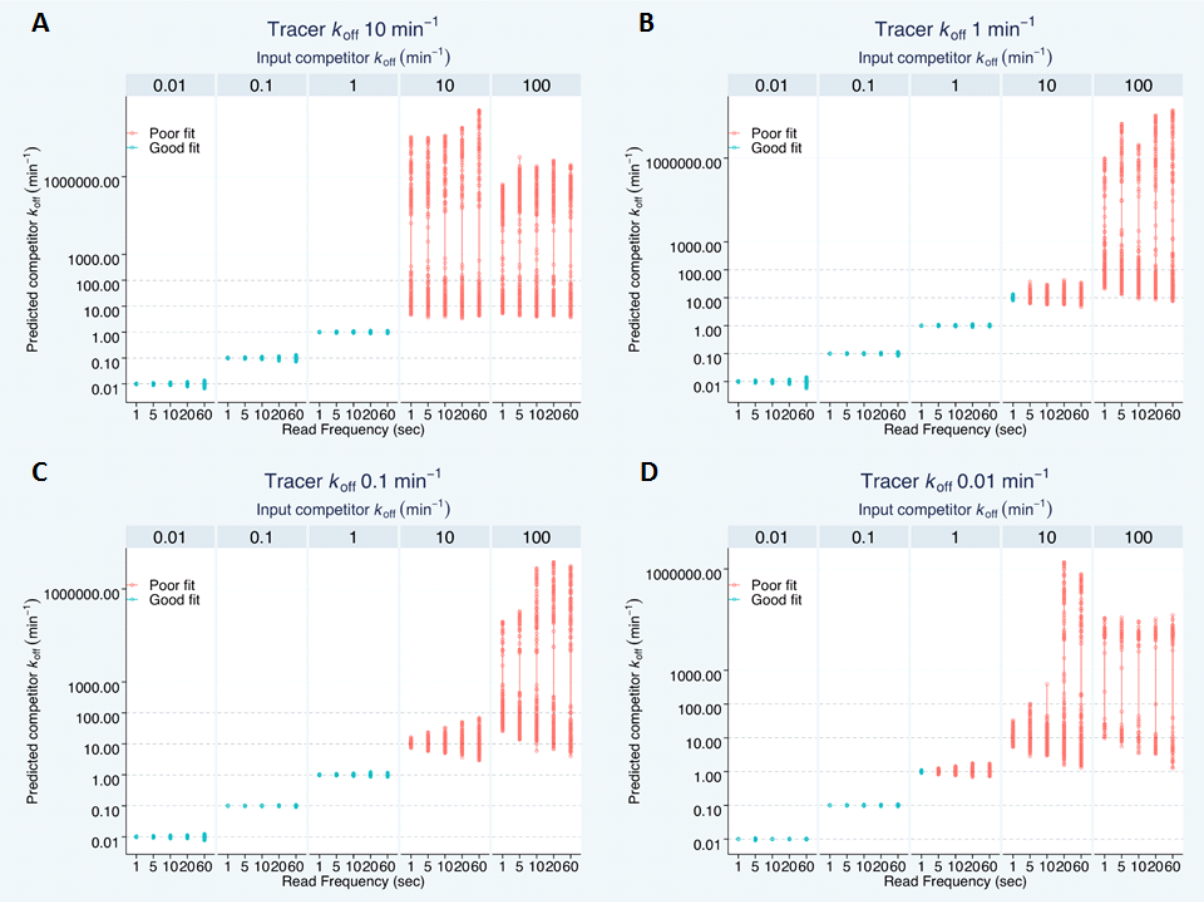

Downloaded from molpharm.aspetjournals.org at ASPET Journals on April 19, 2024

Molecular Pharmacology Fast Forward. Published on July 10, 2019 as DOI: 10.1124/mol.119.116764
This article has not been copyedited and formatted. The final version may differ from this version.

Figure 4

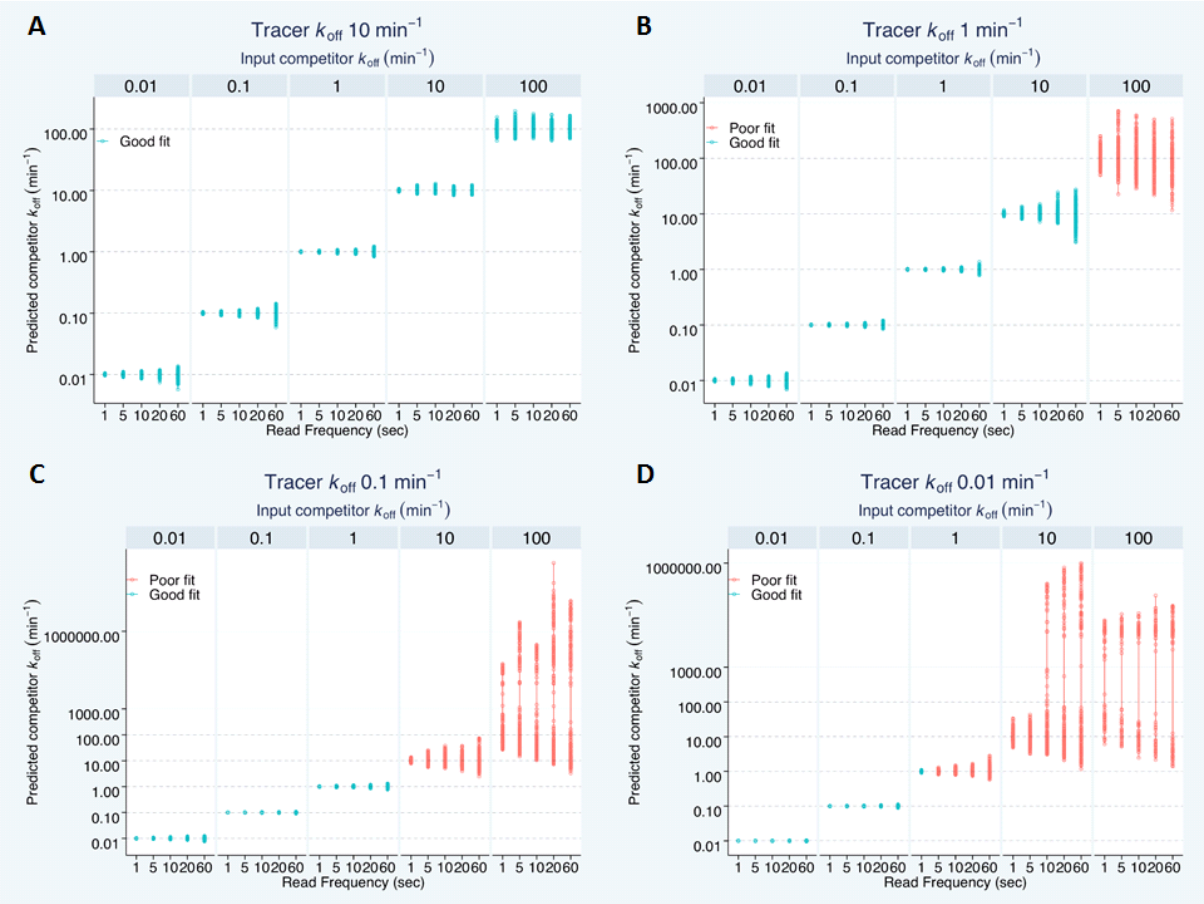

Downloaded from molpharm.aspetjournals.org at ASPET Journals on April 19, 2024

Molecular Pharmacology Fast Forward. Published on July 10, 2019 as DOI: 10.1124/mol.119.116764
This article has not been copyedited and formatted. The final version may differ from this version.

Figure 5

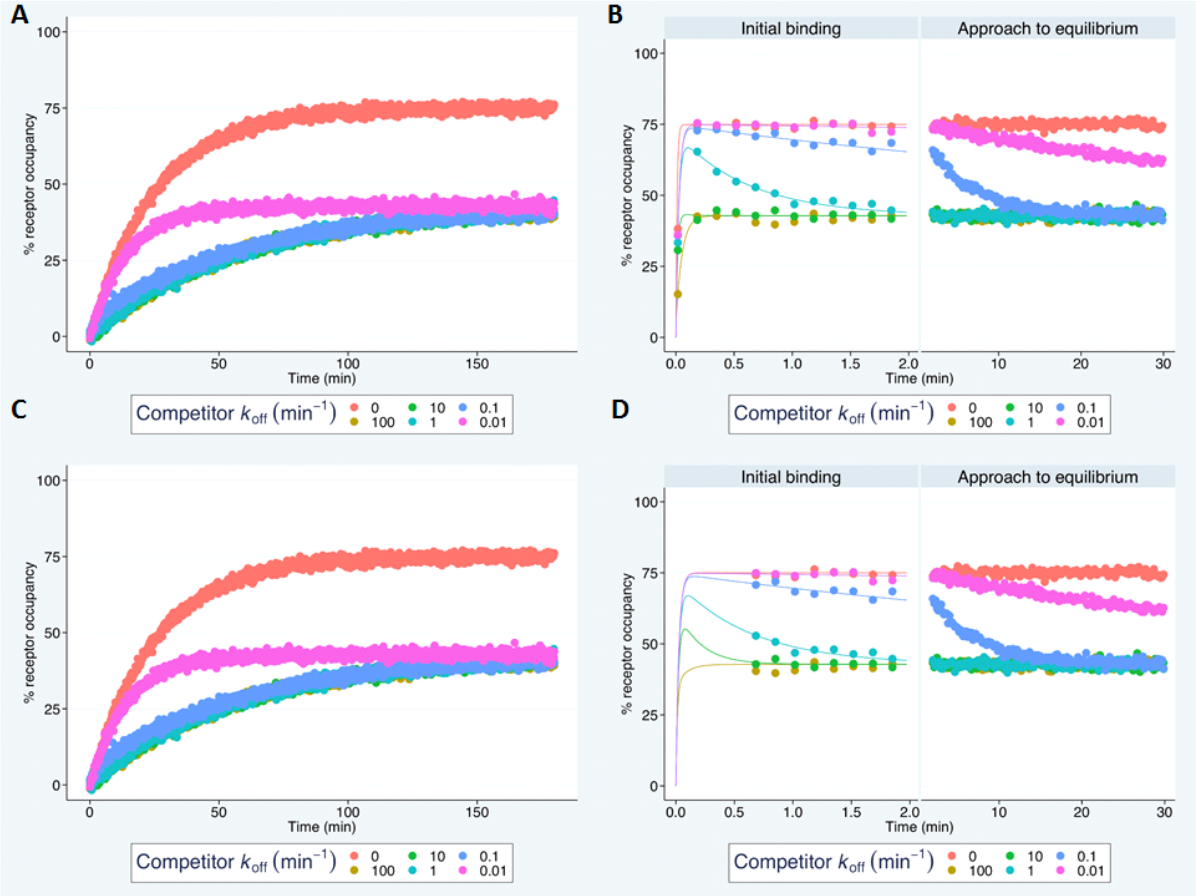

Downloaded from molpharm.aspetjournals.org at ASPET Journals on April 19, 2024

Molecular Pharmacology Fast Forward. Published on July 10, 2019 as DOI: 10.1124/mol.119.116764
This article has not been copyedited and formatted. The final version may differ from this version.

Figure 6

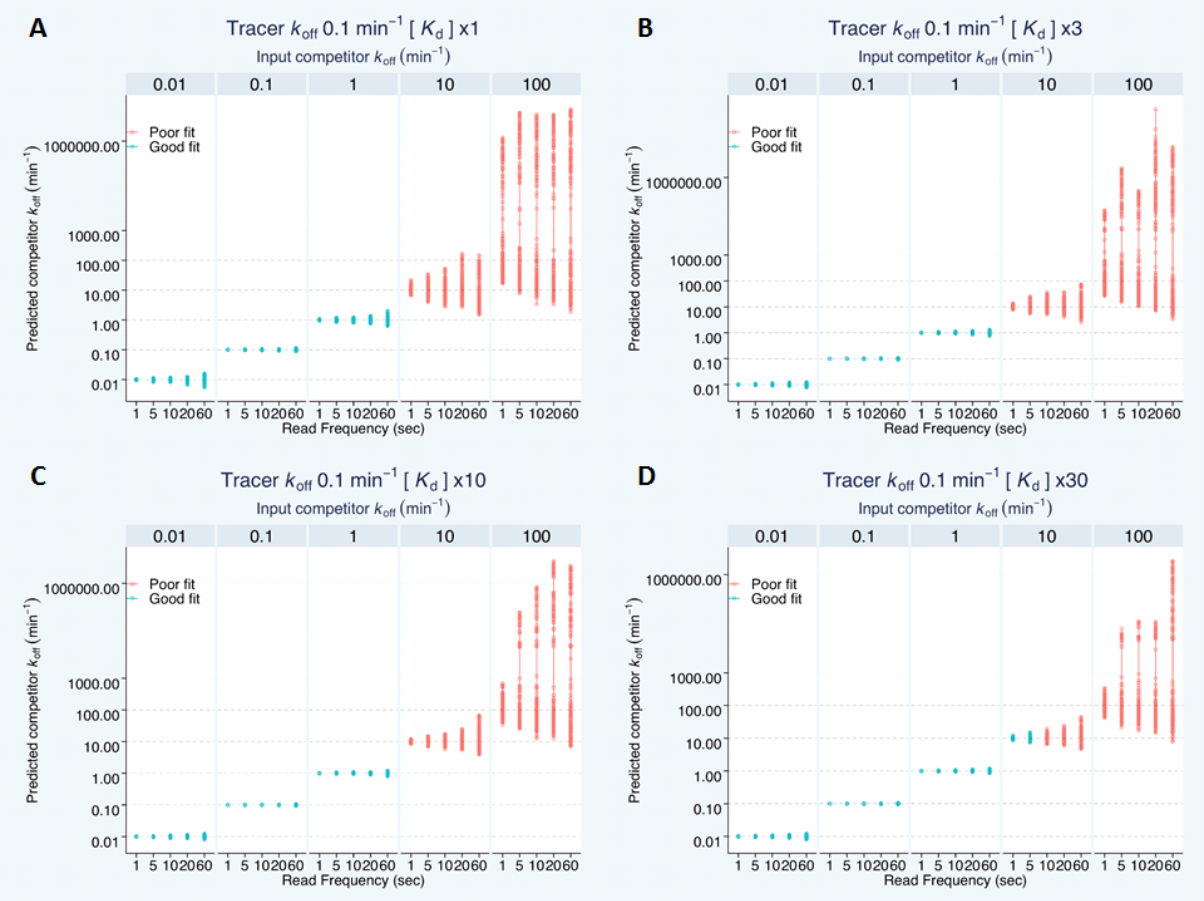

Downloaded from molpharm.aspetjournals.org at ASPET Journals on April 19, 2024

Molecular Pharmacology Fast Forward. Published on July 10, 2019 as DOI: 10.1124/mol.119.116764
This article has not been copyedited and formatted. The final version may differ from this version.

Figure 7

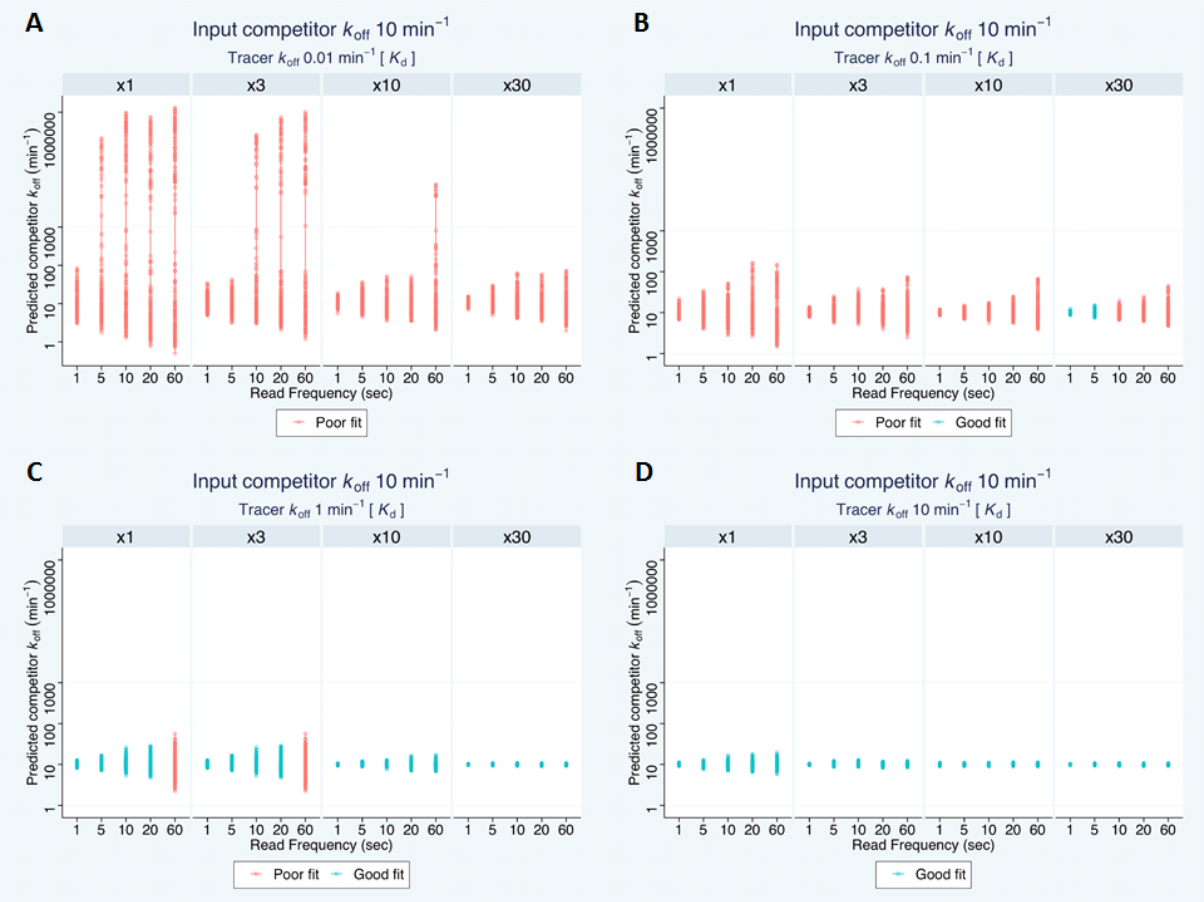

Downloaded from molpharm.aspetjournals.org at ASPET Journals on April 19, 2024

Molecular Pharmacology Fast Forward. Published on July 10, 2019 as DOI: 10.1124/mol.119.116764
This article has not been copyedited and formatted. The final version may differ from this version.

Figure 8

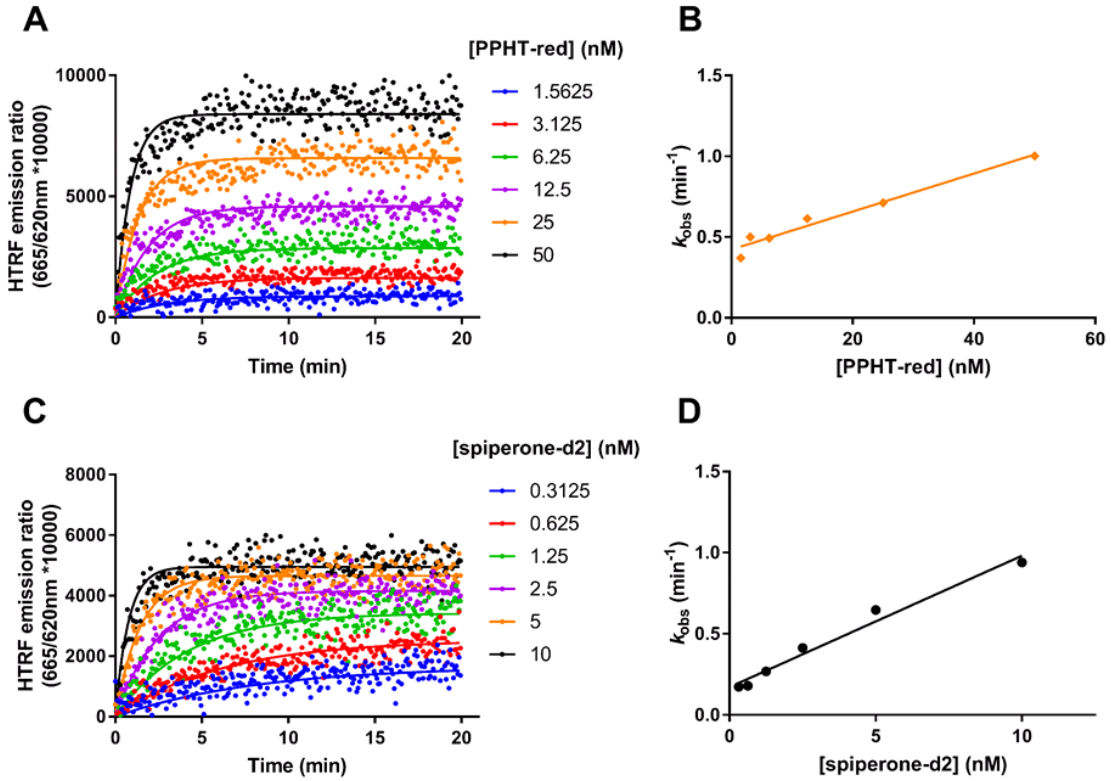

Downloaded from molpharm.aspetjournals.org at ASPET Journals on April 19, 2024

Molecular Pharmacology Fast Forward. Published on July 10, 2019 as DOI: 10.1124/mol.119.116764
This article has not been copyedited and formatted. The final version may differ from this version.

Figure 9

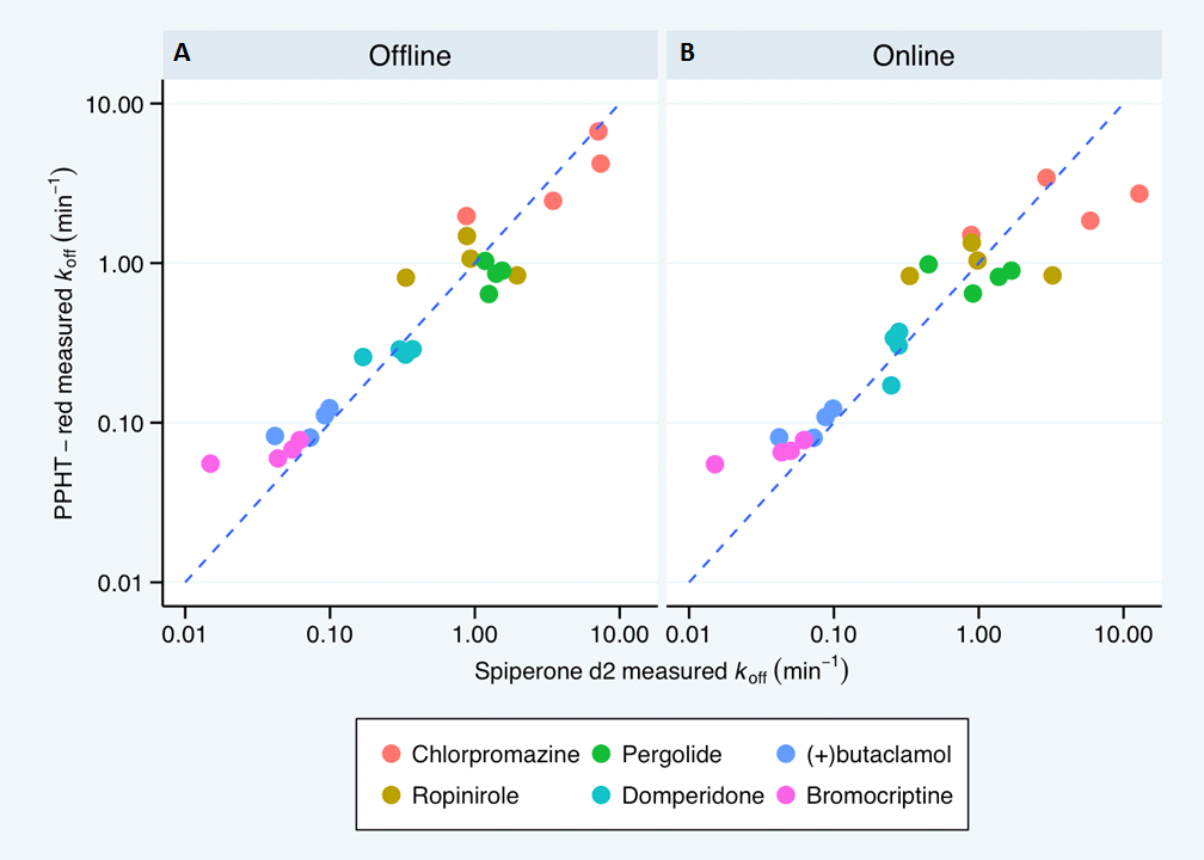

Downloaded from molpharm.aspetjournals.org at ASPET Journals on April 19, 2024

Investigating the influence of tracer kinetics on competition-kinetic association binding assays; identifying the optimal conditions for assessing the kinetics of low affinity compounds.

David A Sykes, Palash Jain & Steven J Charlton

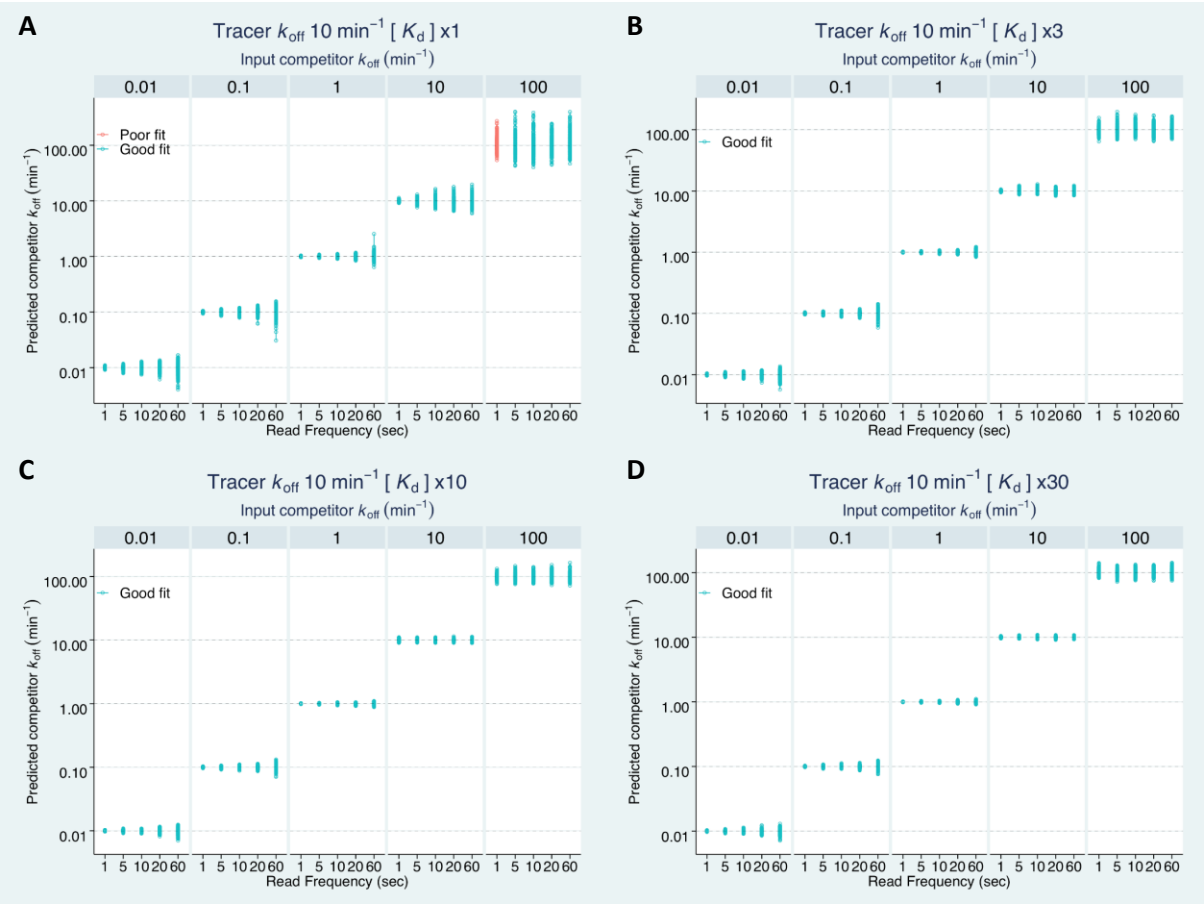

Supplemental Figure 1. Monte-Carlo simulation results exploring the effect of tracer kinetics and assay start and read frequency time on the accurate determination of competitor kinetic parameters representative of online addition protocol. Effect of assay read frequency on measured k_{off} of unlabelled competitor compounds with varied kinetics in competition with different concentrations of a slowly dissociating tracer with kinetic parameters; k_{off} of 10min^{-1}, k_{on} of 3x10^{7} M^{-1} min^{-1}. Tracer concentrations were **(A)** 1x K_d , **(B)** 3x K_d **(C)** 10x K_d and **(D)** 30x K_d. Blue open symbols represent conditions which returned >90% reliable fits. Red open symbols

represent conditions which returned <90% reliable fits. In all cases tracer simulations were performed with an initial start time of 1sec representative of addition of receptor to a reaction containing free tracer (L) and unlabelled competitor (I), all of 200 values (minus outliers) for each simulated condition are plotted.

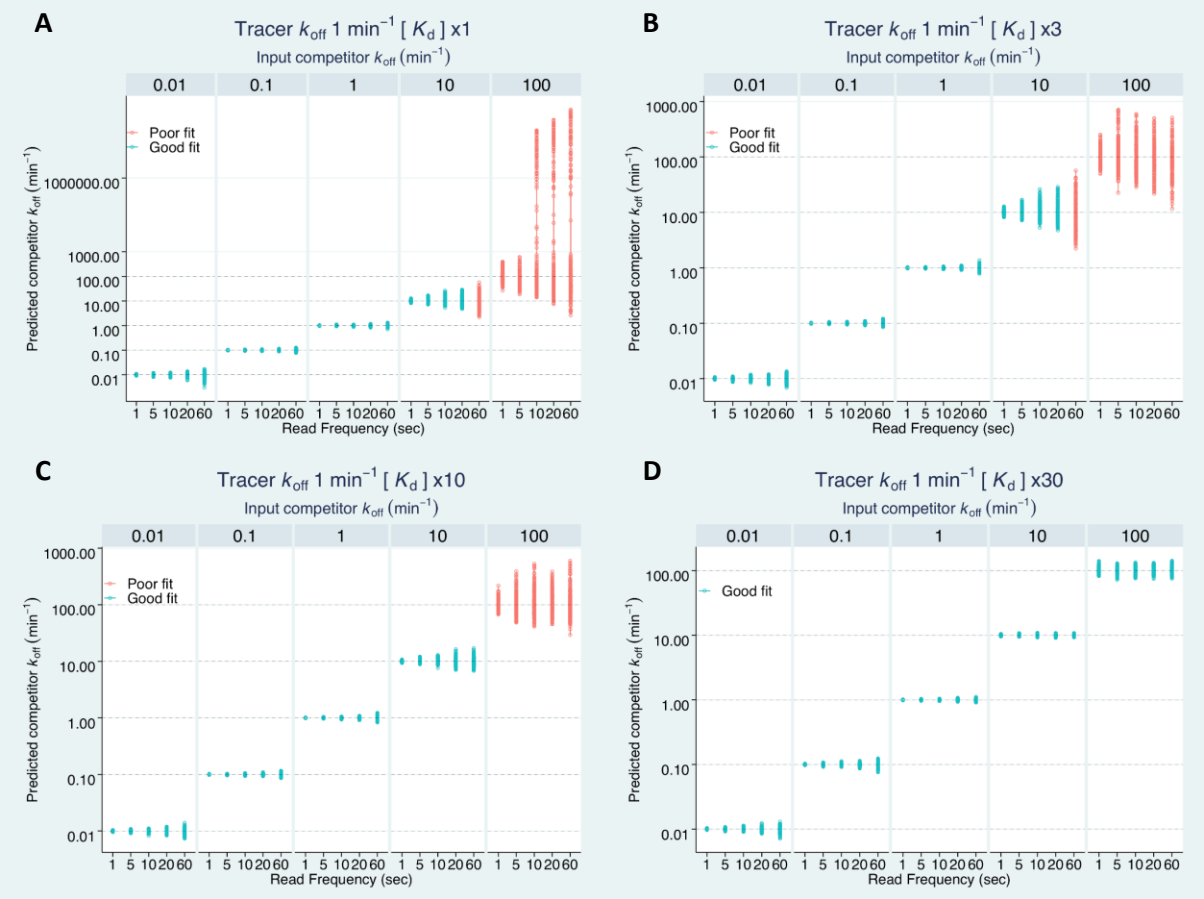

Supplemental Figure 2. Monte-Carlo simulation results exploring the effect of tracer kinetics and assay start and read frequency time on the accurate determination of competitor kinetic parameters representative of online addition protocol. Effect of assay read frequency on measured k_{off} of unlabelled competitor compounds with varied kinetics in competition with different concentrations of a slowly dissociating tracer with kinetic parameters; k_{off} of 1min^{-1}, k_{on} of 1x10^{7} M^{-1} min^{-1}. Tracer concentrations were **(A)** 1x K_d **(B)** 3x K_d **(C)** 10x K_d and **(D)** 30x K_d. Blue open symbols represent conditions which returned >90% reliable fits. Red open symbols represent conditions which returned <90% reliable fits. In all cases tracer simulations were performed with an initial start time of 1sec representative of addition of receptor to a reaction containing free tracer (L) and competitor (I), all of 200 values (minus outliers) for each simulated condition are plotted.

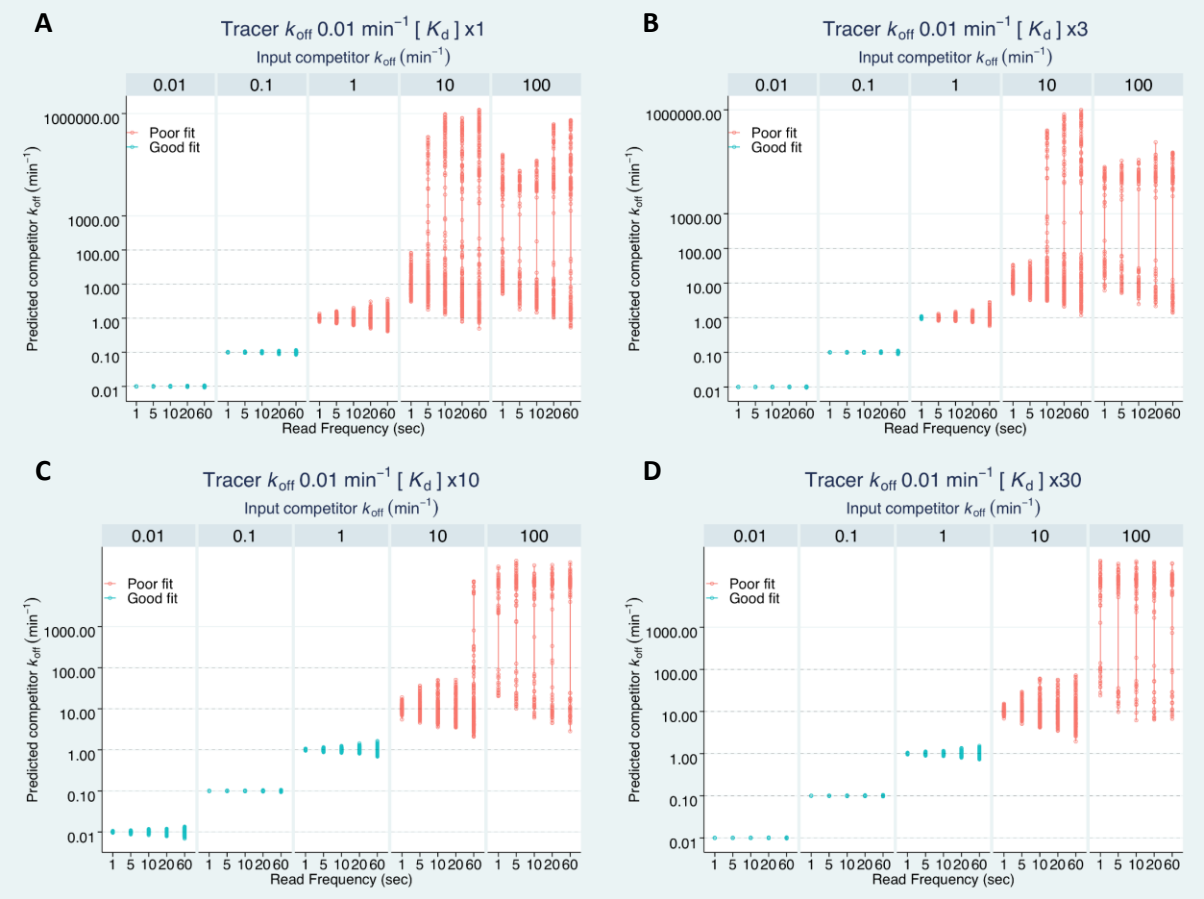

Supplemental Figure 3. Monte-Carlo simulation results exploring the effect of tracer kinetics and assay start and read frequency time on the accurate determination of competitor kinetic parameters representative of online addition protocol. Effect of assay read frequency on measured k_{off} of unlabelled competitor compounds with varied kinetics in competition with different concentrations of a slowly dissociating tracer with kinetic parameters; k_{off} of 0.01min^{-1}, k_{on} of 1x10^{9} M^{-1} min^{-1}. Tracer concentrations were **(A)** 1x K_d **(B)** 3x K_d **(C)** 10x K_d and **(D)** 30x K_d. Blue open symbols represent conditions which returned >90% reliable fits. Red open symbols represent conditions which returned <90% reliable fits. In all cases tracer simulations were performed with an initial start time of 1sec representative of addition of receptor to a reaction containing free tracer (L) and competitor (I), all of 200 values (minus outliers) for each simulated condition are plotted.

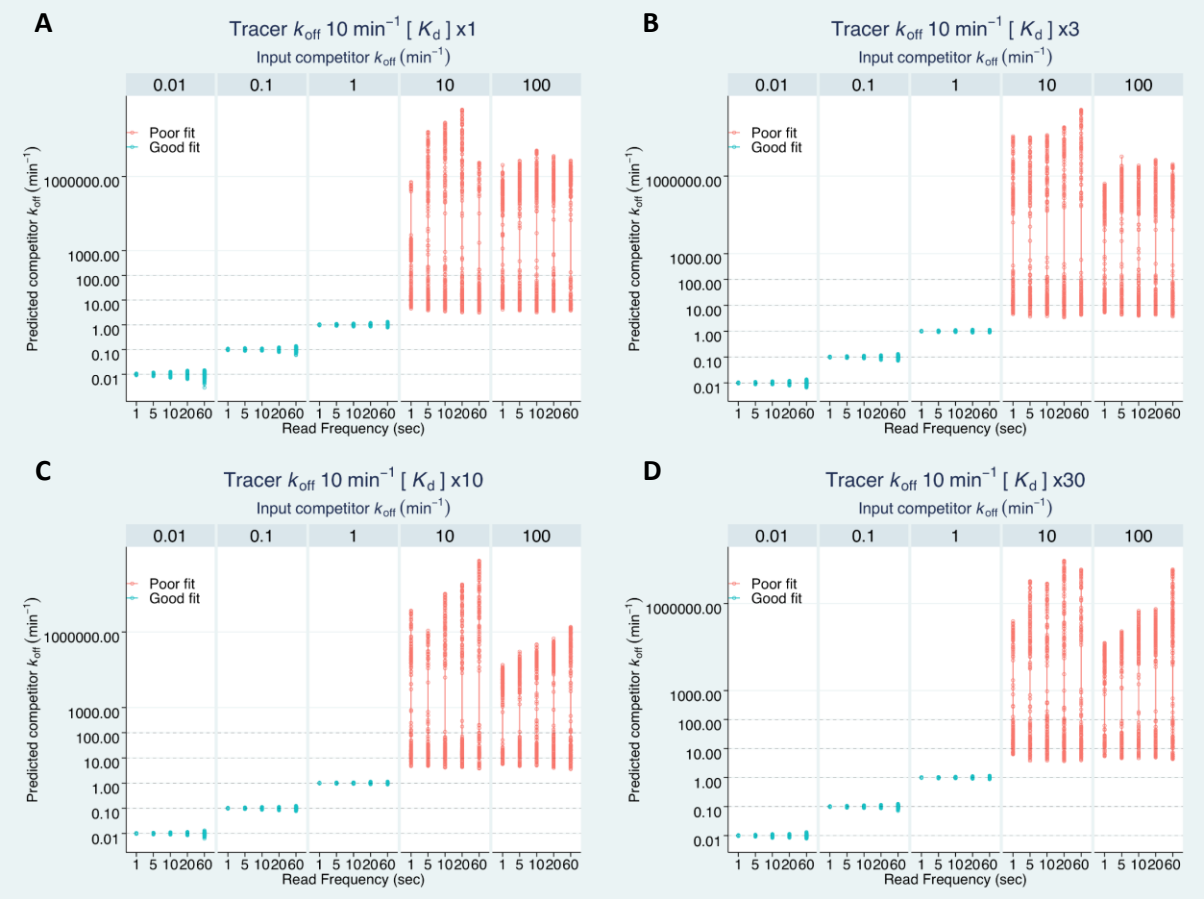

Supplemental Figure 4. Monte-Carlo simulation results exploring the effect of tracer kinetics and assay start and read frequency time on the accurate determination of competitor kinetic parameters representative of offline addition protocol. Effect of assay read frequency on measured k_{off} of unlabelled competitor compounds with varied kinetics in competition with different concentrations of a slowly dissociating tracer with kinetic parameters; k_{off} of 10min^{-1}, k_{on} of 3x10^{7} M^{-1} min^{-1}. Tracer concentrations were **(A)** 1x K_d **(B)** 3x K_d , **(C)** 10x K_d and **(D)** 30x K_d. Blue open symbols represent conditions which returned >90% reliable fits. Red open symbols represent conditions which returned <90% reliable fits. In all cases tracer simulations were performed with an initial start time of 30sec representative of addition of receptor to a reaction containing free tracer (L) and competitor (I), all of 200 values (minus outliers) for each simulated condition are plotted.

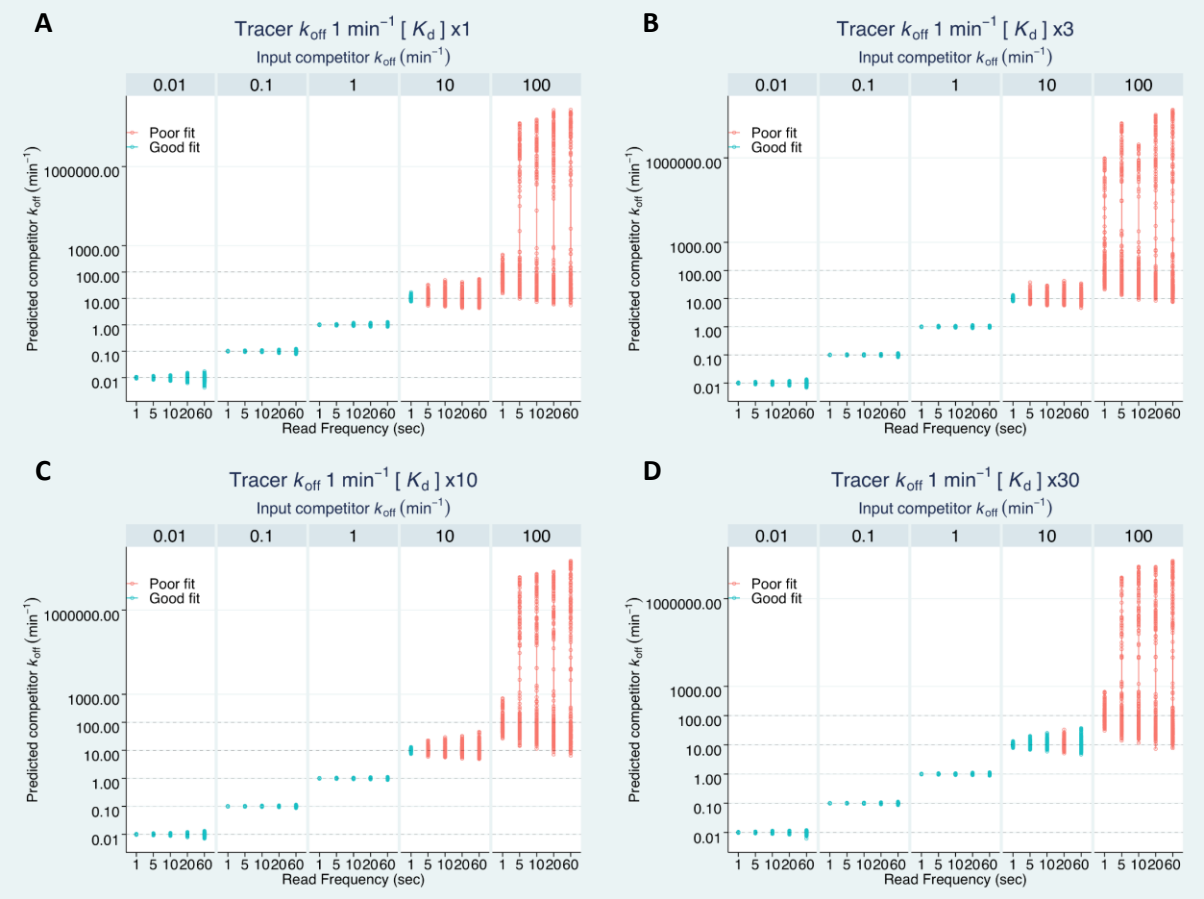

Supplemental Figure 5. Monte-Carlo simulation results exploring the effect of tracer kinetics and assay start and read frequency time on the accurate determination of competitor kinetic parameters representative of offline addition protocol. Effect of assay read frequency on measured k_{off} of unlabelled competitor compounds with varied kinetics in competition with different concentrations of a slowly dissociating tracer with kinetic parameters; k_{off} of 1min^{-1}, k_{on} of 1x10^{7} min^{-1}. Tracer concentrations were **(A)** 1x K_d **(B)** 3x K_d **(C)** 10x K_d and **(D)** 30x K_d. Blue open symbols represent conditions which returned >90% reliable fits. Red open symbols represent conditions which returned <90% reliable fits. In all cases tracer simulations were performed with an initial start time of 30sec representative of addition of receptor to a reaction containing free tracer (L) and competitor (I), all of 200 values (minus outliers) for each simulated condition are plotted.

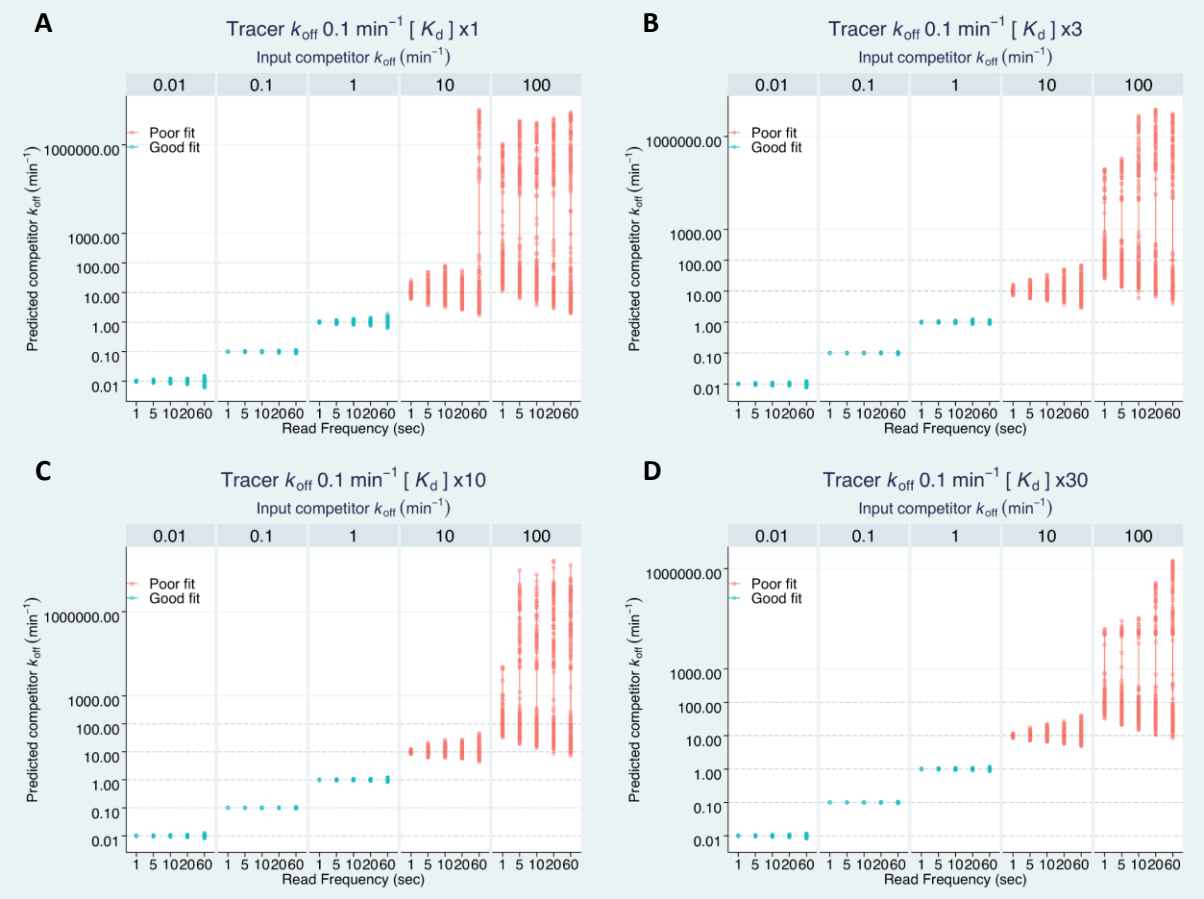

Supplemental Figure 6. Monte-Carlo simulation results exploring the effect of tracer kinetics and assay start and read frequency time on the accurate determination of competitor kinetic parameters representative of offline addition protocol. Effect of assay read frequency on measured k_{off} of unlabelled competitor compounds with varied kinetics in competition with different concentrations of a slowly dissociating tracer with kinetic parameters; k_{off} of 0.1min^{-1}, k_{on} of 1x10^8 min^{-1}. Tracer concentrations were **(A)** 1x K_d , **(B)** 3x K_d , **(C)** 10x K_d and **(D)** 30x K_d. Blue open symbols represent conditions which returned >90% reliable fits. Red open symbols represent conditions which returned <90% reliable fits. In all cases tracer simulations were performed with an initial start time of 30sec representative of addition of receptor to a reaction containing free tracer (L) and competitor (I), all of 200 values (minus outliers) for each simulated condition are plotted.

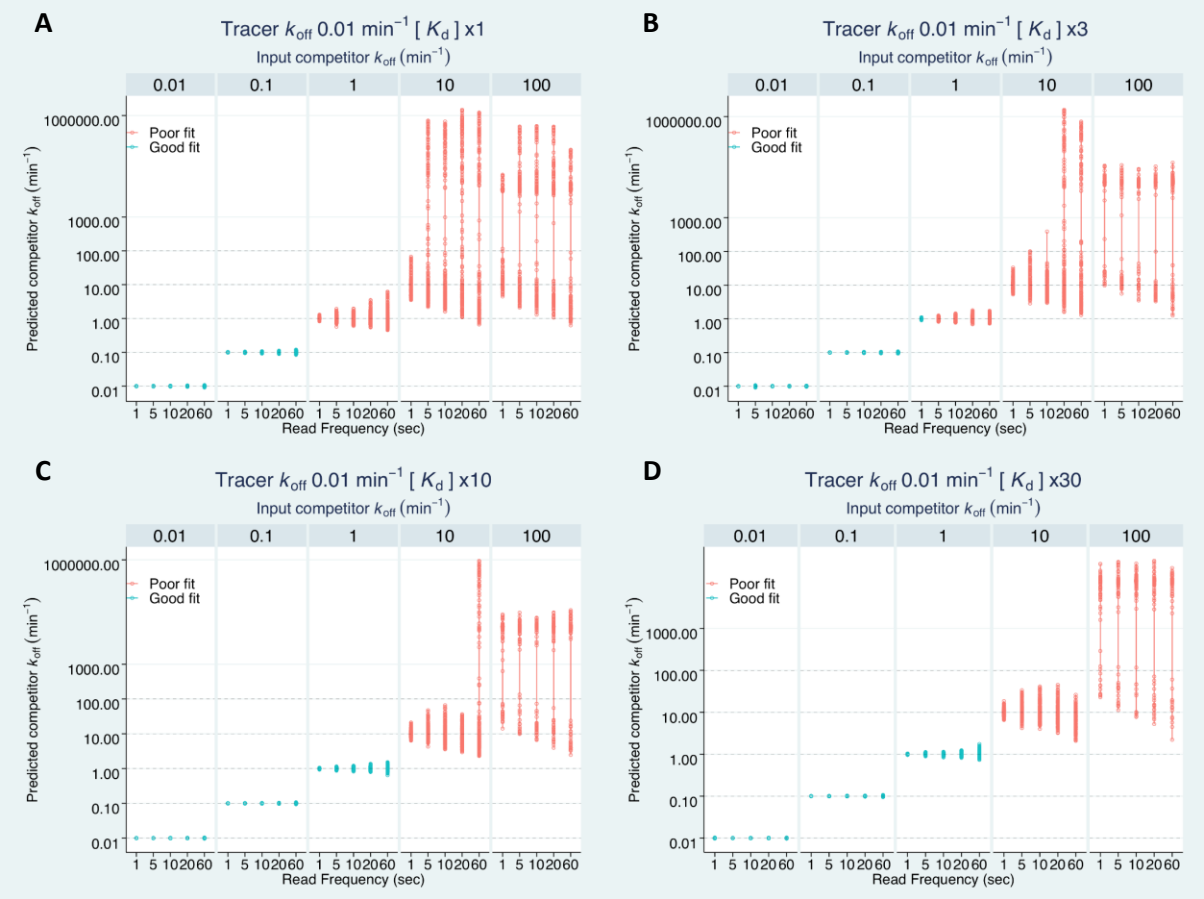

Supplemental Figure 7. Monte-Carlo simulation results exploring the effect of tracer kinetics and assay start and read frequency time on the accurate determination of competitor kinetic parameters representative of offline addition protocol. Effect of assay read frequency on measured k_{off} of unlabelled competitor compounds with varied kinetics in competition with different concentrations of a slowly dissociating tracer with kinetic parameters; k_{off} of 0.01min^{-1}, k_{on} of 1x10^{9} min^{-1}. Tracer concentrations were **(A)** 1x K_d , **(B)** 3x K_d , **(C)** 10x K_d and **(D)** 30x K_d. Blue oipen symbols represent conditions which returned >90% reliable fits. Red open symbols represent conditions which returned <90% reliable fits. In all cases tracer simulations were performed with an initial start time of 30sec representative of addition of receptor to a reaction containing free tracer (L) and competitor (I), all of 200 values (minus outliers) for each simulated condition are plotted.

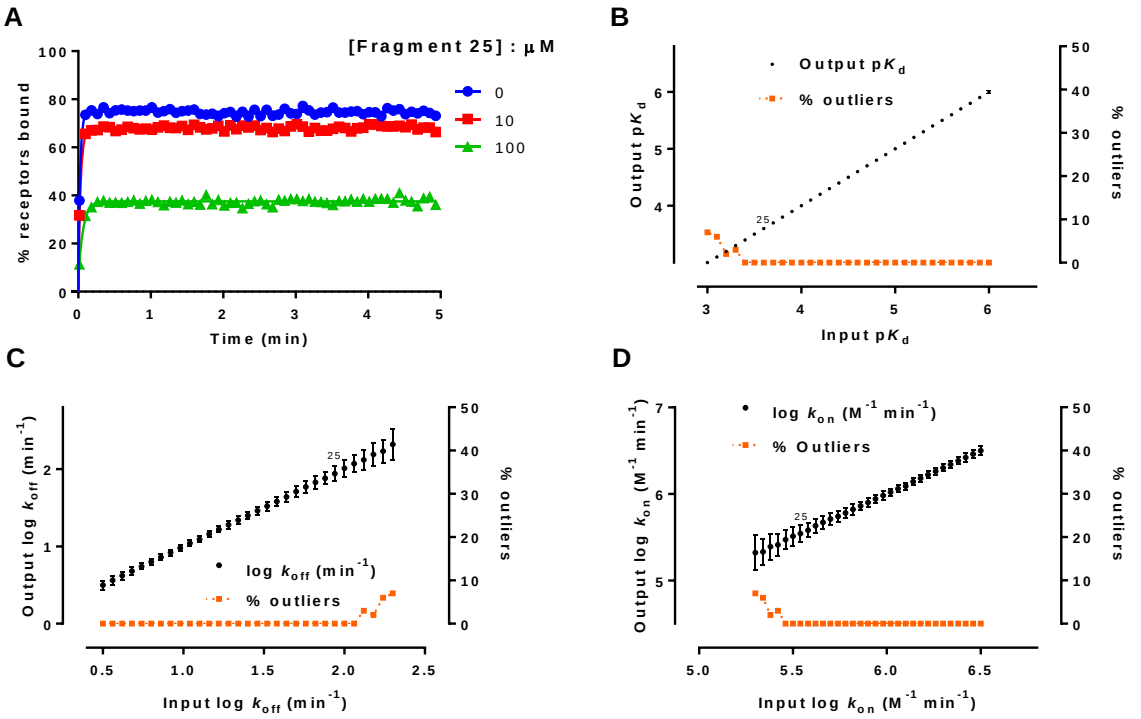

Supplemental Figure 8. Monte-Carlo simulation results representative of the competition profile observed between low affinity fragments 1 to 31 (affinities ranging from 1-1000 µM) tested at 10 and 100 µM in competition with a fixed concentration of a rapidly dissociating tracer. **(A)** Competition between a fixed concentration (3x K_d) of a rapidly dissociating tracer with the following kinetic parameters; k_{off} of $10min^{-1}$, k_{on} of $3x10^7$ M^{-1} min^{-1}, and competitor fragment 25 with the following kinetic parameters; k_{off} of 87.1 min^{-1}, k_{on} of $5 x10^5$ M^{-1} min^{-1}, data shown are representative of 200 simulations. **(B)** Correlation between input K_d and output K_d, **(C)** between input k_{off} and output k_{off}, **(D)** between input k_{on} and output k_{on}. In each case tracer and competitor binding simulations were performed with an initial start time of 1sec (representative of injection of receptor to a reaction containing tracer) and a read frequency of 5sec, the data shown points shown in the correlations plots are the average of 200 simulations**.**

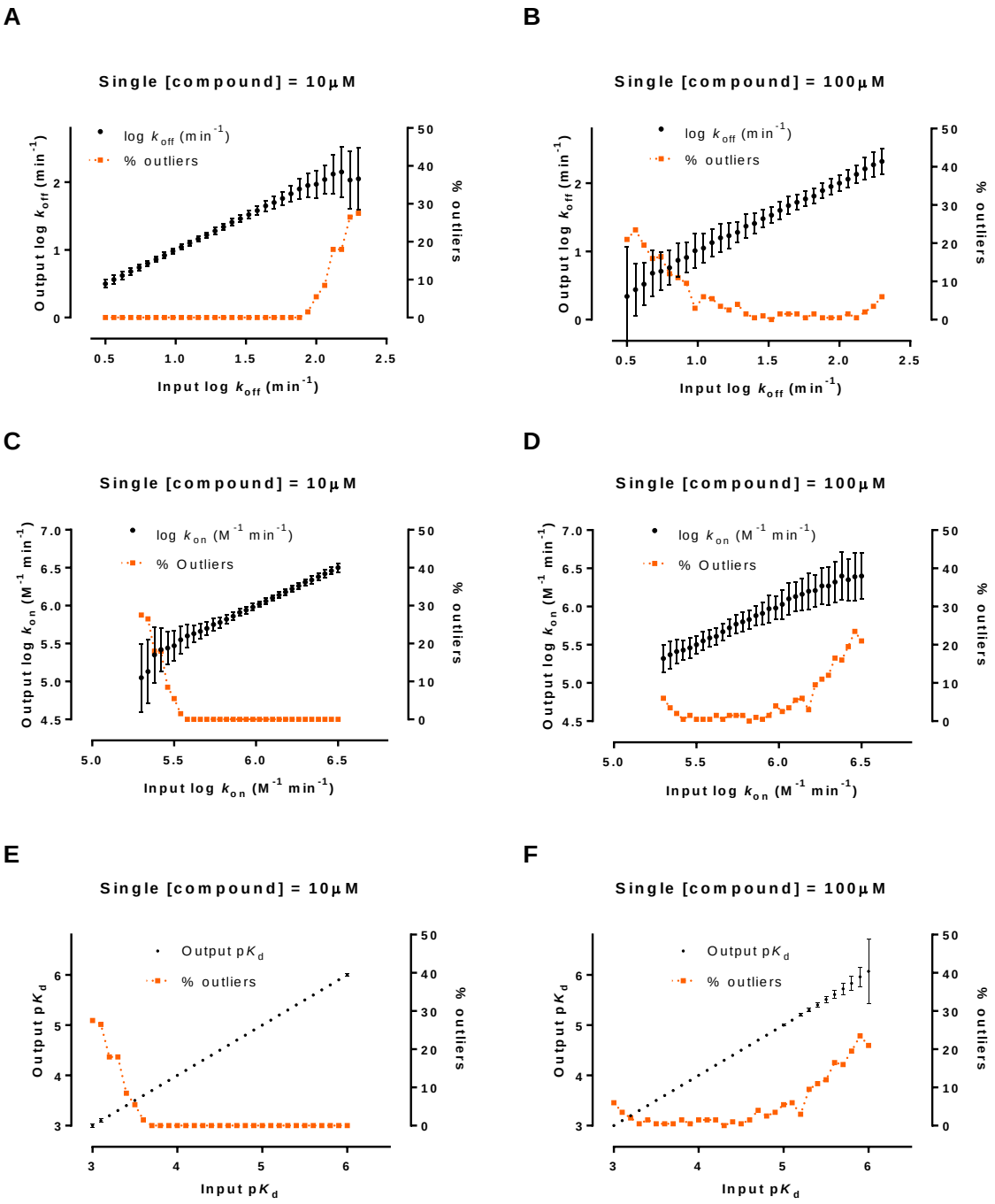

Supplemental Figure 9. Monte-Carlo simulation results representative of the competition profile observed between low affinity fragments (1-1000µM) tested at 10 and 100µM in competition with a fixed concentration (3x K_d) of a rapidly dissociating tracer with the following kinetic parameters; k_{off} of 10min^{-1}, k_{on} of 3x10^7 M^{-1} min^{-1}. Correlation between **A)** input k_{off} and output k_{off} at 10µM **B)** input k_{off} and output k_{off} at 100µM. **C)** input k_{on} and output k_{off} at 10µM. **D)** input k_{on} and output k_{off} at 100µM. **E)** input K_d and output K_d, at 10µM. **F)** input K_d and output K_d, at 100µM. In each case tracer and competitor binding

simulations were performed with an initial start time of 1sec (representative of injection of receptor to a reaction containing tracer) and a read frequency of 5sec, the data shown points shown in the correlations plots are the average of 200 simulations.

Supplemental data files

Supplemental Table 1. Summary of the kinetic input parameters and their estimates for the tracer described in Table 1, under conditions which mimic online and offline addition, determined from 200 simulated data sets using the global association model equation (see Figure 1).

Online injection first read time 1sec							
Number of : (Ambiguous fits; Outliers)	Read frequency (sec)	Input K_d (Output K_d) nM	K_d %CV	Input k_{on} (Output k_{on}) $M^{-1}min^{-1}$	k_{on} %CV	Input k_{off} (Output k_{off}) min^{-1}	k_{off} %CV
(0; 0)	1	333 (333)	0.21	3E7 (3E7)	1.29	10 (10.01)	1.32
(0; 0)	5	333 (333)	0.47	3E7 (3E7)	2.31	10 (10.01)	2.27
(0; 0)	10	333 (333)	0.72	3E7 (3E7)	2.49	10 (10.01)	2.50
(0; 0)	20	333 (334)	0.96	3E7 (3.01E7)	2.34	10 (10.05)	2.40
(0; 0)	60	333 (333)	1.67	3E7 (3E7)	2.72	10 (9.99)	3.07
(0; 0)	1	100 (100)	0.26	1E7 (1E7)	0.44	1 (1.00)	0.53
(0; 0)	5	100 (100)	0.55	1E7 (1E7)	0.93	1 (1.00)	1.18
(0; 0)	10	100 (100)	0.81	1E7 (1E7)	1.34	1 (1.00)	1.71
(0; 0)	20	100 (100)	1.10	1E7 (1E7)	1.62	1 (1.00)	2.10
(0; 0)	60	100 (100)	2.14	1E7 (1E7)	2.74	1 (1.00)	3.52
(0; 0)	1	1 (1)	0.14	1E8 (1E8)	0.14	0.1 (0.1)	0.22

(0; 0)	5	1 (1)	0.32	1E8 (1E8)	0.32	0.1 (0.1)	0.51
(0; 0)	10	1 (1)	0.49	1E8 (1E8)	0.40	0.1 (0.1)	0.70
(0; 0)	20	1 (1)	0.61	1E8 (1E8)	0.64	0.1 (0.1)	1.02
(0; 0)	60	1 (1)	1.03	1E8 (1E8)	1.14	0.1 (0.1)	1.75
(0; 0)	1	0.01 (0.01)	0.29	1E9 (1E9)	0.06	0.01 (0.01)	0.32
(0; 0)	5	0.01 (0.01)	0.68	1E9 (1E9)	0.15	0.01 (0.01)	0.76
(0; 0)	10	0.01 (0.01)	0.91	1E9 (1E9)	0.20	0.01 (0.01)	1.02
(0; 0)	20	0.01 (0.01)	1.51	1E9 (1E9)	0.29	0.01 (0.01)	1.38
(0; 0)	60	0.01 (0.01)	2.50	1E9 (1E9)	0.55	0.01 (0.01)	2.19

Offline addition first read time 30 sec							
Number of : (Ambiguous fits; Outliers)	Read frequency (sec)	Input K_d (Output K_d) nM	K_d %CV	Input k_{on} (Output k_{on}) $M^{-1}min^{-1}$	k_{on} %CV	Input k_{off} (Output k_{off}) min^{-1}	k_{off} %CV
(197; 0)	1	333 (333)	0.21	3E7 (1.12E7)	41.38	10 (37.17)	41.36
(199; 8)	5	333 (333)	0.44	3E7 (1.71E8)	4.92	10 (56.90)	4.86
(200; 2)	10	333 (333)	0.72	3E7 (2.30E8)	9.54	10 (76.78)	9.54
(192; 0)	20	333 (333)	0.95	3E7 (1.67E8)	31.98	10 (55.54)	32.02
(139; 2)	60	333 (333)	1.68	3E7 (1.13E8)	92.76	10 (37.69)	92.28

(0; 0)	1	100 (100)	0.27	1E7 (9.66E6)	0.67	1 (1.00)	0.80
(0; 0)	5	100 (100)	0.55	1E7 (1E7)	1.47	1 (1.00)	1.74
(0; 0)	10	100 (100)	0.83	1E7 (1E7)	2.08	1 (1.00)	2.50
(0; 0)	20	100 (100)	1.16	1E7 (1E7)	2.65	1 (1.00)	3.09
(0; 0)	60	100 (100)	1.94	1E7 (1E7)	3.39	1 (1.00)	4.27
(0; 0)	1	1 (1)	0.14	1E8 (1E8)	0.13	0.1 (0.1)	0.22
(0; 0)	5	1 (1)	0.33	1E8 (1E8)	0.33	0.1 (0.1)	0.52
(0; 0)	10	1 (1)	0.44	1E8 (1E8)	0.47	0.1 (0.1)	0.72
(0; 0)	20	1 (1)	0.63	1E8 (1E8)	0.63	0.1 (0.1)	0.97
(0; 0)	60	1 (1)	1.03	1E8 (1E8)	1.17	0.1 (0.1)	1.77
(0; 0)	1	0.01 (0.01)	0.30	1E9 (1E9)	0.06	0.01 (0.01)	0.33
(0; 0)	5	0.01 (0.01)	0.68	1E9 (1E9)	0.15	0.01 (0.01)	0.77
(0; 0)	10	0.01 (0.099)	0.94	1E9 (1E9)	0.20	0.01 (0.01)	1.05
(0; 0)	20	0.01 (0.01)	1.25	1E9 (1E9)	0.31	0.01 (0.01)	1.41
(0; 0)	60	0.01 (0.01)	2.30	1E9 (9.99E8)	0.53	0.01 (0.01)	2.61

Supplemental Table 2. Summary of the kinetic input parameters and their estimates for unlabelled compounds under conditions which mimic online injection and offline addition of membranes, values are determined from 200 simulated data sets using the Motulsky-Mahan model equation and the very low affinity tracer (k_{on} = 3x10^{7} M^{-1}min^{-1}; k_{off} = 10min^{-1} K_d= 3μM).

Online injection first read time 1sec							
Number of : (Ambiguous fits; Outliers)	Read frequency (sec)	Input K_d (Output K_d)	K_d %CV	Input k_{on} (Output k_{on}) M^{-1}min^{-1}	k_{on} %CV	Input k_{off} (Output k_{off}) min^{-1}	k_{off} %CV
(0; 0)	1	10pM (10pM)	1.62	1E9 (1E9)	0.18	0.01 (0.01)	1.77
(0; 0)	5	10pM (10pM)	3.44	1E9 (1E9)	0.41	0.01 (0.01)	3.78
(0; 0)	10	10pM (10pM)	5.29	1E9 (1E9)	0.57	0.01 (0.01)	5.74
(0; 0)	20	10pM (10pM)	6.82	1E9 (1E9)	0.78	0.01 (0.01)	7.42
(0; 0)	60	10pM (10pM)	12.75	1E9 (0.999E8)	1.32	0.01 (0.01)	13.70
(0; 0)	1	1nM (1nM)	1.12	1E8 (1E8)	0.34	0.1 (0.1)	1.38
(0; 0)	5	1nM (0.99nM)	2.73	1E8 (1E8)	0.78	0.1 (0.1)	3.29
(0; 0)	10	1nM (1nM)	3.98	1E8 (1E8)	1.29	0.1 (0.1)	4.99
(0; 0)	20	1nM (0.996nM)	5.37	1E8 (1E8)	1.51	0.1 (0.1)	6.49
(0; 0)	60	1nM (0.991nM)	12.13	1E8 (1E8)	3.31	0.1 (0.1)	14.79
(0; 0)	1	100nM (100nM)	0.30	1E7 (9.99E6)	0.68	1 (1)	0.77
(0; 0)	5	100nM (99.9nM)	0.62	1E7 (1E7)	1.47	1 (1)	1.64

(0; 0)	10	100nM (100nM)	0.90	1E7 (1E7)	2.06	1 (1)	2.38
(0; 0)	20	100nM (99.9nM)	1.42	1E7 (1E7)	2.94	1 (1)	3.42
(0; 0)	60	100nM (99.8nM)	2.47	1E7 (1.01E7)	6.86	1 (1.01)	7.42
(0; 0)	1	10µM (10µM)	0.25	1E6 (1E6)	2.06	10 (10)	2.08
(0; 0)	5	10µM (10µM)	0.62	1E6 (1E6)	5.68	10 (10.02)	5.74
(0; 0)	10	10µM (10µM)	0.92	1E6 (1.01E6)	7.27	10 (10.05)	7.33
(0; 0)	20	10µM (9.99µM)	1.30	1E6 (1.01E6)	6.94	10 (10.05)	7.03
(0; 0)	60	10µM (9.98µM)	2.54	1E6 (1.01E6)	7.93	10 (10.06)	7.73
(0; 0)	1	1mM (1mM)	0.26	1E5 (9.98E4)	14.41	100 (99.81)	14.42
(0; 0)	5	1mM (1mM)	0.58	1E5 (1.04E5)	20.54	100 (103.86)	20.57
(0; 0)	10	1mM (1mM)	0.86	1E5 (1.03E5)	18.60	100 (103.48)	18.71
(0; 0)	20	1mM (1mM)	1.14	1E5 (1.02E5)	16.86	100 (101.83)	17.11
(0; 1)	60	1mM (1mM)	2.36	1E5 (1.02E5)	17.26	100 (102.38)	17.57

Offline addition first read time 30 sec							
Number of : (Ambiguous fits; Outliers)	Read frequency (sec)	Input K_d (Output K_d)	K_d %CV	Input k_{on} (Output k_{on}) $M^{-1}min^{-1}$	k_{on} %CV	Input k_{off} (Output k_{off}) min^{-1}	k_{off} %CV

(0; 0)	1	10pM (10pM)	1.55	1E9 (1E9)	0.17	0.01 (0.01)	1.67
(0; 0)	5	10pM (9.98pM)	3.74	1E9 (1E9)	0.43	0.01 (0.01)	4.09
(0; 0)	10	10pM (10pM)	4.95	1E9 (1E9)	0.56	0.01 (0.01)	5.43
(0; 0)	20	10pM (10pM)	6.79	1E9 (1E9)	0.86	0.01 (0.01)	7.47
(0; 0)	60	10pM (9.94pM)	12.31	1E9 (1E9)	1.42	0.01 (0.01)	13.39
(0; 0)	1	1nM (0.999nM)	1.24	1E8 (1E8)	0.37	0.1 (0.1)	1.52
(0; 0)	5	1nM (1nM)	2.68	1E8 (1E8)	0.90	0.1 (0.1)	3.39
(0; 0)	10	1nM (1nM)	3.79	1E8 (1E8)	1.24	0.1 (0.1)	4.77
(0; 0)	20	1nM (1nM)	5.42	1E8 (1E8)	1.70	0.1 (0.1)	6.73
(0; 0)	60	1nM (0.998nM)	9.62	1E8 (1E8)	2.78	0.1 (0.1)	11.83
(0; 0)	1	100nM (100nM)	0.33	1E7 (1E7)	1.04	1 (1)	1.18
(0; 0)	5	100nM (100nM)	0.70	1E7 (1E7)	2.18	1 (1)	2.38
(0; 0)	10	100nM (100nM)	0.92	1E7 (1E7)	3.05	1 (1)	3.30
(0; 0)	20	100nM (100nM)	1.41	1E7 (9.99E6)	4.28	1 (1)	4.79
(0; 0)	60	100nM (100nM)	1.30	1E7 (1E7)	3.85	1 (1)	4.26
(193; 6)	1	10µM (10µM)	0.28	1E6 (2.42E11)	277.73	10 (2.42E6)	277.65
(192; 19)	5	10µM (10µM)	0.58	1E6 (2.43E11)	261.24	10 (2.44E6)	261.33

(187; 27)	10	10μM (10μM)	0.93	1E6 (3.21E11)	241.99	10 (3.20E6)	241.45
(174; 30)	20	10μM (9.98μM)	1.18	1E6 (5.96E11)	258.44	10 (5.96E6)	258.67
(177; 31)	60	10μM (10μM)	2.19	1E6 (2.70E12)	275.64	10 (2.70E7)	275.21
(197; 0)	1	1mM (1mM)	0.26	1E5 (7.89E7)	143.79	100 (78893.74)	143.79
(191; 5)	5	1mM (1mM)	0.62	1E5 (3.01E8)	209.63	100 (3.01E5)	209.59
(188; 9)	10	1mM (1mM)	0.87	1E5 (2.50E8)	205.46	100 (2.51E5)	205.66
(192; 22)	20	1mM (9.99E-4)	1.14	1E5 (3.84E8)	209.43	100 (3.84E5)	209.53
(191; 36)	60	1mM (1mM)	1.51	1E5 (3.29E8)	170.69	100 (3.30E5)	171.09

Supplemental Table 3. Summary of the kinetic input parameters and their estimates for unlabelled compounds under conditions which mimic online injection and offline addition of membranes, values are determined from 200 simulated data sets using the Motulsky-Mahan model equation and the low affinity tracer (k_{on} = 1x10^{7}M^{-1}min^{-1}; k_{off} = 1min^{-1} K_d= 0.1μM).

Online injection first read time 1sec							
Number of : (Ambiguous fits; Outliers)	Read frequency (sec)	Input K_d (Output K_d)	K_d %CV	Input k_{on} (Output k_{on}) M^{-1}min^{-1}	k_{on} %CV	Input k_{off} (Output k_{off}) min^{-1}	k_{off} %CV
(0; 0)	1	10pM (10.03pM)	1.72	1E9 (1E9)	0.21	0.01 (0.01)	1.90
(0; 0)	5	10pM (10.01pM)	3.49	1E9 (1E9)	0.38	0.01 (0.01)	3.78
(0; 0)	10	10pM (10.03pM)	5.17	1E9 (1E9)	0.61	0.01 (0.01)	5.68
(0; 0)	20	10pM (9.96pM)	8.02	1E9 (1E9)	0.90	0.01 (0.01)	8.75
(0; 0)	60	10pM (9.97pM)	12.56	1E9 (0.999E8)	1.49	0.01 (0.01)	13.80
(0; 0)	1	1nM (1nM)	0.48	1E8 (1E8)	0.32	0.1 (0.1)	0.74
(0; 0)	5	1nM (0.9993nM)	1.05	1E8 (1E8)	0.66	0.1 (0.1)	1.53
(0; 0)	10	1nM (1nM)	1.54	1E8 (1E8)	0.98	0.1 (0.1)	2.32
(0; 0)	20	1nM (0.996nM)	2.25	1E8 (9.99E7)	1.35	0.1 (0.1)	3.22
(0; 0)	60	1nM (1.002nM	4.06	1E8 (1E8)	2.67	0.1 (0.1)	6.12
(0; 0)	1	100nM (100nM)	0.20	1E7 (1E7)	0.81	1 (1)	0.88
(0; 0)	5	100nM (100nM)	0.47	1E7 (9.99E6)	1.41	1 (1)	1.53

(0; 0)	10	100nM (100nM)	0.62	1E7 (1E7)	2.20	1 (1)	2.29
(0; 0)	20	100nM (100nM)	0.90	1E7 (1E7)	3.24	1 (1)	3.48
(0; 0)	60	100nM (100nM)	1.67	1E7 (1E7)	7.85	1 (1)	8.46
(0; 0)	1	10µM (10µM)	0.18	1E6 (1.01E6)	4.04	10 (10.07)	4.07
(0; 0)	5	10µM (10µM)	0.43	1E6 (1.01E6)	9.08	10 (10.06)	9.13
(0; 0)	10	10µM (10µM)	0.64	1E6 (1.01E6)	13.24	10 (10.14)	13.32
(0; 0)	20	10µM (10µM)	0.85	1E6 (1.06E6)	27.32	10 (10.57)	27.51
(0; 4)	60	10µM (10µM)	1.52	1E6 (1.03E6)	48.92	10 (10.29)	49.03
(200; 4)	1	1mM (1mM)	0.19	1E5 (1.07E5)	35.44	100 (107.40)	35.47
(194; 23)	5	1mM (1mM)	0.47	1E5 (1.45E5)	96.89	100 (145.64)	97.11
(188; 30)	10	1mM (1mM)	0.56	1E5 (1.25E5)	82.92	100 (124.57)	82.98
(161; 34)	20	1mM (1mM)	0.89	1E5 (1.10E5)	84.50	100 (109.54)	84.29
(110; 54)	60	1mM (1mM)	1.51	1E5 (1.08E5)	79.17	100 (108.44)	79.07

Offline addition first read time 30 sec							
Number of : (Ambiguous fits; Outliers)	Read frequency (sec)	Input K_d (Output K_d)	K_d %CV	Input k_{on} (Output k_{on}) $M^{-1}min^{-1}$	k_{on} %CV	Input k_{off} (Output k_{off}) min^{-1}	k_{off} %CV

(0; 0)	1	10pM (10.02pM)	1.59	1E9 (1E9)	0.19	0.01 (0.01)	1.74
(0; 0)	5	10pM (10.02pM)	3.85	1E9 (1E9)	0.43	0.01 (0.01)	4.20
(0; 0)	10	10pM (10.02pM)	5.34	1E9 (1E9)	0.63	0.01 (0.01)	5.85
(0; 0)	20	10pM (10.05pM)	7.15	1E9 (1E9)	0.81	0.01 (0.01)	7.77
(0; 0)	60	10pM (9.73pM)	13.56	1E9 (9.97E8)	1.53	0.01 (0.01)	14.84
(0; 0)	1	1nM (1nM)	0.53	1E8 (1E8)	0.33	0.1 (0.1)	0.77
(0; 0)	5	1nM (1nM)	1.10	1E8 (9.99E7)	0.79	0.1 (0.1)	1.70
(0; 0)	10	1nM (1nM)	1.52	1E8 (1E8)	1.01	0.1 (0.1)	2.30
(0; 0)	20	1nM (1.002nM)	2.36	1E8 (1E8)	1.44	0.1 (0.1)	3.37
(0; 0)	60	1nM (1.002nM)	3.59	1E8 (1E8)	2.45	0.1 (0.1)	5.39
(0; 0)	1	100nM (100nM)	0.22	1E7 (1E7)	0.87	1 (1)	0.96
(0; 0)	5	100nM (100nM)	0.44	1E7 (1E7)	2.07	1 (1)	2.15
(0; 0)	10	100nM (100nM)	0.67	1E7 (1E7)	2.67	1 (1)	2.85
(0; 0)	20	100nM (99.99nM)	0.91	1E7 (1E7)	3.92	1 (1)	4.14
(0; 0)	60	100nM (100nM)	0.97	1E7 (1E7)	3.75	1 (1)	3.96
(10; 0)	1	10µM (9.998µM)	0.21	1E6 (1.02E6)	11.41	10 (10.22)	11.46
(25; 0)	5	10µM (9.998µM)	0.41	1E6 (1.06E6)	35.34	10 (10.60)	35.44

(24; 9)	10	10μM (9.998μM)	0.64	1E6 (1.01E6)	36.20	10 (11.02)	36.30
(33; 5)	20	10μM (10μM)	0.95	1E6 (1.21E6)	53.14	10 (12.14)	53.50
(15; 11)	60	10μM (10μM)	1.50	1E6 (1.13E6)	48.06	10 (11.35)	48.33
(200; 23)	1	1mM (0.994mM)	0.19	1E5 (6.05E7)	312.35	100 (6.06E4)	312.28
(200; 12)	5	1mM (1mM)	0.44	1E5 (1.47E9)	249.83	100 (1.47E6)	249.81
(192; 33)	10	1mM (1mM)	0.65	1E5 (2.15E8)	273.44	100 (2.16E5)	273.47
(173; 13)	20	1mM (9.99E-4)	0.91	1E5 (2.83E9)	236.28	100 (2.83E6)	235.84
(138; 11)	60	1mM (9.98E-4)	1.42	1E5 (4.33E9)	252.26	100 (4.34E6)	252.33

Supplemental Table 4. Summary of the kinetic input parameters and their estimates for unlabelled compounds under conditions which mimic online injection and offline addition of membranes, values are determined from 200 simulated data sets using the Motulsky-Mahan model equation and the low affinity tracer (k_{on} = 1x10^{8}M^{-1} min^{-1}; k_{off} = 0.1min^{-1} K_d= 1nM).

Online injection first read time 1sec							
Number of : (Ambiguous fits; Outliers)	Read frequency (sec)	Input K_d (Output K_d)	K_d %CV	Input k_{on} (Output k_{on}) M^{-1}min^{-1}	k_{on} %CV	Input k_{off} (Output k_{off}) min^{-1}	k_{off} %CV
(0; 0)	1	10pM (10pM)	1.07	1E9 (1E9)	0.18	0.01 (0.01)	1.22
(0; 0)	5	10pM (9.99pM)	2.41	1E9 (1E9)	0.42	0.01 (0.01)	2.74
(0; 0)	10	10pM (10pM)	3.52	1E9 (1E9)	0.62	0.01 (0.01)	4.06
(0; 0)	20	10pM (10pM)	5.05	1E9 (1E9)	0.88	0.01 (0.01)	5.05
(0; 0)	60	10pM (10pM)	8.33	1E9 (1E9)	1.54	0.01 (0.01)	9.55
(0; 0)	1	1nM (1nM)	0.17	1E8 (1E8)	0.29	0.1 (0.1)	0.38
(0; 0)	5	1nM (0.9993nM)	0.38	1E8 (1E8)	0.57	0.1 (0.1)	0.75
(0; 0)	10	1nM (1nM)	0.56	1E8 (1E8)	0.92	0.1 (0.1)	1.24
(0; 0)	20	1nM (0.999nM)	0.81	1E8 (9.98E7)	1.27	0.1 (0.1)	1.73
(0; 0)	60	1nM (0.999nM)	1.34	1E8 (9.99E7)	2.04	0.1 (0.1)	2.78
(0; 0)	1	100nM (100nM)	0.12	1E7 (1E7)	1.23	1 (1)	1.27
(0; 0)	5	100nM (100nM)	0.25	1E7 (1.01E7)	3.10	1 (1)	3.20

(0; 0)	10	100nM (100nM)	0.38	1.01E7 (1E7)	4.0	1 (1.01)	4.15
(0; 0)	20	100nM (100nM)	0.59	1E7 (9.99E6)	6.0	1 (1)	6.17
(0; 0)	60	100nM (99.9nM)	0.99	1E7 (1.02E7)	10.71	1 (1.02)	10.87
(198; 0)	1	10µM (10µM)	0.12	1E6 (1.01E6)	11.55	10 (10.07)	11.57
(167; 1)	5	10µM (10µM)	0.27	1E6 (1.08E6)	30.83	10 (10.84)	30.90
(165; 6)	10	10µM (10µM)	0.35	1E6 (1.17E6)	46.26	10 (11.74)	46.37
(145; 12)	20	10µM (10µM)	0.51	1E6 (1.14E6)	52.10	10 (11.45)	52.30
(138; 38)	60	10µM (9.99µM)	0.98	1E6 (1.31E6)	104.83	10 (13.12)	104.98
(200; 29)	1	1mM (1mM)	0.12	1E5 (3.79E6)	283.24	100 (3789.78)	283.25
(200; 6)	5	1mM (1mM)	0.27	1E5 (1.72E8)	251.19	100 (1.72E5)	251.26
(200; 35)	10	1mM (0.994mM)	7.82	1E5 (2.89E7)	261.12	100 (2.56E4)	245.84
(197; 24)	20	1mM (1mM)	0.54	1E5 (2.52E8)	277.58	100 (2.52E5)	277.30
(175; 13)	60	1mM (1mM)	0.86	1E5 (1.18E9)	240.35	100 (1.18E6)	240.04

Offline addition first read time 30 sec							
Number of : (Ambiguous fits; Outliers)	Read frequency (sec)	Input K_d (Output K_d)	K_d %CV	Input k_{on} (Output k_{on}) $M^{-1}min^{-1}$	k_{on} %CV	Input k_{off} (Output k_{off}) min^{-1}	k_{off} %CV

(0; 0)	1	10pM (10.02pM)	1.21	1E9 (1E9)	0.20	0.01 (0.01)	1.38
(0; 0)	5	10pM (9.99pM)	2.37	1E9 (1E9)	0.43	0.01 (0.01)	2.73
(0; 0)	10	10pM (10.02pM)	3.72	1E9 (1E9)	0.59	0.01 (0.01)	4.21
(0; 0)	20	10pM (10.1pM)	4.55	1E9 (1E9)	0.86	0.01 (0.01)	5.23
(0; 0)	60	10pM (10pM)	8.39	1E9 (9.97E8)	1.51	0.01 (0.01)	9.60
(0; 0)	1	1nM (1nM)	0.17	1E8 (1E8)	0.27	0.1 (0.1)	0.38
(0; 0)	5	1nM (1nM)	0.37	1E8 (1E8)	0.66	0.1 (0.1)	0.88
(0; 0)	10	1nM (1nM)	0.50	1E8 (1E8)	0.88	0.1 (0.1)	1.14
(0; 0)	20	1nM (1nM)	0.74	1E8 (1E8)	1.35	0.1 (0.1)	1.78
(0; 0)	60	1nM (1nM)	1.27	1E8 (1E8)	2.34	0.1 (0.1)	3.13
(0; 0)	1	100nM (100nM)	0.28	1E7 (1E7)	1.57	1 (1)	1.71
(0; 0)	5	100nM (100nM)	0.44	1E7 (1E7)	2.07	1 (1)	2.15
(0; 0)	10	100nM (100nM)	0.35	1E7 (9.96E6)	3.76	1 (1)	3.80
(0; 0)	20	100nM (100nM)	0.51	1E7 (1E7)	5.80	1 (1)	5.91
(0; 0)	60	100nM (100nM)	0.55	1E7 (1E7)	5.52	1 (1)	5.64
(200; 0)	1	10µM (10µM)	0.11	1E6 (1.05E6)	13.71	10 (10.47)	13.74
(189; 5)	5	10µM (10µM)	0.26	1E6 (1.10E6)	30.09	10 (10.96)	30.17

(160; 3)	10	10μM (10μM)	0.35	1E6 (1.11E6)	44.94	10 (11.10)	45.04
(146; 9)	20	10μM (10μM)	0.51	1E6 (1.21E6)	67.30	10 (12.15)	67.49
(127; 32)	60	10μM (9.98μM)	0.96	1E6 (1.33E6)	90.67	10 (13.30)	91.04
(200; 16)	1	1mM (0.994mM)	7.39	1E5 (5.92E6)	326.01	100 (5.30E3)	328.85
(200; 36)	5	1mM (1mM)	0.25	1E5 (1.51E7)	248.87	100 (1.51E4)	249.0
(199; 8)	10	1mM (1mM)	0.33	1E5 (3.17E8)	283.26	100 (3.17E5)	283.26
(173; 23)	20	1mM (9.99E-4)	0.96	1E5 (6.49E8)	235.89	100 (2.83E6)	235.57
(180; 13)	60	1mM (1mM)	0.99	1E5 (5.02E8)	217.62	100 (5.02E5)	217.31

Supplemental Table 5. Summary of the kinetic input parameters and their estimates for unlabelled compounds under conditions which mimic online injection and offline addition of membranes, values are determined from 200 simulated data sets using the Motulsky-Mahan model equation and the low affinity tracer (k_{on} = 1x10^{9}M^{-1}min^{-1}; k_{off} = 0.01min^{-1} K_d= 10pM).

Online injection first read time 1sec							
Number of : (Ambiguous fits; Outliers)	Read frequency (sec)	Input K_d (Output K_d)	K_d %CV	Input k_{on} (Output k_{on}) M^{-1}min^{-1}	k_{on} %CV	Input k_{off} (Output k_{off}) min^{-1}	k_{off} %CV
(0; 0)	1	10pM (10pM)	0.10	1E9 (1E9)	0.11	0.01 (0.01)	0.18
(0; 0)	5	10pM (10pM)	0.22	1E9 (1E9)	0.25	0.01 (0.01)	0.41
(0; 0)	10	10pM (10pM)	0.33	1E9 (1E9)	0.34	0.01 (0.01)	0.61
(0; 0)	20	10pM (10pM)	0.45	1E9 (1E9)	0.54	0.01 (0.01)	0.89
(0; 0)	60	10pM (10pM)	0.86	1E9 (9.99E8)	0.84	0.01 (0.01)	1.51
(0; 0)	1	1nM (1nM)	0.05	1E8 (1E8)	0.44	0.1 (0.1)	0.46
(0; 0)	5	1nM (1nM)	0.12	1E8 (1E8)	0.88	0.1 (0.1)	0.93
(0; 0)	10	1nM (1nM)	0.17	1E8 (1E8)	1.47	0.1 (0.1)	1.51
(0; 0)	20	1nM (1nM)	0.24	1E8 (1E8)	1.92	0.1 (0.1)	2.01
(0; 0)	60	1nM (1nM)	0.47	1E8 (1E8)	3.53	0.1 (0.1)	3.75
(7; 0)	1	100nM (100nM)	0.05	1E7 (9.97E6)	3.58	1 (1)	3.59
(43; 0)	5	100nM (100nM)	0.11	1E7 (1.01E7)	8.31	1 (1.01)	8.36

(50; 0)	10	100nM (100nM)	0.15	1E7 (1.01E7)	11.68	1 (1.01)	11.74
(66; 0)	20	100nM (100nM)	0.22	1E7 (1.03E7)	15.59	1 (1.03)	15.65
(80; 2)	60	100nM (99.9nM)	0.37	1E7 (1.07E7)	35.12	1 (1.07)	35.29
1							
(200; 1)	1	10µM (10µM)	0.05	1E6 (1.15E6)	43.79	10 (11.52)	43.81
(200; 29)	5	10µM (10µM)	0.12	1E6 (1.12E6)	66.90	10 (11.25)	66.95
(200; 14)	10	10µM (10µM)	0.16	1E6 (1.75E9)	294.79	10 (17548.04)	294.76
(200; 8)	20	10µM (10µM)	0.24	1E6 (5.64E9)	250.94	10 (56466.86)	251.01
(200; 6)	60	10µM (10µM)	0.39	1E6 (8.72E9)	230.45	10 (87216.14)	230.35
(200; 11)	1	1mM (1mM)	0.05	1E5 (9.55E6)	48.48	100 (9553.29)	48.47
(200; 21)	5	1mM (1mM)	0.12	1E5 (9.79E6)	54.05	100 (9787.06)	54.05
(200; 16)	10	1mM (1mM)	0.15	1E5 (9.77E6)	59.74	100 (9770.79)	59.74
(200; 22)	20	1mM (1mM)	0.21	1E5 (1.17 E7)	98.96	100 (11729.2)	99.01
(200; 16)	60	1mM (1mM)	0.36	1E5 (1.27E7)	92.39	100 (12507.79)	92.30

Online injection first read time 1sec							
Number of : (Ambiguous fits; Outliers)	Read frequency (sec)	Input K_d (Output K_d)	K_d %CV	Input k_{on} (Output k_{on}) $M^{-1}min^{-1}$	k_{on} %CV	Input k_{off} (Output k_{off}) min^{-1}	k_{off} %CV

(0; 0)	1	10pM (10pM)	0.10	1E9 (1E9)	0.12	0.01 (0.01)	0.20
(0; 0)	5	10pM (9.99pM)	2.43	1E9 (1E9)	0.46	0.01 (0.01)	2.81
(0; 0)	10	10pM (10pM)	0.33	1E9 (1E9)	0.37	0.01 (0.01)	0.62
(0; 0)	20	10pM (10pM)	0.43	1E9 (1E9)	0.53	0.01 (0.01)	0.86
(0; 0)	60	10pM (10pM)	0.78	1E9	0.87	0.01 (0.01)	1.46
(0; 0)	1	1nM (1nM)	0.05	1E8 (1E8)	0.46	0.1 (0.1)	0.48
(0; 0)	5	1nM (1nM)	0.12	1E8 (9.99E7)	0.89	0.1 (0.1)	0.93
(0; 0)	10	1nM (1nM)	0.16	1E8 (1E8)	1.36	0.1 (0.1)	1.43
(0; 0)	20	1nM (1nM)	0.25	1E8 (1E8)	1.76	0.1 (0.1)	1.88
(0; 0)	60	1nM (1nM)	0.40	1E8 (9.99E7)	2.91	0.1 (0.1)	3.07
(9; 0)	1	100nM (100nM)	0.05	1E7 (1E7)	3.33	1 (1)	3.35
(58; 0)	5	100nM (100nM)	0.12	1E7 (1.01E7)	8.81	1 (1.01)	8.85
(51; 0)	10	100nM (100nM)	0.17	1E7 (1.01E7)	11.53	1 (1.01)	11.59
(68; 0)	20	100nM (100nM)	0.22	1E7 (1.02E7)	18.16	1 (1.02)	18.24
(77; 0)	60	100nM (100nM)	0.23	1E7 (1.05E7)	17.87	1 (1.05)	17.95
(200; 8)	1	10μM (10μM)	0.05	1E6 (1.16E6)	44.00	10 (11.61)	44.02
(200; 17)	5	10μM (10μM)	0.11	1E6 (1.54E6)	115.22	10 (15.39)	115.24

(200; 52)	10	10μM (10μM)	0.14	1E6 (1.28E6)	247.86	10 (12.84)	248.29
(200; 6)	20	10μM (10μM)	0.22	1E6 (1.08E10)	285.87	10 (1.08E5)	285.94
(200; 16)	60	10μM (10μM)	0.39	1E6 (5.38E9)	252.64	10 (53811.80)	252.71
(200; 13)	1	1mM (1mM)	0.05	1E5 (1.02E7)	55.30	100 (10237.89)	55.30
(200; 14)	5	1mM (1mM)	0.11	1E5 (9.95E6)	55.06	100 (9950.64)	55.05
(200; 16)	10	1mM (1mM)	0.15	1E5 (9.68E6))	49.20	100 (9683.19)	49.20
(200; 8)	20	1mM (1mM)	0.20	1E5 (9.63E6)	55.35	100 (9632.49)	55.33
(200; 16)	60	1mM (1mM)	0.40	1E5 (9.98E6)	60.23	100 (9977.35)	60.20

Supplemental Methods

How to conduct a Monte Carlo Analysis in GraphPad Prism

This analysis will repeat simulations many times, and tabulate selected results. There are essentially 3 steps to follow in order to perform a Monte Carlo analysis:

1. Simulating a data table

To simulate a family of XY data sets with random error, start from any data table or graph, click **Analyze**, open the **Simulate data** category, and then select **Simulate XY Data**.

X values tab. This allows you to generate a regular series of X values.

The example described below is performed using the Equation the '**Kinetics of competitive binding**', and forms a small part of our whole analysis.

We chose to simulate X values time (min), using a 30sec start time (i.e. 0.5min, representing offline addition) and generate X values up to 180min, at 20sec intervals (i.e. plus 0.3333min).

These simulations include random scatter, so will produce new results when they are updated.

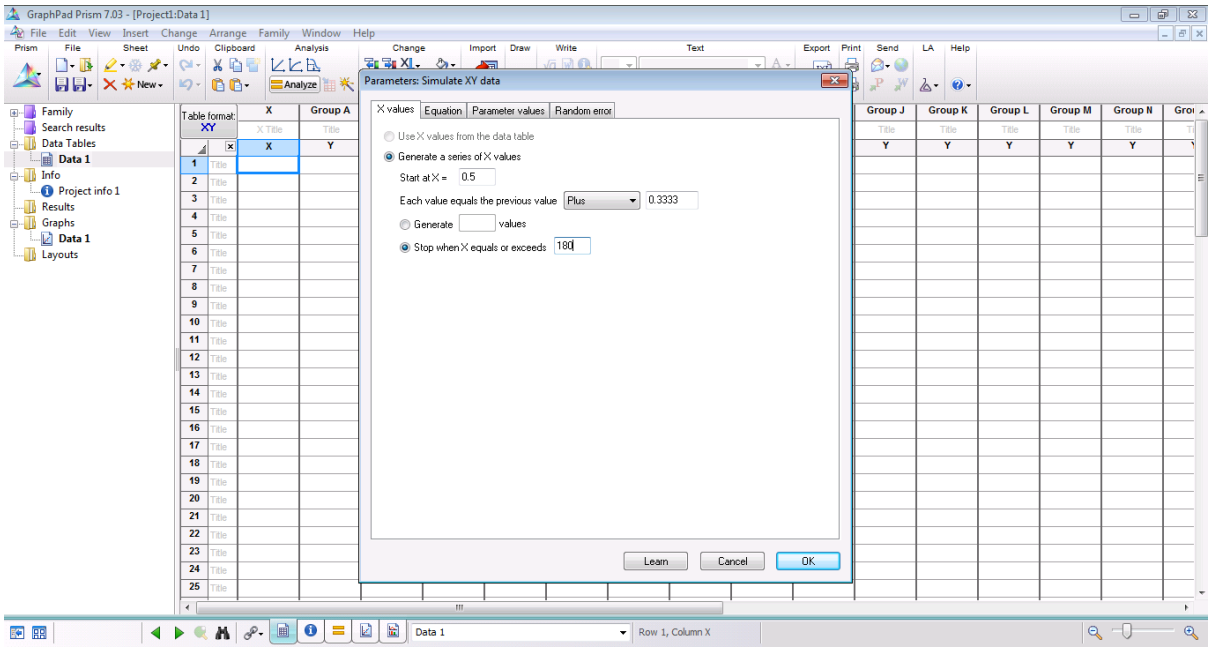

Equation tab. Choose the '**Kinetics of competitive binding' equation** on this tab found listed in '**Binding-Kinetics**' option.

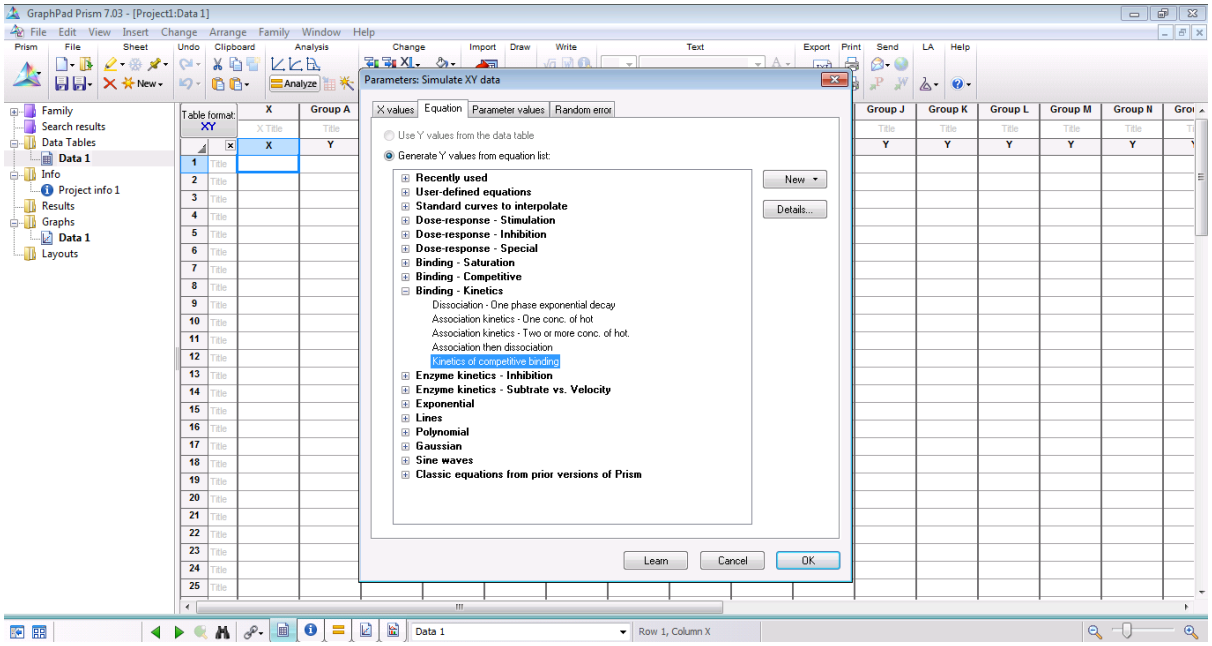

Parameter values tab. On top of the tab, choose how many data sets you wish to simulate, and how many replicates each data set will have.

In this example we chose to simulate using one replicate our tracer (K1 =1e9$M^{-1}min^{-1}$; K2 =0.01min^{-1}) in the absence of competitor at a concentration (L) 3* K_d (0.03nM), Data set A, column title 0 and our tracer in the presence of a competitor (K3 =1e9$M^{-1}min^{-1}$, K3 0.1min^{-1}), employing five different competitor concentrations (I) ranging from 100 to 1nM*K_d, Data set B to F, column titles 100 to 1. Note for simulation input purposes units are omitted.

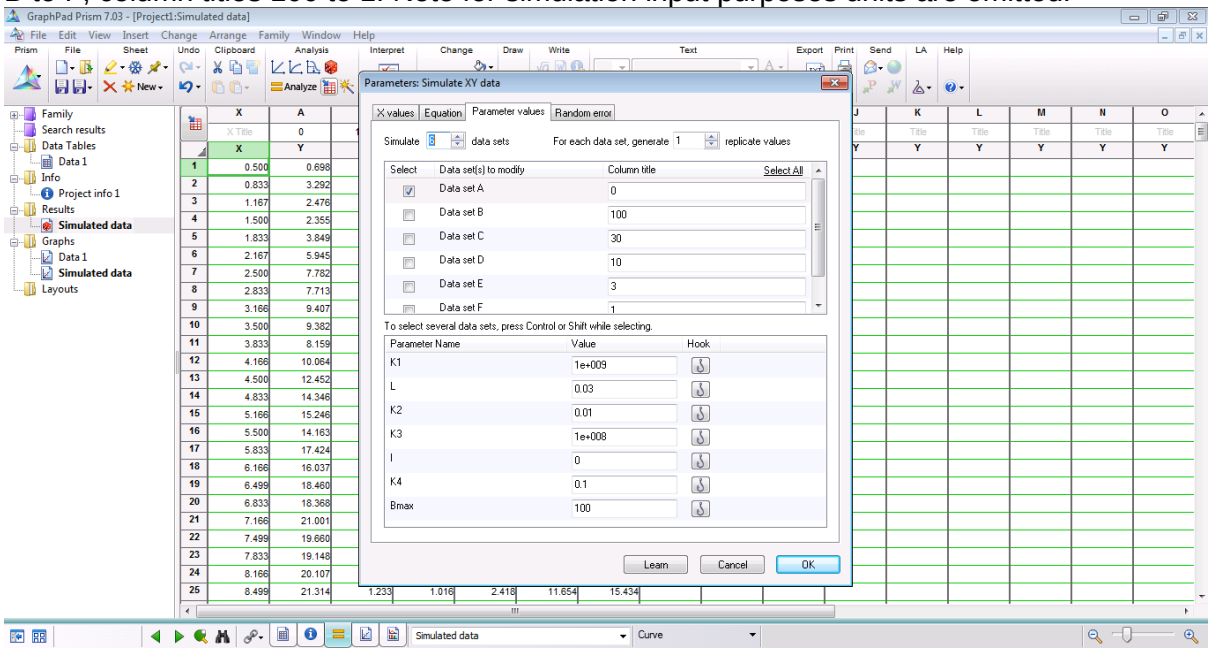

You can choose to simulate multiple data sets (Global fitting), choosing to enter a parameter value for just for one data set (eg. competitor concentrations or I), or to enter a parameter that applies to all data sets, or all, curves (eg. the tracer parameters K1, K2 and L and the competitor parameters K3 K4 plus Bmax).

Random error tab. There are several methods for generating random scatter (and if desired also adding outliers).

GraphPad Prism allows the user to add random error to the generated *Y* values by taking each theoretical (i.e. 'correct') value and adding to it a random number taken from a uniformly distributed population with a standard deviation (SD) defined by the user and equivalent at all concentrations. The random error chosen for simulation was Guassian absolute to directly reflect the pattern of error observed in our experimental data.

We took the decision to run simulations with minimal error (a standard deviation equal to one) reflecting a high quality assay to test the theoretical limitations of the Motulsky-Mahan model rather than being restricted by what we perceive as technical assay limitations.

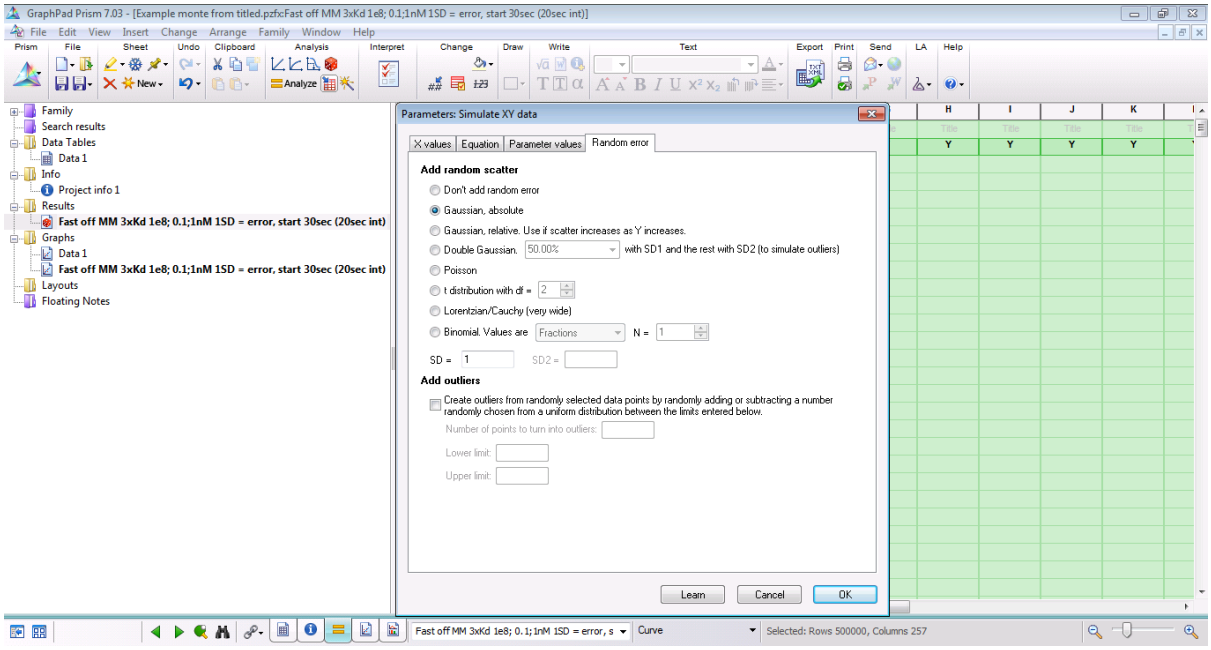

Finally, **title** the 'simulation' as you will likely create several varying one or more parameter at a time.

2. Analyze the simulated data set using the equation Kinetics of competitive binding.

To do this click **Analyse**, and choose **XY analyses (Non-linear regression curve fit)**

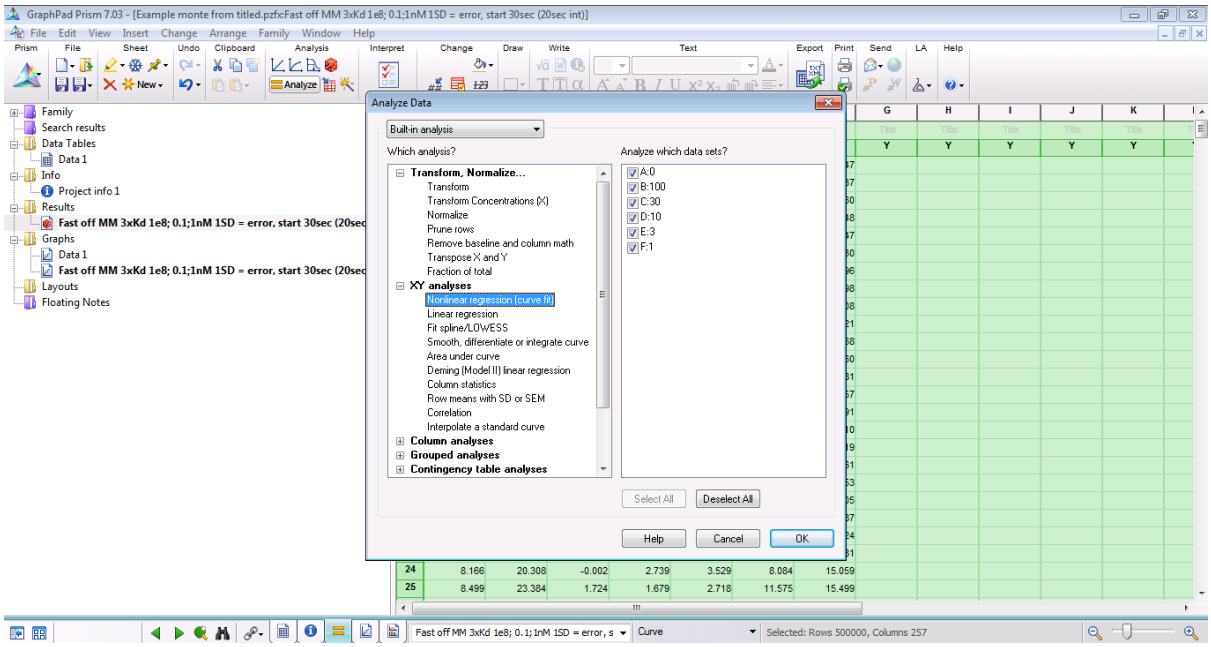

Then choose the **Kinetics of competitive binding** equation on this tab found listed in '**Binding-Kinetics'** option.

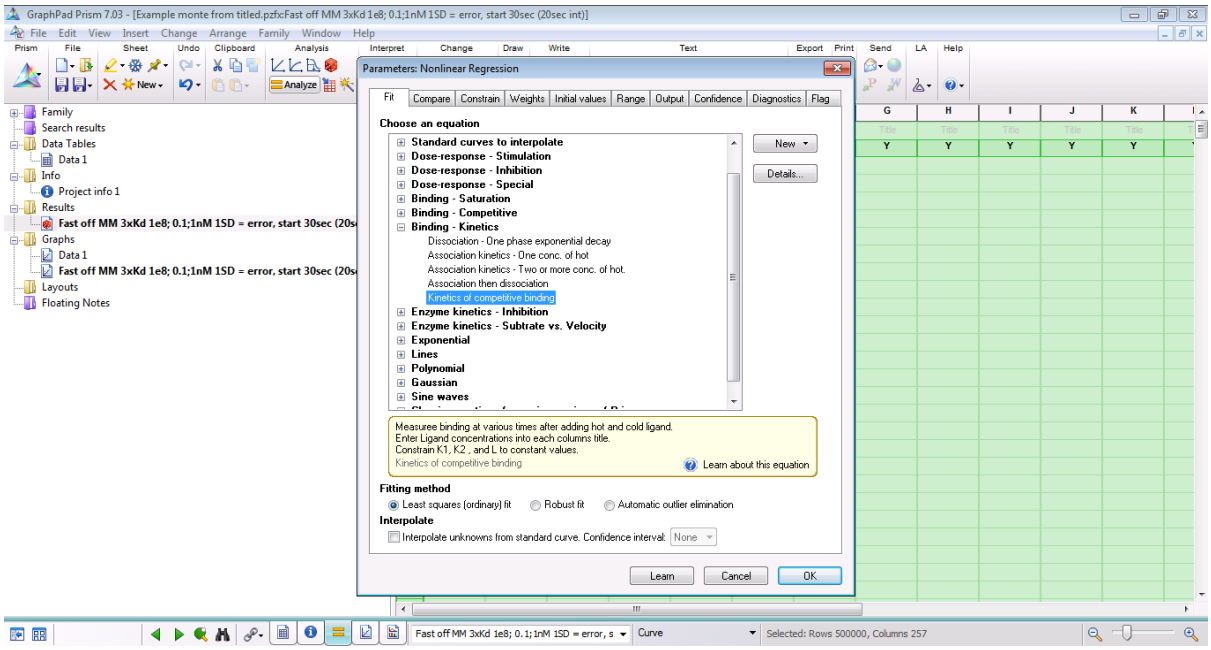

Then click on the **constrain** tab and constrain the parameters of the tracer eg k1, k2 and L, as described above.

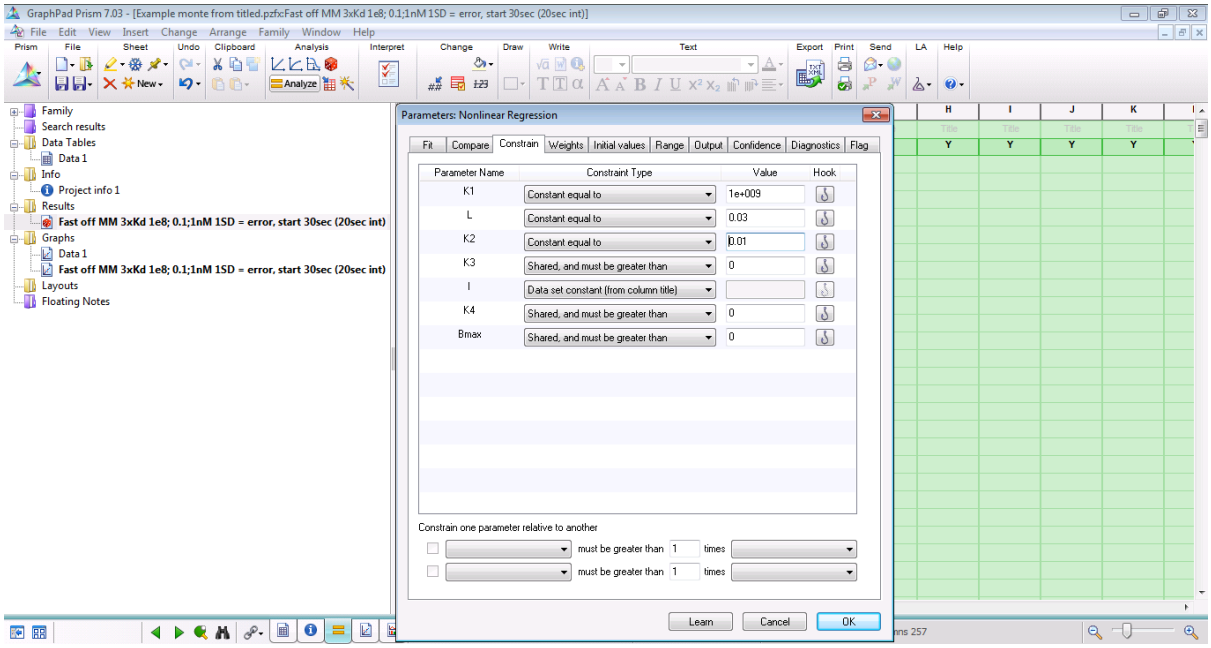

3. Perform the Monte-Carlo analysis.

Start from the nonlinear regression **results page**, click **Analyze** and choose **Monte Carlo** simulation.

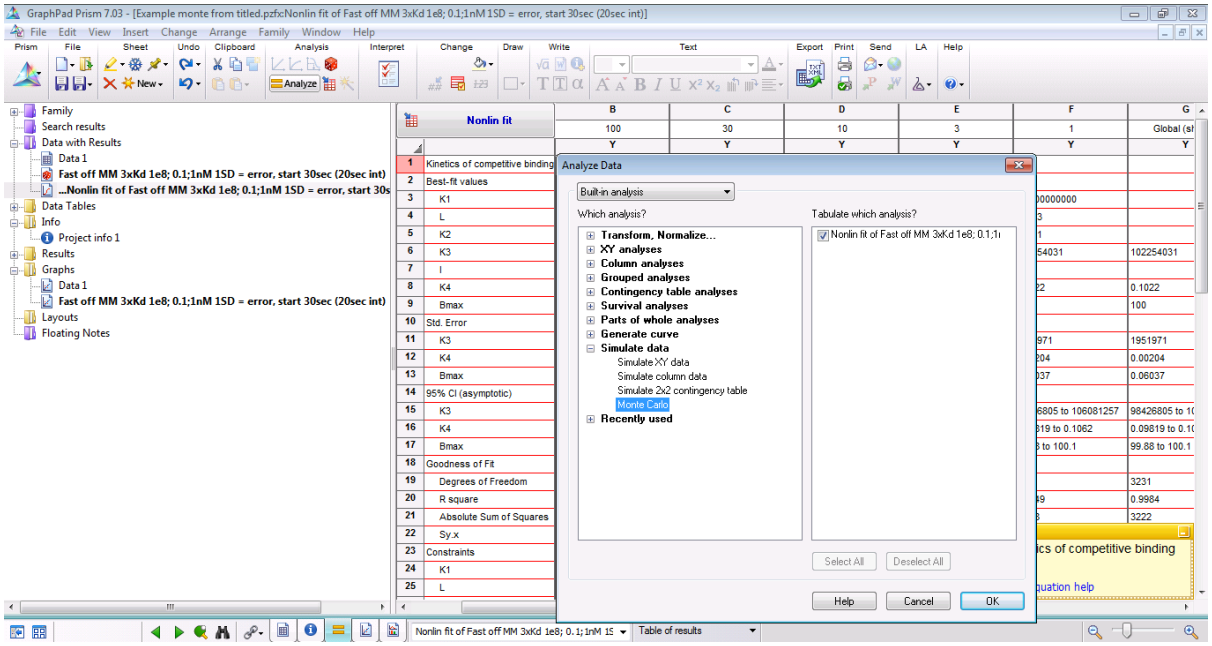

On the first (simulations) tab, choose how many simulations you want Prism to perform. We chose to perform 200 simulations per test condition.

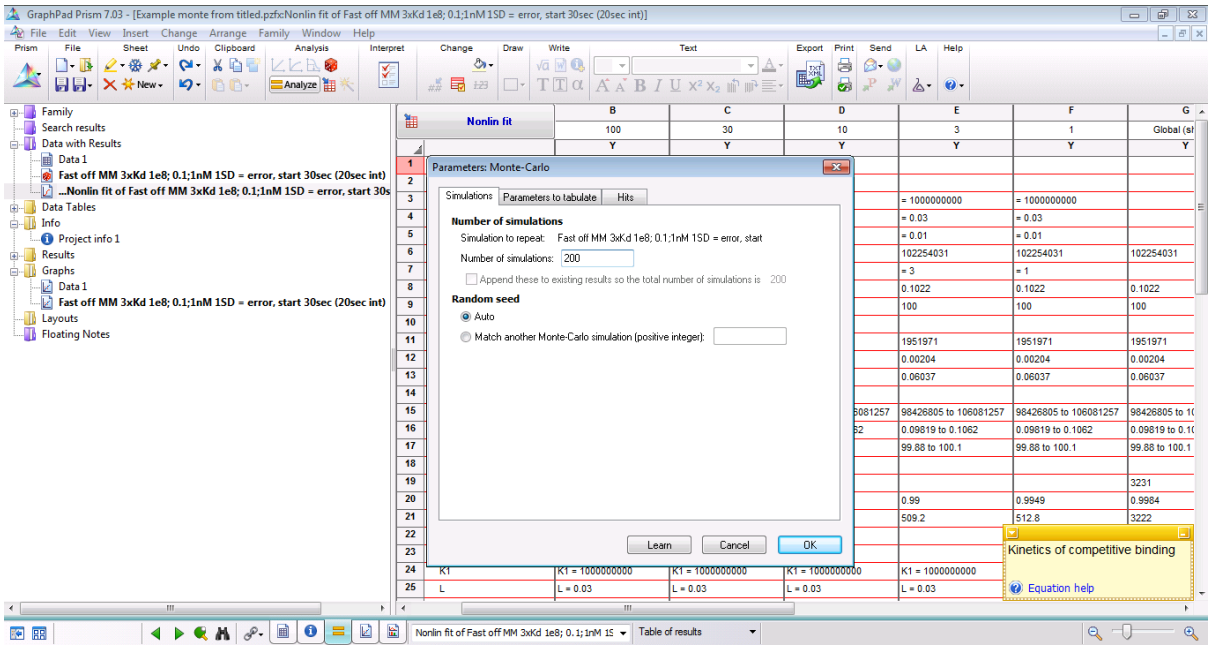

On the **Parameters to tabulate** tab, choose which parameters you want to tabulate. The choice is the list of analysis constants that Prism creates when it analyses the data.

For this example, we chose to tabulate all the **Global (shared) parameters**.

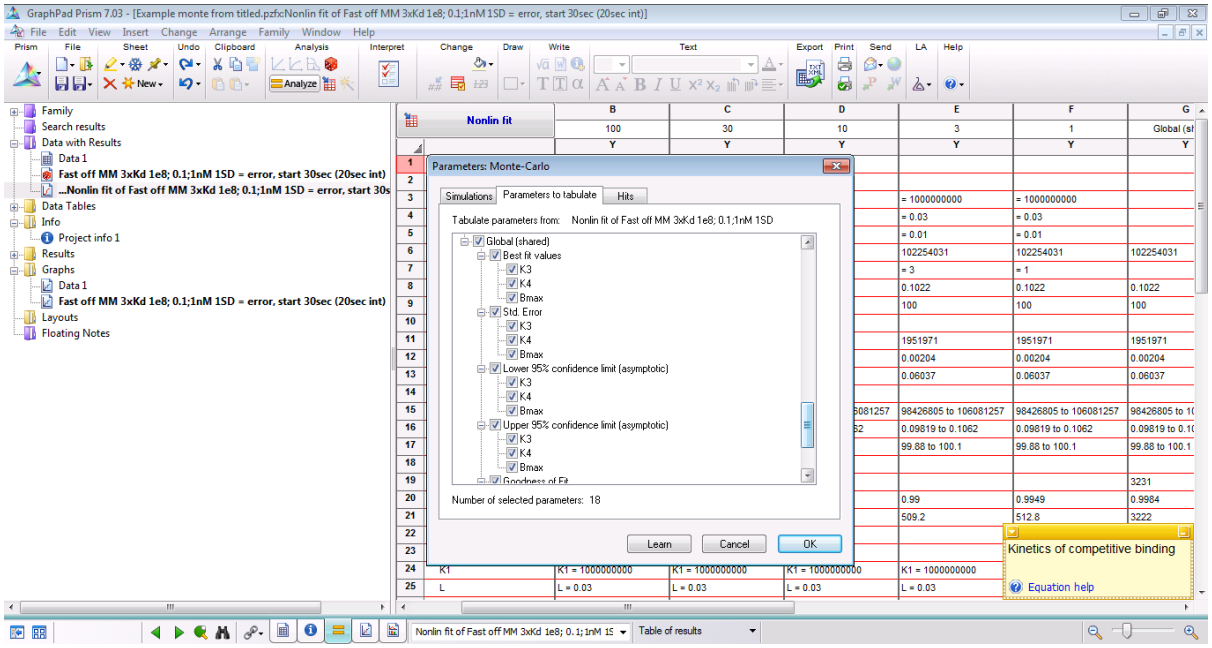

On the **Hits tab**, you can define a criterion which makes a given simulated results a "hit". We copied all the reported data (Parameters to tabulate) to Excel for further analysis and so chose to report all individual simulations.

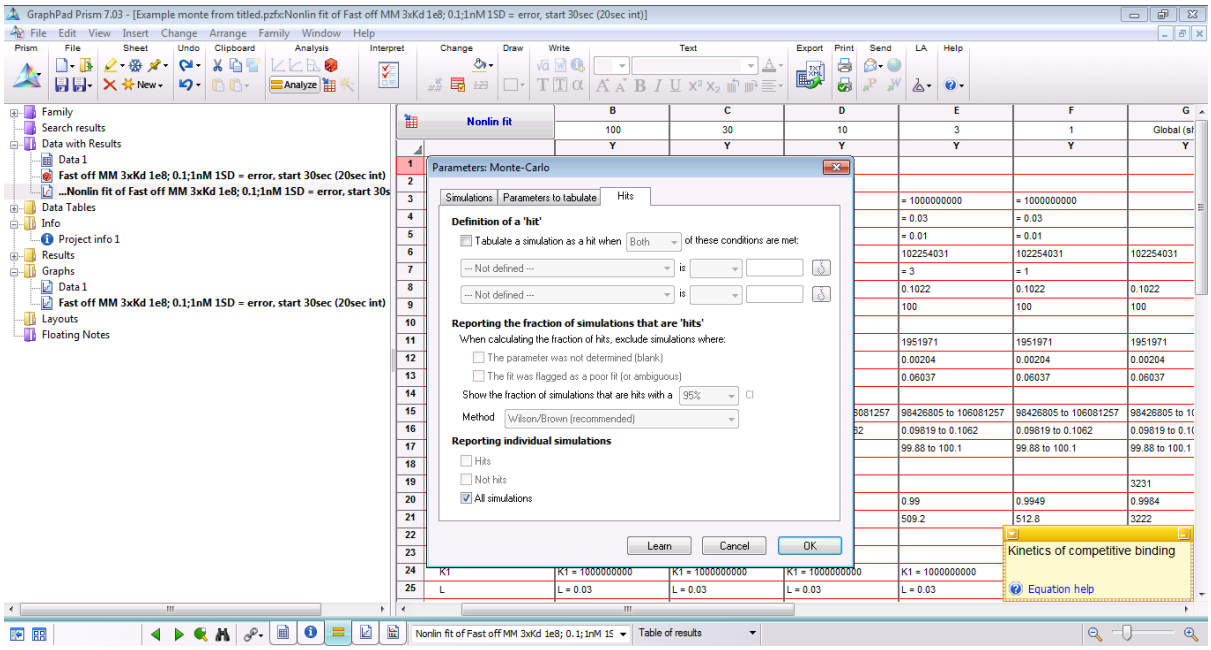

Full instructions can be found in the online Prism guide found through the following link under Simulating data and Monte Carlo simulations
https://www.graphpad.com/guides/prism/7/user-guide/index.htm?simulating_data.htm

Example Monte Carlo file.pzfx